National Library of Canada | Bibliothèque nationale du Canada | CANADIAN THESES ON MICROFICHE | THÈSES CANADIENNES SUR MICROFICHE

54200

0-315-06280-0

NAME OF AUTHOR/*NOM DE L'AUTEUR* James D. Ray

TITLE OF THESIS/*TITRE DE LA THÈSE* A Study of the Interfacial Reaction Kinetics in the Fe-CaF_2 System at 1450 Deg. C.

UNIVERSITY/*UNIVERSITÉ* McMaster University

DEGREE FOR WHICH THESIS WAS PRESENTED/*GRADE POUR LEQUEL CETTE THÈSE FUT PRÉSENTÉE* Ph.D.

YEAR THIS DEGREE CONFERRED/*ANNÉE D'OBTENTION DE CE DEGRÉ* 1981

NAME OF SUPERVISOR/*NOM DU DIRECTEUR DE THÈSE* Dr. W.K. Lu

DATED/*DATÉ* September 18, 1981 SIGNED/*SIGNÉ* [signature]

PERMANENT ADDRESS/*RÉSIDENCE FIXÉ*

A STUDY OF THE INTERFACIAL REACTION KINETICS IN THE Fe-CaF_2 SYSTEM AT 1450°C

by

© J. D. Ray, B.Sc. (Hons.)

A Thesis

Submitted to the School of Graduate Studies

in Partial Fullfilment of the Requirements

for the Degree

Doctor of Philosophy

McMaster University

May, 1981

Doctor of Philosophy (1981)

McMaster University
Hamilton, Ontario

TITLE: A Study of the Interfacial Reaction Kinetics in the Fe-CaF_2 System at 1450°C

AUTHOR: James Douglas Ray, B.Sc. (McMaster University)

SUPERVISOR: Professor W-K. Lu

NUMBER OF PAGES: x, 157

ABSTRACT

An understanding of the chemical reaction kinetics at a slag/metal interface requires knowledge of both transport and interfacial properties. However, fundamental interfacial reaction rate data are largely unavailable. Consequently, the ion exchange current density and interfacial capacitance have been measured with the double pulse galvanostatic method for the anodic dissolution of an iron electrode in liquid CaF_2 and CaF_2-CaO slags. Both the exchange current and capacitance are strongly increasing functions of concentration. The measured exchange current densities are large (ranging from 4.5 to 400 amperes/cm^2), so that a non-linear extrapolation of the experimental data is necessary.

The kinetics of oxygen transfer at the Fe/CaF_2 interface was studied in independent experiments. The reaction was driven by an FeO activity gradient. The kinetic information obtained in this manner compares favourably with that derived from the electrochemical technique.

With suitable information on the relative magnitudes of transport and reaction rates, it is possible to predict the kinetic regime for the entire system (i.e. transport, reaction, or mixed control). The experimental data indicate that mixed control of the reaction kinetics will prevail at the Fe/CaF_2 interface in the absence of forced stirring. If the kinetic parameters in more complex metallurgical systems are similar to those measured at the Fe/CaF_2 interface, the influence of interfacial charge transfer reactions may be greater than is normally supposed.

ACKNOWLEDGMENTS

The author wishes to express his sincere gratitude to Professor W-K. Lu for his guidance during the course of this project, and his countless efforts to provide a broad educational experience. The assistance of the other members of the supervisory committee, Professors J.A. Morrison, G.R. Purdy and W.W. Smeltzer, is greatly appreciated.

Sincere thanks are extended to Professor K. Schwerdtfeger and Dr. R. Prange for their valued contributions while the author studied at the Max-Planck-Institut für Eisenforschung, Düsseldorf.

The author also expresses his appreciation to the Algoma Steel Corporation of Sault Ste. Marie for their support and encouragement, and to the faculty, staff, and graduate students of the Department of Metallurgy and Materials Science, McMaster University, for their helpful discussions and assistance.

Finally, many thanks are due for the drawings by Mr. M. van Oosten and the typing by Mrs. J. Reinholt.

TABLE OF CONTENTS

LIST OF TABLES

LIST OF FIGURES

CHAPTER 1: INTRODUCTION

1.1 INTRODUCTION

Many pyrometallurgical smelting and refining reactions involve the simultaneous presence of a slag and a metal phase. Such reactions are heterogeneous and occur only at an interface.

Any heterogeneous reaction can be considered as consisting of three principal steps:

(1) transport of the reactants from the bulk phases to the metal/slag interface,

(2) the reaction or series of reactions at the slag/metal interface,

(3) transport of the reaction products from the slag/metal interface into the bulk phases.

The three steps could be stated in an equivalent way which better lends itself to analysis:

(1) transport in the slag of reactants and products,

(2) reaction at the interface,

(3) transport in the metal of reactants and products.

Kinetic expressions are typically written as linear relations between fluxes and forces. Although linear relationships should not be expected to be universally true, they have been successfully applied on many occasions and are always justifiable approximations for sufficiently small forces. Of particular interest in any such flux/force relationship is the constant of proportionality, whether it be a diffusivity in a diffusing system or a fundamental rate constant in a

reacting system.

In the case of multicomponent systems, a phenomenological framework is necessary in order to describe the manner in which the various fluxes are interrelated or coupled. Such a framework, as it applies to diffusing systems is developed and summarized in Chapter 2.

The study of slag/metal reaction kinetics has intensified significantly in the past two decades although fundamental interfacial reaction rate data are still largely unavailable. In the classic work of King and Remachandran[1, 2] it was reported that chemical reaction at the slag/metal interface was electrochemical in nature. More recent experiments lead to a similar conclusion. Thus, it is possible in principle at least to use established electrochemical techniques to evaluate kinetic parameters in slag/metal systems. This subject is pursued in Chapter 3 as applied to the Fe/CaF_2 system. An alternate approach to the interfacial kinetics based on a chemical driving force is developed in Chapter 4. The theory and experimental results of the chemical and electrochemical approaches are compared and discussed in Chapter 5.

1.2 RATE CONTROL

As introduced previously, a heterogeneous reaction consists of three definable steps: transport to, reaction at, and transport from the interface. In this section, a single component reaction will be considered, although the arguments can be generalized. The steps are arranged in series and can be considered analogous to three resistances arranged in series in an electrical circuit (Figure 1.1). One can

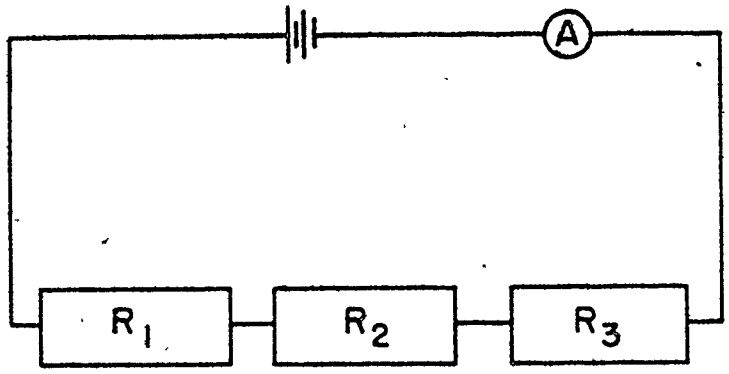

Figure 1.1: Electrical Circuit Analogy for Rate Control

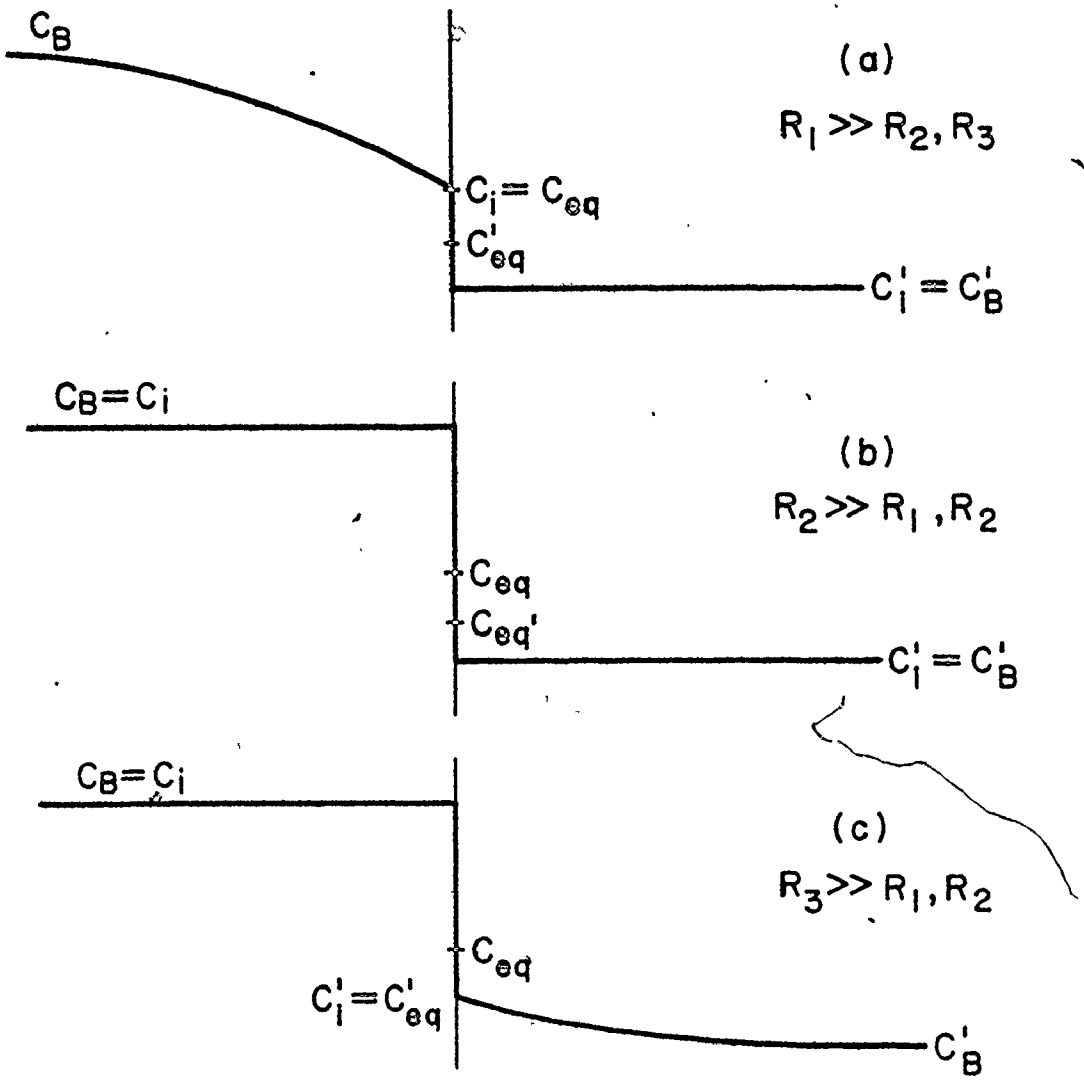

Figure 1.2: Rate Control - Limiting Cases

readily visualize three limiting cases in the electrical circuit analogy.

If $R_1 >> R_2, R_3$ then most of the voltage drop (i.e. driving force) will be allocated to R_1. Moreover, the total current (i.e. flux or reaction rate) in the circuit will be determined by R_1. Identical arguments can be advanced for $R_2 >> R_1, R_3$ and $R_3 >> R_1, R_2$. If one lets R_1 represent the "resistance" due to reactant transport towards the interface, R_2 the resistance due to reaction at the interface, and R_3 the resistance due to the transport of product, one can now consider limiting cases analogous to those above.

(1) When $R_1 >> R_2, R_3$, the interfacial reaction approaches closely to equilibrium, and the interfacial concentration of the product approaches the bulk value (Figure 1.2a). In this limiting case, the overall reaction rate is determined by the ability to transport reactant to the interface.

(2) When $R_2 >> R_1, R_3$, the rate of the interfacial reaction is slow relative to those for the processes that supply reactant and remove product. In this case, the differences between the bulk and interfacial concentrations of both reactant and product are insignificant, and the overall rate is determined by the interfacial reaction (Figure 1.2b).

(3) When $R_3 >> R_1, R_2$ the situation is similar to (1) except that the overall rate is limited by transport of product from the interface (Figure 1.2c).

Case (2) is commonly referred to as reaction rate control. Cases (2) and (3) are usually grouped under the name transport control.

In addition to the limiting cases, it is important to consider the intermediate situation (i.e. mixed control) when none of the three steps dominates. For simplicity, $R_1 \approx R_2 >> R_3$ will be assumed in the following analysis. The steady state condition (time independent) will be considered intially, i.e. $\frac{\partial}{\partial x} D \frac{\partial c}{\partial x} = \frac{\partial c}{\partial t} = 0$. The situation is summarized in Figure 1.3. In the steady state one can write $J_1 = J_2 = J_3$ and solve for C_i (independent of time) to determine the overall rate. In the unsteady state, $\frac{\partial C}{\partial t} \neq 0$ and C_i is a function of time. In this case, $J_1 \neq J_2 = J_3$ and no simple analytic solution to the problem exists. Often, however, the quasi-steady state approximation can be made (i.e. $J_1 \approx J_2 = J_3$). Then, an approximate analytical solution can be obtained at a specified time.

Alternatively, the solution to the unsteady state problem may be approached numerically. Yamanda[3] has used this approach to solve for reaction rates in a theoretical multicomponent slag/metal system. The transport equations for the slag and metal are solved simultaneously using the interfacial reaction rate as a common boundary condition. Numerical solutions can be obtained for unsteady state mixed control reactions.

The equations arising from the theories of both material transport and interfacial reaction rates must be solved simultaneously to obtain the overall rate. It is important to emphasize at this point that the rate theories for interfacial reaction, transport in the slag, and transport in the metal can be developed independently of each other without loss of generality. The overall rate for the system may then be obtained through one of the approaches discussed.

Knowledge of the regime (transport, reaction or mixed) in which a slag/metal system is operating is of significant practical and theoretical importance. Although reactions of metallurgical interest are often assumed to be controlled by mass transport in the slag, supporting experimental evidence is sparse. This question is addressed again in Chapter 5.

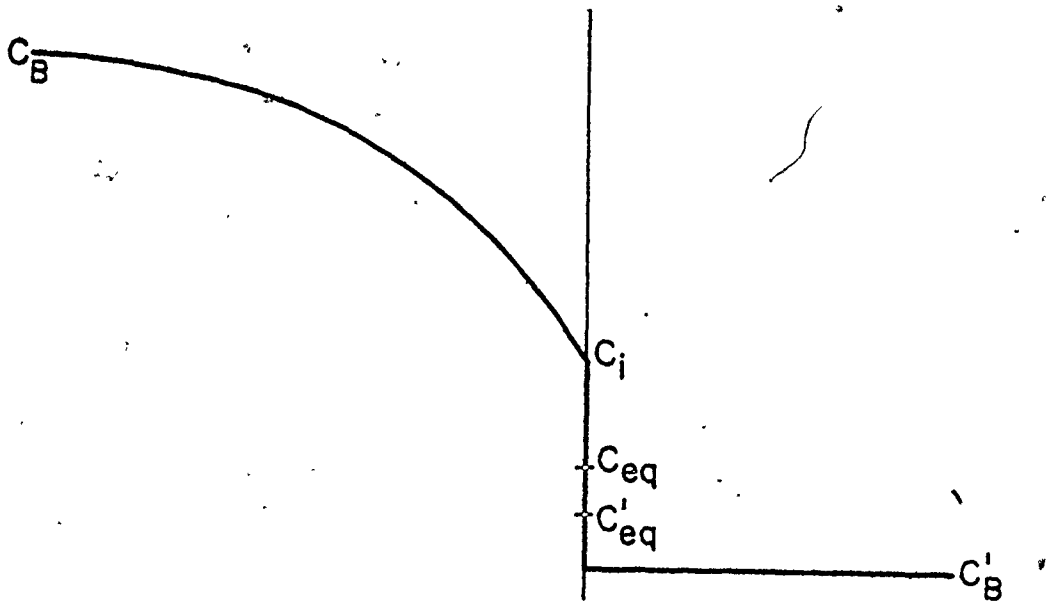

Figure 1.3: Rate Control - Mixed Case

CHAPTER 2: TRANSPORT IN METALS AND SLAGS

2.1 INTRODUCTION: BULK FLOW AND DIFFUSION

Transport to a slag/metal interface is commonly described by convective mass transfer. Far from the reaction interface, bulk flow (eg. due to turbulence) is presumed to be the dominant transport mechanism. Closer to the reaction interface, the influence of bulk flow diminishes and is replaced by diffusion as the dominant mode of mass transfer. The concept of a boundary layer thickness is introduced as an indication of the region in which diffusion begins to dominate. This boundary layer concept has not proven to be entirely satisfactory. The layer thickness will generally differ for heat, momentum, and mass transfer. Furthermore, it will be dependent upon the species being transferred. Frequently, an empirical mass transfer coefficient is introduced which is intended to represent a sum-average of the diffusional and bulk flow contributions.

Although the interrelation of bulk and diffusional flow is complex, it is clear that, close to the interface, diffusion must be considered. Diffusion will have a major impact on the role of transport in the progress of the overall reaction, and play a primary role in the system with mixed control kinetics. This, coupled with the generally complex and theoretically intractable interaction between bulk and diffussive flow, suggests that bulk flow should not be considered further, except through the introduction of an empirical boundary thickness.

One of the most important concepts which comes out of a phenomenological treatment of diffusion is the possibility, in fact neces-

sity, of interrelated fluxes, i.e., coupling. In this work, coupling is intended to refer to any interdependence of simultaneous reactions or diffusion events. The acceleration or deceleration of a diffusing species due to the effect of simultaneous diffusion of another species is considered to be evidence of coupling. In the limit, one could anticipate that strong coupling could result in the reversal of a flux as the system proceeds towards equilibrium.

By thermodynamic coupling, one implies a coupling which arises due to interaction of elements that can be described through activity coefficients. A classic example of this type of coupling can be found in the work of Darken,[4] who studied a diffusion couple containing iron, silicon and carbon. An increase in the carbon concentration on the silicon-deficient side of the couple, followed by a gradual decrease can be attributed to the effect of the silicon concentration on the activity of the carbon. Thus, carbon concentration as a function of time exhibits a reversal. However, the driving forces (i.e., chemical potential gradients) show a monotonic decrease with time.

In contrast, kinetic coupling implies that the potential gradient of one species will have an effect on the motion of a second species with respect to a specified reference frame. It will be shown in a later section that kinetic coupling might arise due to charge interactions in ionic systems. Such coupling can, in principle, result in the reversal of a chemical potential gradient with time. One might anticipate the possibility of coupled reactions even in ideal or henrian solutions.

It is interesting to reflect briefly on potential implications

of coupled reactions. Consideration of such coupling may lead to a better understanding of reactions proceeding in a multicomponent system. It is also clear that in any situation where the coupling is significant, the alteration in rates encountered in multicomponent systems could be profound when compared with individual rates determined in separate experiments. It is then reasonable to ask whether such an alteration in rates might be exploited in order to achieve some result which would not otherwise be possible.

2.2 IRREVERSIBLE THERMODYNAMICS AND THE PHENOMENOLOGICAL BASIS FOR DIFFUSION

Experiment has firmly established the following theoretical presentation as a reasonable approximation for diffusion in non-ionic systems and it should be applicable to metallic diffusion in slag/metal systems. However, liquid metal tracer diffusivities are normally about one order of magnitude greater than those in slag. The generally lower viscosity of metal will also result in increased bulk transport. Consequently, transport in metals will not, in general, limit the kinetics of the overall reaction sequence and need not be considered further in a study of slag/metal kinetics.

Nonetheless, a sound background in metallic transport is important for understanding transport in slags, since most of the important concepts of ionic diffusion are simple extensions of those in non-ionic diffusion.

The experimental work of Kirkendall and Smigelskas[5] using a

copper-zinc diffusion couple served to stimulate analysis of diffusion in binary systems. Darken[6] formulated an analytical solution to the binary problem and used it to explain the experimental work of Kirkendall. Darken's concept has since been extended to include ternary and more complicated systems. An excellent introduction may be found in Shewmon's book.[7]

The fundamentals of irreversible thermodynamics and the phenomenological approach are detailed in de Groot and Mazur,[8] and reviewed by Kirkaldy.[9] The development will be summarized briefly. Many "forces" X_i such as temperature, chemical, and potential gradients give rise to irreversible phenomena. Generally, fluxes J_i will result from such forces. One should consider that any force X_k can give rise or contribute to <u>any</u> flux J_i. The algebraic form of any such relationship is not clear, but when the force is sufficiently small (i.e. close to equilibrium) a linear approximation arising from the truncation of a Taylor series is applicable. Thus, the general form of the phenomenological equations for irreversible phenomena may be written

$$J_i = \sum_{k=1}^{n} L_{ik} X_k \qquad (2.1)$$

where the L_{ik} form a mobility matrix.

Onsager's Theorem[10] states that, provided that the rate of entropy production can be expressed as a bilinear function of independent fluxes and forces, the matrix of phenomenological coefficients L_{ik} is symmetric, i.e., $L_{ik} = L_{ki}$. Onsager's Theorem, which was justified by treating the behavior of fluctuations from equilibrium will

be taken as an axiom. In practice, the symmetry of the L_{ik} matrix has limited impact on the theories of isothermal metallic diffusion, since this matrix is generally approximated as diagonal, and hence the symmetry of the off-diagonal terms is unimportant.

By considering mass and energy conservation, and the Gibbs-Duhem relation, one can formulate an entropy balance $\rho\frac{\partial s}{\partial t} = -\ \text{div}\ J_s + \sigma$ where div J_s can be taken as the entropy flux term and σ as the entropy source. For isothermal, isobaric diffusion,

$$\sigma = -\frac{1}{T}\sum_{k=1}^{n} J_k \cdot \nabla\mu_k \qquad (2.2)$$

where $\nabla\mu_k$ is the chemical potential gradient. The entropy production rate is shown in the required bilinear, although not as yet independent form.

The fluxes and forces are not independent in the equation above. Among the fluxes there exists an arbitrary linear dependence of the form

$$\sum_{i=1}^{n} \alpha_i J_i = 0 \qquad (2.3)$$

arising from the need to choose a reference frame. The chemical potential gradients are linearly related through the Gibbs-Duhem relation

$$\Sigma N_i \frac{\partial \mu_i}{\partial x} = 0. \qquad (2.4)$$

Following de Groot and Mazur[11] one can demonstrate that symmetry of the L_{ik} is preserved even with a linear relationship between the

fluxes and forces. Alternatively, one could solve and eliminate the n^{th} flux and force from the set of equations. This approach will be used in the next section on ionic diffusion.

In order for the phenomenological formalism to be of practical significance, the L_{ik} matrix must be evaluated. Some model or models must be applied, and some approximations made. First, a general comment on the matrix is in order. The diagonal terms L_{ii} in the matrix represent the contribution to the flux J_i as a result of the chemical potential of species i. The off-diagonal terms represent the contribution to the flux of J_i as a result of forces or chemical potential gradients in the system from other species. For example, these cross terms may indicate the effect on the flux of manganese through iron due to the chemical potential gradient for nickel.

Normally, assumptions are introduced and a model developed which postulates the existence of some reference frame in which the fluxes are approximately independent. As an immediate consequence of such a model, the cross terms in the mobility matrix are approximately zero. That is, the matrix is assumed to be diagonal. Kirkaldy and Lane[12] have proposed such a model for close packed solids by applying transition state theory for a vacancy diffusion mechanism, with the constraint that sufficient vacancy sources and sinks exist to preserve local equilibrium of vacancies.[13] In their work, they assume that the correlated motion of atomic groups in the vicinity of a vacancy is negligible and then demonstrate that, with such an assumption, the mobility matrix for the lattice fixed or "Kirkendall" frame is diagonal. If such correlated motion in a lattice proved

significant in such a system, no reference frame would exist in which the fluxes were independent. Manning[14] has proposed a vacancy model in which non-zero mobility cross terms arise in the lattice fixed frame due to a vacancy wind effect. However, the net effect is small and remains experimentally unsubstantiated.

Zeibold and Cooper,[15] and Cooper[21] have developed equations similar to those of Kirkaldy with three assumptions:

(1) that the relaxation velocity is always great enough to cancel the net flux,

(2) that the mobilities remain unchanged by the introduction of chemical potential gradients,

(3) that there is no coupling mechanism between the species other than that caused by the relaxation velocity.

In addition to the vacancy mechanism, they further postulate hydrodynamic flow as an alternative source of a relaxation velocity in noncrystalline materials.

Although the diagonal mobility matrix in the lattice fixed or Kirkendall frame is commonly accepted, the complications of this approximation should be examined further. Consider first the number of independent coefficients generated by the approximation. Because the matrix is diagonal, one has n independent mobility coefficients in an n component system. In general, however, one can reduce an nxn matrix (n^2 coefficients) through Gibbs-Duhem and reference frame choice to an (n-1) x (n-1) matrix ($(n-1)^2$ coefficients). Further, the Onsager Reciprocity Relations give n(n-1)/2 independent mobility coefficients. Consider the two equations for 2, 3 and 4 component

systems:

n	= 2	3	4	diagonal approximation
n(n-1)/2	= 1	3	6	fundamental coefficients.

For a two-component system, only one fundamental mobility coefficient is defined. The two mobilities (commonly related to tracer diffusivities through the Einstein equation $L_{ii} = D_i^* C_i/RT$) must be related, as they are in Darken's equation. In a ternary system, the number of available tracer diffusivities equals the number of fundamental coefficients. In a four-component system, the number of fundamental coefficients necessary to define the system fully exceeds the number of available tracer diffusivities. This simple analysis shows that it is not sufficient to measure tracer diffusivities in any system of four or more components where the mobility matrix written in the lattice fixed frame cannot be approximated as diagonal.

It should be clear that the use of the terms "coupling" and "cross effects" refer to the existence of non-zero off-diagonal elements in the mobility matrix. It will be shown that even when the mobility matrix is assumed to be diagonal in the Kirkendall frame (i.e., lattice-fixed), one will, in general, generate non-zero off-diagonal elements in the mobility matrix when the matrix expressed in any experimentally accessible reference frame (eg. mass-fixed, volume-fixed). The presence of such cross terms, when due to the choice of reference frame, will be referred to as "reference frame coupling".

On the same basis, any non-zero terms in the Kirkendall (lattice)

frame (eg. due to correlated atom-vacancy interactions) will be attributed to "fundamental coupling".

Using the above definitions, the third assumption of Zeibold and Cooper may be restated: reference frame coupling is the dominant coupling mechanism. The effect of fundamental coupling is negligible by comparison.

De Groot and Mazur[8] have shown that any linear relation of the form $\sum_{i=1}^{n} \alpha_i J_i = 0$ will provide a suitable choice of reference frame. With specific choices for α_i, the common reference frames can be expressed as follows:

Reference Frame	Definition of α_i	
Number-Fixed	$\alpha_i = 1$ for $i = 1, \ldots, n$	
Volume-Fixed	$\alpha_i = \bar{v}_i$ for $i = 1, \ldots, n$	($\bar{v}_i$ partial molar volume)
Solvent (Anion)-Fixed	$\alpha_i = 0$ for $i = 1, \ldots, (n-1)$	
	$\alpha_n = 1$	

The volume fixed frame is of particular interest, since it is coincidental with the laboratory frame when the partial molar volumes are independent of concentration. When a volume change of mixing occurs, a volume change will also occur during diffusion. A bulk flow term must then be included to relate the volume fixed frame to the experimentally fixed frame. This bulk velocity is considered in Kirkwood et. al.[16] but will not be considered further in this report.

In systems where the partial molar volumes are nearly equal, the number-fixed frame is a good approximation to the volume-fixed

one. Because of great simplicity, without significant loss in generality, the number-fixed frame will be considered in the balance of this section.

In the absence of fundamental coupling, starting from a diagonal matrix in the Kirkendall frame, the phenomenological scheme can be expressed as a symmetric matrix in the number-fixed frame following Kirkaldy.[12] The starting point for a ternary system is the following system of three equations:

$$\begin{bmatrix} J_1 \\ J_2 \\ J_3 \end{bmatrix} = \begin{bmatrix} L_1 & 0 & 0 \\ 0 & L_2 & 0 \\ 0 & 0 & L_3 \end{bmatrix} \begin{bmatrix} \nabla\mu_1 \\ \nabla\mu_2 \\ \nabla\mu_3 \end{bmatrix} \qquad (2.5)$$

This matrix can be transformed to a 3 x 3 matrix in the number-fixed frame which retains one degree of arbitrariness. It is then reduced to a unique 2 x 2 symmetric matrix with the requirement that the fluxes be expressed in terms of the correct thermodynamic forces ($(\nabla\mu_1 - \nabla\mu_3)$ and $(\nabla\mu_2 - \nabla\mu_3)$) for the number-fixed frame.

In this manner, the elements of the symmetric matrix are found to be:

$$\begin{aligned} (L_{11})_N &= L_1 (1 - 2N_1) + N_1^2 \sum_{i=1}^{3} L_i \\ (L_{12})_N &= (L_{21})_N = -N_1 L_2 - N_1 L_2 + N_1 N_2 \sum_{i=1}^{3} L_i \\ (L_{22})_N &= L_2 (1 - 2n_2) + N_2^2 \sum_{i=1}^{3} L_i \end{aligned} \qquad (2.6)$$

where N_1, N_2 are the mole fractions of components 1 and 2 respectively,

and $(L_{11})_N$, $(L_{12})_N$, etc. are now expressed in the number-fixed frame of reference.

Several points should be emphasized. The cross terms in the number-fixed frame are non-zero. We have assumed the fundamental coupling to be zero in this derivation, and so cross term coupling has arisen strictly from the choice of reference frame. The sign and magnitude of this coupling will be a direct result of the reference frame chosen. It is the existence of this reference frame coupling which is conventionally used to explain the marker movement in the Kirkendall and Smigilskas experiment. Note that the presence of N_i in all of the reference frame "correction terms" implies that the coupling effect will be very small in dilute solutions.

Finally, recall that the mobility matrix in the lattice-fixed frame was assumed diagonal. Thus, the Onsager Reciprocity Relations (O.R.R.) are satisfied in any transformation from this lattice-fixed frame. The number-fixed mobility matrix is symmetric as an immediate consequence of the mathematical transformation of a matrix previously assumed to be symmetric, and only indirectly as a result of O.R.R.

2.3 THE STRUCTURE OF SILICATE MELTS

Slags are generally considered to be ionic in character. Although the principles of transport are similar to those in metals, due consideration must also be given to the effect of charge in the system. Bulk flow is a macroscopic process and as such, the influence of charge will not be significant. Diffusion, however, is a microscopic process. Consequently, the charges on the atoms or

molecules in the system must have a profound effect on the progress of diffusion. At this stage, our primary interest is the examination of reaction kinetics of the iron and steel making process. The slags involved are based primarily on oxygen, with silicon normally being present in significant amounts.

The model of the vitreous silica structure as a random three-dimensional network of SiO_4 tetrahedra is a basis for nearly all theories of silicate structure but usually, only the qualitative effect of metal oxides in modifying the silica structure is considered. Only brief comments on some theories will be offered because none appears to be sufficiently detailed or quantitative to elucidate the mechanisms of the process of diffusion.

Theories of silicate structures can be divided into two broad groups. A short summary of the first group, including the random network model and the various modifications of the discrete polyanion model can be found in Bockris and Reddy.[17] These approaches consider the breaking of silica networks or discrete polyanions with network modifiers (eg. Na, K, Ca, Fe, etc.) to form smaller chains or rings. The presence of O^{2-} anions is not considered at compositions below 66 mole % metal oxide. These models postulate the existance of discrete, stable anion complexes whose concentrations depend on metal oxide concentration. The diffusing anion species is specified as a function of those concentrations.

However, the popularity of these models has declined in favor of a polymerisation theory approach advanced by Masson.[18] From simple tetrahedral SiO_4^{4-} monomers, branched polyanion chains are

formed through polymerisation reactions which produce free O^{2-} anions, eg.:

$$SiO_4^{4-} + SiO_4^{4-} = Si_2O_7^{6-} + O^{2-}$$

Equilibrium constants involving O^{2-} can be written for this and higher order polymerisation reactions. With certain assumptions, one can generate polyanion fractions as a function of mole fraction SiO_2. Thus, one has equilibrium probability distributions of anion chain and ring sizes as functions of the molar concentration of metal oxide.

Unfortunately, this model yields little or no information about kinetic phenomena - in particular, about the nature of the diffusing anion species. However, it seems clear that at least one of the diffusing anions should be free O^{2-}. This appears to be substantiated in work by Schwerdtfeger[19] which indicates substantially different tracer diffusivities for Si and O in calcium silicate melts in the range .48 to .64 mole fraction SiO_2.

2.4 THE ELECTROCHEMICAL DIFFUSION POTENTIAL AND THE CHARGE BALANCE

The effect of charge on a system has conventionally been described by defining an effective chemical potential known as an electrochemical potential for an ion. The electrochemical potential is taken to be the sum of the standard chemical potential and a field term (i.e., $\mu_i + Z_iF\phi$). The driving force for ionic diffusion then becomes the electrochemical potential gradient $\nabla(\mu_i + Z_iF\phi)$. Kirkaldy[20] has recently discussed the nature of this diffusion potential. He demonstrates that in the absence of an external electrical field, the field term in the electrochemical potential gradient is due entirely to diffusion-induced dipoles.

The diffusion-induced field is not supposed to be experimentally accessible. It is normally eliminated from the phenomenological equations by introducing the constraint of no net flux of real charge (i.e., $\Sigma Z_iJ_i = I = 0$). Conventionally, this is justified on the basis of physical plausibility or a comparison of the magnitudes of driving forces due to chemical potential driving force and the field resulting from real charge separation. However, Kirkaldy[20]

also demonstrated that the zero current constraint represents a quasi-steady state of minumum entropy production. This constraint is shown to be applicable when the relaxation time for the neutralization of real charge is short in comparison with the relaxation time for the chemical potentials of the neutral components in the system (i.e., a form of the quasi-steady state approximation).

2.5 THE PHENOMENOLOGICAL BASIS FOR IONIC DIFFUSION

The phenomenological approach to ionic diffusion is analogous to that for metallic diffusion. One can write the flux equations for the ions as a function of the electrochemical potential and eliminate the linear dependencies due to the reference frame choice

$$\sum_{i=1}^{n} \alpha_i J_i = 0 \qquad (2.3)$$

and the charge balance

$$\sum_{i=1}^{n} z_i J_i = 0. \qquad (2.7)$$

It is interesting to note the mathematical similarity of these two summations. In Section 2.2, it was shown that the reference frame choice gave rise to non-zero off-diagonal elements and was termed reference frame coupling. The similarity of the above equations leads to the expectation that the summation $\sum_{i=1}^{n} z_i J_i = 0$ also generates a coupling effect. The development of this coupling wil be demonstrated in the following, when three recent ionic diffusion theories are reviewed. The coupling will be referred to as charge balance coupling.

Three basic origins of kinetic coupling have been identified:

(1) fundamental coupling,

(2) reference frame coupling,

(3) charge balance coupling.

Although all three theories for ionic diffusion start from a common basis, they differ in their assumptions regarding the relative importance of these three kinetic coupling effects. It is generally conceded that reference frame coupling is large in comparison with fundamental coupling in metals. Assumptions of a similar nature may or may not be valid in ionic systems. On one aspect all agree: the paramount importance of charge balance coupling.

Cooper[21, 22] extends the theory for multicomponent metallic diffusion to ionic systems by introducing a local electrical field through the electrochemical potential gradient. He postulates the existance of a bulk relaxation velocity and assumes other coupling mechanisms to be negligible. That is, he proposed to ignore fundamental coupling, but include reference frame coupling effects.

In the development, he approximates $\tilde{v}_{cations} = 0$ by reasoning that the volume of ionic materials is largely determined by the anions, with the cations occupying interstitial sites. Thus, he has chosen the anion fixed lattice as a good approximation for the laboratory frame.

In order to relate the experimentally measurable chemical potential of neutral components to the ionic chemical potentials, Cooper adopts the convention

$$\nabla\mu_{CO} = |z_C|\ \nabla\mu_O + |z_O|\ \nabla\mu_C \qquad (2.8)$$

To eliminate the degree of arbitrariness involved in splitting the chemical potential gradients, Cooper has chosen $\nabla\mu_o = 0$. The zero net current flux constraint is then imposed on the system to generate charge balance coupling terms by eliminating the electric field.

By neglecting physical coupling, Cooper can write

$$\begin{aligned} j_1 &= -L_i(\nabla\mu_1 + Z_1F\nabla\phi) + N_1V \\ j_2 &= -L_2(\nabla\mu_2 + Z_2F\nabla\phi) + N_2V \\ j_3 &= -L_3(\nabla\mu_3 + Z_3F\nabla\phi) + N_3V \\ j_4 &= -L_4(\nabla\mu_4 + Z_4F\nabla\phi) + N_4V \end{aligned} \tag{2.9}$$

where j_1, j_2, j_3 represent cation fluxes, and j_4 is the common anion flux. V is the velocity of the reference frame relative to the Kirdendall frame.

The system of equations is subject to the constraints

$$\sum_{i=1}^{4} Z_i j_i = 0 \quad \text{charge balance} \tag{2.10}$$

and

$$\sum_{i=1}^{4} \bar{\nu}_i j_i = 0 \quad \text{volume fixed reference frame.} \tag{2.11}$$

If $\bar{\nu}_i = 0$ for the cations, $\bar{\nu}_4 j_4 = 0$, that is $j_4 = 0$. The solution for $j_4 = 0$ is

$$V = \frac{L_4}{N_4}(\nabla\mu_4 + Z_4F\nabla\phi). \tag{2.12}$$

The charge balance is then applied to

$$j_1 = -L_i(\nabla\mu_{14} + Z_i F\nabla\phi) + \frac{L_4}{N_4} Z_4 F\nabla\phi, \tag{2.13}$$

with $\nabla\mu_{14} = |Z_4|\mu_i$ since it is assumed that $\nabla\mu_4 = 0$. Cooper obtains an equation of the form

$$J_i = -\frac{N_{i4}}{RT}\left\{\sum_{k=1}^{3}(\delta_{ik} + N_{k4}Z_k\psi_{i4})D_k\nabla\mu_{k4}\right\}, \tag{2.14}$$

where $$\psi_{i4} = \frac{(D_4Z_4 - D_iZ_i)}{\sum_{k=1}^{3}(D_kZ_k - D_4Z_4)Z_kN_{k4}} .$$

The system is now uniquely defined by two fluxes, J_1 and J_2, with J_3 being determined by the charge balance. The equation is correct in form, although minor algebraic errors involving N_{k4} and Z_k exist. The cross terms are clearly of the form

$$L_{ik} = \frac{1}{RT}(N_{i4}N_{k4}Z_k\psi_{i4}D_k) . \tag{2.15}$$

The expression for J_i as written still contains a linear dependence of forces due to the Gibbs-Duhem relation. Cooper then writes the flux equations in the form

$$J_1 = \tilde{D}_{11}\nabla C_{14} + \tilde{D}_{12}\nabla C_{24}$$
$$J_2 = \tilde{D}_{21}\nabla C_{14} + \tilde{D}_{22}\nabla C_{24} \tag{2.16}$$

and solves for the chemical diffusivities. The solutions are correct in principle and include thermodynamic nonideality although minor algebraic errors exist, apparently due to the incorrect application

of the Gibbs-Duhem relation.

Several important features should be noted. The starting point is a 4 x 4 diagonal matrix (i.e., 4 component system). With the application of two constraints on the fluxes (reference frame and charge balance) and two constraints on the forces (molecular chemical potentials and Gibbs-Duhem), a 2 x 2 matrix of independent fluxes and concentration gradients is obtained. The magnitude of the cross terms is significant, indicating a major coupling effect due to the charge balance constraint.

Experimental work was carried out by Varshneya and Cooper for the K_2O-SrO-SiO_2 system. The work clearly demonstrated reversals in concentration during diffusion. It was shown that the phenomenological theory was qualitatively adequate to describe the observations.

The starting point for the development due to Okongwu[23, 24, 25] is the familiar linear flux-force phenomenological equation

$$J_i = -\sum_{k=1}^{n} L_{ik}(\nabla\mu_k - Z_k FE). \qquad (2.17)$$

With Lane and Kirkaldy[12] and Cooper,[21] Okongwu assumes fundamental coupling to be negligible and writes

$$J_i = -L_i(\nabla\mu_i - Z_i FE) + C_i V \qquad (2.18)$$

where V is the velocity as defined previously. Whereas, Cooper chooses

$$V = \frac{L_4}{N_4}(\nabla\mu_4 + Z\ FE), \qquad (2.12)$$

the anion fixed lattice, Okongwu assumes $V \simeq 0$, taking the Kirkendall frame as a good approximation of the laboratory frame. That is, he

has also assumed reference frame coupling to be negligible.

For an ideal solution with $E = -\frac{\partial \phi}{\partial x}$ and the Einstein approximation $L_i = D_i C_i / RT$, Okongwu determines the assumptions to reduce the equations to the Nernst-Planck relation

$$J_i = -D_i^* \left[\frac{\partial C_i}{\partial x} + \frac{Z_i F C_i}{RT} \frac{\partial \phi}{\partial x} \right] . \qquad (2.19)$$

This equation is then used as the basis of subsequent analysis.

In an approach similar to that of Cooper, the charge balance constraint is used to eliminate the electrical field from the equations. However, it is important to recognize a significant difference between the two approaches. Okongwu carried out work in the K_2O-CaO-SiO_2 glass system which is experimentally similar to the K_2O-SrO-SiO_2 system of Cooper. Cooper assumed that each element constituted a separate ionic species in the glass, thus considering a system with three cations and one anion. This approach is consistent with the polymerization model of Masson. Okongwu has apparently based his approach on the discrete polyanion model. Consequently, he does not consider the existence of free O^{2-} in the system and binds all of the silicon in an anion complex. The immediate consequence of this approach is the complete loss of one cation in the system. Therefore, the system consists of two cations and one anion complex or distribution of complexes. Whereas the Cooper approach generates a molecular ternary system, the Okongwu formalism must be considered as a molecular binary system. This leads to two problems: firstly, the tracer diffusivity of an anion complex cannot be determined experimentally. Furthermore, although Okongwu does not consider

the linear dependence of the fluxes due to the reference frame, or the linear dependence of forces due to the Gibbs-Duhem relation, (or alternately $\Sigma \frac{\partial C_i}{\partial x} = 0$ for condensed phases), the implications are clear. The molecular binary system (i.e., 2 x 2) will reduce with independent fluxes and forces to a 1 x 1 matrix (i.e., a scaler) which is not capable of exhibiting coupling. Although the theory is employed fairly successfully in interpreting experiments by curve-fitting to find the tracer diffusivity for the anion complex, it is not formally correct.

In the most comprehensive analysis of ionic diffusion to date, Goto[26] examines the phonomenological basis of diffusion and then applies it quantitatively to the CaO-SiO_2-Al_2O_3 system.

Starting from the linear flux-force phenomenological relation of irreversible thermodynamics, i.e.,

$$j_i = - \sum_{k=1}^{n} L_{ik} \nabla \eta_k, \qquad \text{with } \nabla \eta_k = \nabla \mu_i + z_1 F \nabla \phi, \tag{2.20}$$

Goto writes the equation in the number fixed frame ($\sum_{i=1}^{n} j_i = 0$).

Unlike the previous work on ionic and metallic diffusion, Goto makes no initial assumptions about the magnitude of the cross terms in the mobility matrix. Thus, by implication, it is his intention to include, if possible, any fundamental coupling effects in the formalism. This requires additional experimental information beyond tracer diffusivity data. Consequently, Goto introduces conductivity and transference number information.

In principle, the approach is sound theoretically but there is

some confusion regarding the choice of reference frame. Some of it has been removed,[27] but there are still implicit and explicit approximations which have the effect of assuming reference frame coupling to be negligible.

The main approximation centres around the use of mixed reference frames in the mobility matrix. Goto derives the Einstein approximation ($D_i^* = L_{ii}RT/C_i$) to relate mobilities and tracer diffusivities. The derivation is carried out under experimental conditions (i.e., the classic tracer diffusion experiment), in which all reference frames coincide. However, the relation is only applicable in general for the Kirkendall (lattice fixed) frame.

One of the assumptions in this derivation is that fundamental coupling is neglected. If fundamental coupling is not neglected, one obtains the following interesting relation:

$$D_i^* = \left(L_{i^*i^*} - \frac{C_{i^*}}{C_i} L_{i^*i}\right) \frac{RT}{C_{i^*}} \quad . \tag{2.21}$$

The diagonal elements in the mobility matrix are expressed in the Kirkendall frame. By comparison, the off-diagonal elements are calculated from conductivity and transference data and are consequently expressed in the experimental frame (which has been approximated as the number fixed frame). These experimental values will include all three forms of coupling: fundamental, reference frame, and charge balance. The situation is depicted schematically in Figure 2.1.

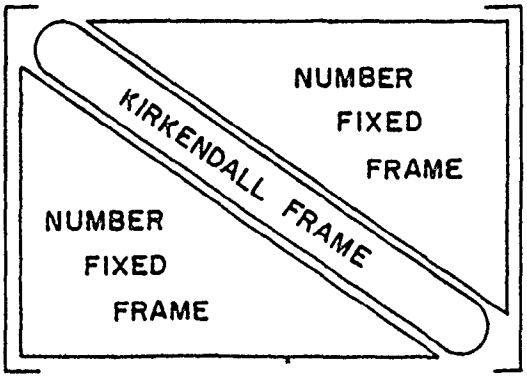

Figure 2.1: Mixed Reference Frames

Finally, the similarities and differences with respect to assumptions in the three approaches are summarized as followed:

	Fundamental	Coupling Effect Reference Frame	Charge Balance
Cooper	Negligible	Important	Important
Okongwu	Negligible	Negligible	Important
Goto	Important	Negligible	Important

Each approach has advantages and disadvantages in terms of simplicity and completeness. One must resort to experiment to determine the overall merits of each.

2.6 QUANTITATIVE APPLICATION OF THE THEORIES FOR IONIC DIFFUSION

The experimental and analytical work of Okongwu, Cooper and Varshneya has been referred to briefly and will not be discussed further. The recent and very impressive work by Goto, Nagata, and Sugawara[28] will be reviewed.

Inter-diffusivity matrices were determined for 52 diffusion runs in the $CaO-Al_2O_3-SiO_2$ (ironmaking type) system in the temperature range 1450°C to 1550°C and compared with the theoretical predictions.

Goto recognizes that the melt will generally contain many ionic species and complexes of the form Ca^{2+}, O^{2-}, AlO_2^{4-}, $Al_2O_5^{4-}$, SiO_4^{4-}, $Si_2O_7^{6-}$, etc. However, he assumes that diffusion in ionic melts can be strictly expressed by fluxes of the elementary ions, provided local equilibrium prevails in the melt. That is, he considers diffusion equations based on fluxes of Ca^{2+}, Al^{3+}, Si^{4+} and O^{2-}. In effect, he is assuming that to a good approximation all of the required physical information on mechanism and ion complexing is supplied to the system by the tracer diffusivities, etc. measured under experimentally similar conditions. A comparison of theoretical and actual penetration curves (Figure 2.2) shows good agreement, and clearly indicates the ability of the theory to predict the experimentally observed concentration reversal of Al_2O_3.

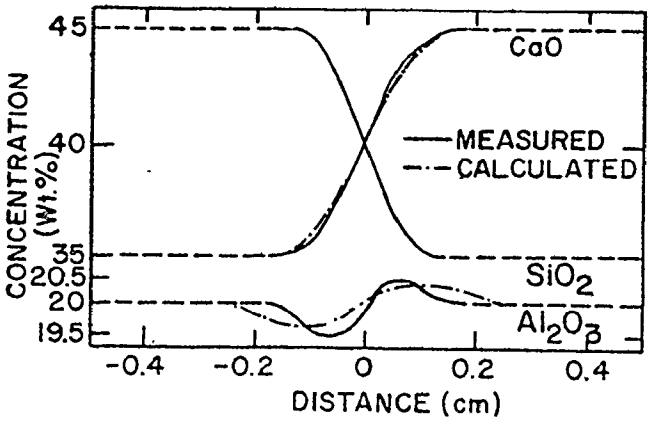

Figure 2.2: Sugawara, Nagata, and Goto[28] - Comparison of Calculated and Measured Penetration Curves

In analysing the three approaches, the question of the relative importance of reference frame coupling is reasonably straightforward, although it will vary somewhat depending on the system and choice of reference frame. Generally speaking, it will not be as strong as the coupling effect attributed to charge balance. As in non-ionic diffusion, however, one must rely on experiment in order to estimate the importance of fundamental coupling.

No concentration gradients exist under the experimental conditions in which tracer diffusivities and high frequency conductivity are measured, so all reference frames coincide under these conditions. Since fundamental coupling is assumed to be negligible during the derivation of the Nernst-Planck equation, a comparison of actual conductivities with those predicted by the Nernst-Planck equation will serve as a direct experimental check on the relative importance of fundamental coupling. Such a comparison is possible when all tracer diffusivities and the conductivity are known for a single system. At least two such investigations have been carried out. Schwerdtfeger and Keller[19] have examined the CaO-SiO_2 system at 1500°C while Schmalzried and Langanke[29] have examined the PbO-SiO_2 system at 850°C. In both cases, the experimentally observed conductivities were significantly lower than those predicted, with the mobility of either one or two of the three ions being able to account fully for the experimental conductivities.

One could conclude that the so-called fundamental coupling is significant under these circumstances. However, this is in direct contradiction with the results from metallic diffusion studies in

which fundamental coupling was found to be negligible. We recall from 2.2 that in order to justify a diagonal matrix in the Kirkendall frame, it was necessary to assume that correlated motion of atomic groups in the vicinity of a vacancy is negligible and that sufficient vacancy sources and sinks existed to preserve the local equilibrium of vacancies. In liquid systems, the situation somewhat simpler (i.e. a convective term is used) but the basic concept the same. In effect it was assumed that in terms of motion, the atoms interact with vacancies alone. That is, the vacancies serve as a mask to screen the motion of one atom from the others, permitting uncorrelated or uncoupled motion.

In an ionic system, the coulombic forces are of much longer range than those in a metallic system. Under such conditions, it is possible that the motions of the ions are not effectively screened from each other, leading to a form of fundamental coupling. A similar situation exists in aqueous solutions. In this case, an empirical law relating conductivity to electrolyte concentration due to Kohlrausch[17] is explained in terms of mobile ionic clouds or atmospheres surrounding the charged particles. Although this aqueous solution approach, based ultimately on the Debye-Hückel model, differs somewhat from the phenomenological diffusion framework, the fundamental basis in the long range coulombic forces is common to both.

In view of the apparent importance of fundamental coupling in ionic diffusion, one would tend to favour the approach due to Goto, over those of Cooper and Okongwu. The implications are not insigni-

ficant. It is not possible to describe fully such a diffusing system in terms of tracer diffusivities alone, as is the case for metallic diffusion. Additional information in the form of transport numbers and conductivity is required.

It is generally agreed (section 2.3) that equilibrium structures in silicon based slags contain silicate polymers of varying complexity. However, the phenomenological theories assume that the motion of simple ions is important and they normally ignore the existence of such silicate complexes. This need not necessarily lead to a contradictory situation since the equilibrium species may not be the effective mobile species. Takada[30] has shown theoretically that the rates of the so called exchange reactions (primarily of Si-O bonds) are important. If such reactions are slow, then the effective diffusing species is the silicate since it has a relatively long lifetime. If, however, the exchange reactions are very fast, then the movements of silicon, oxygen, and aluminum ions, etc. become more or less independent. The net result is a predominance of the simple ions as the effective mobile species. A preliminary analysis of Takada's transport data in the $PbO-SiO_2$ system indicates the latter to be true. That is, it may be reasonable to neglect the existence of complex ions in diffusion theories for slags.

Finally, a comment on the symmetry of the mobility matrix is in order since it is frequently a cause for some confusion. It has been shown that, for systems in which physical coupling is negligible, it is always possible to express the fluxes in terms of a symmetric mobility matrix and a proper choice of forces. For a metallic system,

the proper force is simply

$$X_i = \nabla\mu_i - \frac{\alpha_i}{\alpha}\nabla\mu_n, \qquad (2.22)$$

and aesthetic considerations may justify the additional complexity introduced in generating a symmetric matrix. However, it can be shown that the "proper" force for symmetry in an ionic formalism is of the form

$$X_i = \nabla\mu_1 - \frac{\alpha}{\alpha_n}\nabla\mu_n - \frac{Z_1 - \frac{\alpha_i}{\alpha_n}Z_n}{Z_{n-1} - \frac{\alpha_{n-1}}{\alpha_n}Z_n}\left(\nabla\mu_{n-1} - \frac{\alpha_{n-1}}{\alpha_n}\nabla\mu_n\right). \qquad (2.23)$$

In this case, the complexities are such that efforts to maintain the symmetry of the matrix would not seem justified. However, one must recognize that even if one does not maintain the symmetry of the cross terms, they are related; there still exist only $\frac{1}{2}(n-1)(n-2)$ independent coefficients.

2.7 ELECTRONIC CONDUCTION

Up to this point, it has been assumed that electronic conduction in the ionic system is negligible. Such an assumption is reasonable for stoichiometric compounds, such as CaO, SiO_2, Al_2O_3, Na_2O, etc. and thereby seems applicable to blast furnace type slags.

However, when multivalent transition metal cations such as iron are considered, the validity of the assumption is not so certain. The nonstoichiometry of the iron oxides introduces significant numbers of electronic defects to the system which are then free to act

in maintaining the charge balance. Under these circumstances, the assumption that $I_{ionic} = 0$ may not be reasonable and the equation $I_{ionic} + I_{electronic} = 0$ should be considered. This approach is commonly used in the theories for the formation of semiconducting oxides from transition metals.

From the preceding argument, it is clear that metallic and ionic diffusion should properly be regarded as limiting cases in a unified theory of diffusion. Metallic diffusion can be viewed as the diffusion of positive ions in a system where the full burden for charge balance rests with the highly mobile electrons. Consequently, atomic diffusion is not influenced by the charge balance consideration.

As the other limiting case, pure ionic diffusion can be visualized as a system with no electronic mobility. In this case, the full burden for charge balance rests with the ions. As a result, the charge balance has a profound effect on the diffusion of the ions.

The intermediate cases should be considered as part of a continuum in which the burden for maintaining charge balance progressively shifts from the electronic to the ionic component in the system. Concurrent with this shift is an increased atomic coupling due to charge balance. A metallic system with n atomic species could, when electrons are considered, be considered as an n + 1 component system. When the two constraints are applied to the fluxes and the forces, and independent (n-1)x(n-1) mobility matrix is obtained. In the absence of electronic mobility (i.e., pure ionic), an independent (n-2)x(n-2) mobility matrix is obtained.

The general framework seems suitable for a unified approach to diffusion. The implications are interesting. It suggests that ionic coupling in a steelmaking type slag (high Fe) may be much less than that in a blast furnace type slag. It is possible that some slag/metal systems exist in which charge balance coupling is negligible.

2.8 SUMMARY

The development of ionic diffusion theory parallels closely that of metallic diffusion. Phenomenological theories were introduced which relate experimentally measurable tracer diffusivities in multicomponent systems to interdiffusion coefficients in the presence of concentration gradients. The role of electronic mobility in ionic diffusion was discussed, and the framework laid down for a unified approach to ionic and metallic diffusion.

It has been shown that the principle bases of ionic and non-ionic diffusion theories have been demonstrated experimentally.

CHAPTER 3: KINETICS AT THE Fe/CaF_2 INTERFACE

ELECTROCHEMICAL APPROACH

3.1 INTRODUCTION

A coupling theory equivalent to that for ionic diffusion has been developed for interfacial charge transfer reactions by W-K. Lu,[31] and will be elaborated on in Section 4.2. The formalism requires knowledge of the fundamental reaction rate constant, a phenomenological coefficient whose analogue in diffusion theory is the tracer diffusivity. Wagner[32] has suggested that the interfacial reactions may be considered in terms of anodic and cathodic reactions for which the Butler-Volmer equation may be applicable. Thus, one method of evaluating these rate constant coefficients is the electrochemically determined ion exchange current density.

A double pulse constant current technique was employed to determine the exchange current density at 1450°C for the reaction $Fe \rightarrow Fe^{2+}+2e^{-}$ using a solid iron electrode and a liquid CaF_2 electrolyte.

3.2 THEORY

3.2.1 Electrochemical Kinetics

Following Vetter,[33] the kinetics of metal/ion electrodic reactions may be approached by considering individually the rate of the forward reaction $Fe \rightarrow Fe^{2+}+2e^{-}$ and the back reaction $Fe^{2+}+ 2e \rightarrow Fe$. The temperature dependence of the rate is related to the activation energy of the formation of the intermediate complex between the Fe

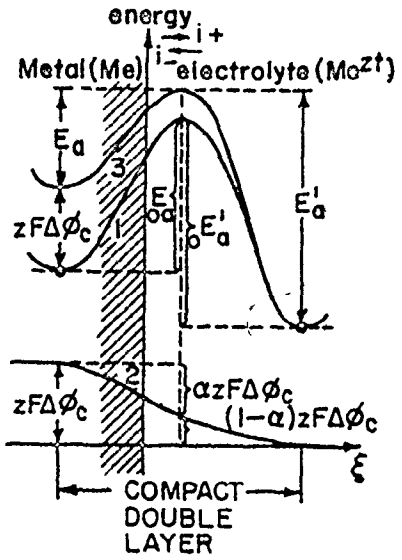

Figure 3.1: Electrochemical Model of Potential vs Reaction Coordinate

and Fe^{2+} states. Consider first, a plot of "chemical" energy* vs reaction coordinate (curve 1, Figure 3.1) indicating activation energies for the forward and reverse reactions ${}_oE_a$ and ${}_oE_a'$. A possible electrical energy vs reaction coordinate is presented in Figure 3.1 (curve 2). The additivity of these energies implies that the effective activation energies will be dependent on the potential curve (curve 3). As indicated in Figure 3.1, the transfer coefficient $0<\alpha<1$ is introduced as a parameter for the shifting of the position of the maximum energy barrier with respect to the reaction coordinates. The derivation carries the implicit assumption that α is independent of the field, although, at present, insufficient experimental and

---

*The electrochemical potential may be defined as $\eta = \mu + ZF\phi$. Any splitting of electrochemical energy into chemical and electrical components, although of conceptual and practical interest, is essentially arbitrary in nature.(34)

theoretical evidence exists to support it.

With this reservation, the approximate field dependence of activation energy may be written

$$E_a' = {}_oE_a' + \alpha ZF\Delta\phi,$$
$$E_a = {}_oE_a - (1 - \alpha)\ ZF\Delta\phi. \tag{3.1}$$

From absolute rate theory, the forward reaction may be taken as proportional to the interfacial reactant concentration C and the Boltzman factor $\exp(-E_a/RT)$. Thus:

$$i = ZFk_o\ C \exp\ (-E_a/RT) = ZFk_o \exp\ \{-({}_oE_a - (1-\alpha)ZF\Delta\phi)/RT\}. \tag{3.2}$$

Similarly for the back reaction:

$$i' = ZFk_o'C' \exp\ (-E_a'/RT) = ZFk_o'C' \exp\ \{-({}_oE_a' + \alpha ZF\Delta\phi)/RT\}. \tag{3.3}$$

The net Faradaic current $i_F = i' - i$ may be written:

$$i_F = ZFk_o'C' \exp\ \{-({}_oE_a' + \alpha ZF\Delta\phi)/RT\}$$
$$- ZFk_oC \exp\ \{-({}_oE_a - (1-\alpha)ZF\Delta\phi)/RT\}. \tag{3.4}$$

At equilibrium, with the potential difference $\Delta\phi_{eq}$ defined such that $i_F = 0$, the relationship $i = i' = i_o$ holds, where i_o denotes the exchange current density. The equation for the net current may be rewritten in terms of the exchange current density with the introduction of a charge transfer overpotential $\eta_t = \Delta\phi - \Delta\phi_{eq}$. Thus:

$$i_F = i_o \left\{ \exp\ \left(-\frac{\alpha ZF}{RT}\ \eta_t\right) - \exp\ \left(\frac{(1-\alpha)ZF}{RT}\ \eta_t\right) \right\}, \tag{3.5a}$$

with $i_o = ZFk'_oC' \exp\{-({}_oE'_a + \alpha ZF\Delta\phi_{eq})/RT\}$

$$= ZFk_oC \exp\{-({}_oE_a - (1-\alpha)ZF\Delta\phi_{eq})/RT\}. \qquad (3.5b)$$

For small deviations from the equilibrium potential the exponential terms may be linearized to give

$$i_F = i_o\left\{1 - \frac{\alpha ZF}{RT}\eta_t - 1 + \frac{(1-\alpha)ZF}{RT}\eta_t\right\} = \frac{ZF}{RT} i_o\eta_t \qquad (3.6)$$

which is independent of α. Thus, when η_t, Z and i_F are known in the linear region, i_o may be evaluated. This equation will be used to interpret the experimental data.

At this point, two comments are necessary regarding the limitations of the equations with respect to experimental parameters. It has been indicated that knowledge of the interfacial concentrations is required. If C and C' are independent of the Faradaic current i_F (i.e. pure interfacial reaction control), the interfacial concentrations will be equal to the bulk values. However, transport will generally play a role in the overall process and the interfacial values will generally be unkown. It is convenient to introduce a diffusion overpotential via the Nernst equation

$$\eta_{dif} = \frac{RT}{ZF} \ln \frac{C'C_o}{C'_oC}, \qquad (3.7)$$

where C_o and C'_o are bulk values. This approach was used by Berzins

and Delahay[35] to show

$$i_F = i_o \left\{ \frac{C'}{C'_o} \exp\left(-\frac{\alpha Z F}{RT}\eta\right) - \frac{C}{C_o} \exp\left(\frac{(1-\alpha) n F}{RT}\eta\right) \right\}, \quad (3.8)$$

with $\eta = \eta_t + \eta_{dif}$ which is experimentally accessible. The exchange current density is then that based on the bulk concentrations.

The experimental determination of the Faradaic current i_F is also difficult due to the simultaneous charging of the double layer. Berzins and Delahay[4] have treated the matter for the single pulse galvanostatic case by assuming a constant double layer capacitance (combination of compact and diffuse). Thus

$$i_C = C_D \left(\frac{\partial \eta}{\partial t}\right), \quad (3.9)$$

with i_C the capacitance current, and C_D the double layer capacitance. The experimentally imposed constant current condition implies

$$i_C + i_F = i_t = \text{const.} \quad (3.10)$$

The resulting boundary value problem was solved to give η as a function of time, bulk concentrations, exchange current density, double layer capacity, diffusivities and total current. These equations have proven successful in the interpretation of data for moderately fast (i.e. $i_o \approx 50 ma/cm^2$) interfacial reactions. However, for very fast reactions, the experimental error in separating contributions due to double layer charging, charge transfer overpotential, and diffusion overpotential is significant. One solution to this problem is the double pulse galvanostatic method, developed by Gerischer and Krause,[36] and treated theoretically by Matsuda et. al.[37]

3.2.2 The Double Pulse Galvanostatic Method

The principal limitation of the single pulse method in the study of very fast electrode processes is the large non-Faradaic current in the brief period before a significant diffusion overpotential develops.

The quantity of interest, the charge transfer overpotential, is squeezed by the short term charging and the longer term diffusion effects so as to make accurate determination difficult. This difficulty is significantly reduced by the double pulse technique developed by Gerischer and Krause.[36] Two constant current pulses are applied successively to the electrode. The first pulse of relatively large current density i_1 is of short duration ($t_1 \approx 1\ \mu sec$). It is intended to charge the electrical double layer to an overpotential which corresponds to the current density of the second pulse (i_2). Typical current vs time and potential vs time curves are shown in Figure 3.2.

By the proper choice of the current ratio i_1/i_2 and t_1, this desired charging of the double layer may be achieved. This implies that at t_1 the capacitance current will be zero, with all of the external current i_2 then being Faradaic. The proper charging corresponds to the mathematical condition $(\partial\eta/\partial t)_{t=t_1} = 0$, which then serves as the experimental criterion (curve 2, Figure 3.3). Curve 1 and cruve 3 indicate under and overcharging respectively of the electrical double layer.

Gerischer and Krause assumed that the effect of the concentration overpotential was negligible at the beginning of the second pulse. With such an assumption, the observed potential at t_1 is

related (when compensated for electrolyte resistance) to the charge transfer overpotential. Thus i_o can be evaluated directly since i_F and η_t are known.

However, Matsuda, et. al.[37] showed that the diffusion overpotential may be significant at t_1 (typically 1 to 2 μsec). They showed that the overpotential would be approximately related to the length of the first pulse in the following way for small t_1:

$$\eta_{t=t_1} = \frac{RTi^2}{ZFi_o} \{1 + wt_1^{\frac{1}{2}} + (1 - \frac{9\pi}{32}) w^2 t_1 + \ldots\}$$

$$\text{with } w = (\frac{4}{3\pi^{\frac{1}{2}}}) (\frac{i_o}{2F}) (\frac{1}{C_o D^{\frac{1}{2}}} + \frac{1}{C_o'(D')^{\frac{1}{2}}}). \qquad (3.11)$$

On the basis of this equation, they suggested that for sufficiently small t_1, $\eta_{t=t_1}$ would be linear with $t_1^{\frac{1}{2}}$. Hence, they proposed an extrapolation of η to $t_1^{\frac{1}{2}} = 0$ to obtain the true i_o.

As reviewed by Yeager,[38] Susbrelles and Delahay[39] also introduced a correction which becomes significant when the "diffusion thickness" $\delta \simeq (\pi Dt)^{\frac{1}{2}}$ is of the same order as the diffuse portion of the electrical double layer. This may be the case for the very short times used in the double pulse method. However, the nature of the double layer in molten salt and slag electrolytes is open to question, particularly in relation to the possible existence of a diffuse double layer. Consequently, this correction will not be considered further.

3.2.3 Polaragraphic Technique for Bulk Concentrations

Since the ion exchange current density is expected to be a function of the bulk concentration, it is necessary to determine C_o'. With the assumption of transport control, a steady state current-

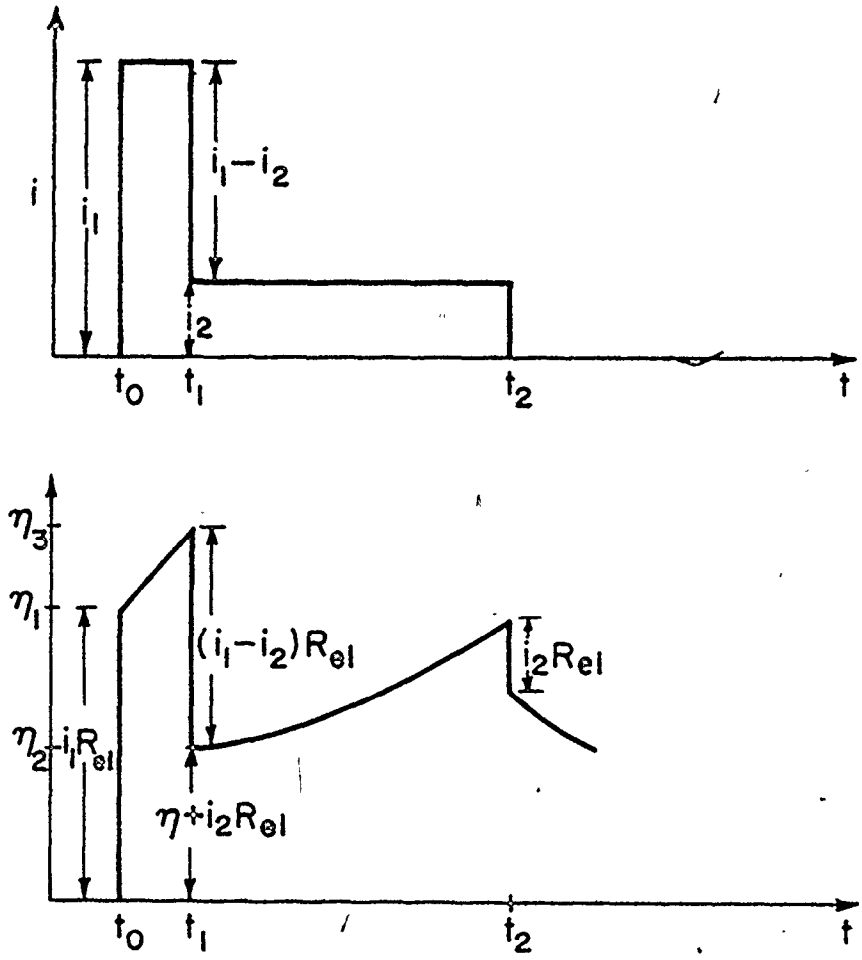

Figure 3.2: Typical Current and Potential vs Time for the Double Pulse Method

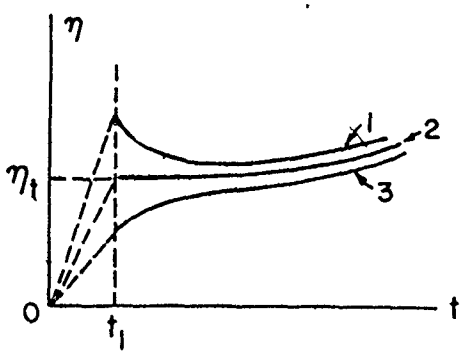

Figure 3.3: The Effects of Over and Under Charging During First Pulse

potential relation may be derived to determine bulk concentrations when it is calibrated for a specified system. The approach has been used recently by Schwerdtfeger, et. al.,[40] and Prange.[41]

The Nernst equation for the diffusion overpotential may be written

$$\eta_{dif} = \frac{RT}{ZF} \ln \frac{C'}{C_o}, \tag{3.12}$$

when the junction potential is negligible and the electrode composition is constant (e.g. pure Fe). The current may be related to the interfacial and bulk concentrations via the mass transfer coefficient K_m, i.e.

$$j = \frac{i}{ZF} = K_m \left[C' - C_o'\right] \tag{3.13}$$

The two equations may be solved to eliminate the interfacial concentration C', giving

$$C_o' = \frac{i}{ZFK_m \left[\exp\ (ZF\eta_{dif}/RT) - 1\right]} . \tag{3.14}$$

The mass transfer coefficient may be determined experimentally for a specific system.

Two further assumptions are required: the valence Z must be known, or at least be constant, and only one reacting species can play a significant role. As will be discussed in the following sections, these assumptions were not always valid in the systems investigated.

3.3 EXPERIMENTAL PROCEDURE

3.3.1 Furnace and Gas System

The furnace employed in this investigation was a Tamann graphite resistance type with an alumina working tube. Because relatively fast heating and cooling rates were possible, the furnace could be loaded cold for each run and taken to operating temperature. The commercial argon used was of 99.999% purity, (see Table 3.1). The gas was further purified by exposure to phosphorous pentoxide for water removal, and to an "Oxysorb" column for O_2 removal. The flow rate was approximately 200 ml/min.

Table 3.1

Argon 5.0 Gas Analysis (Messer Griesheim GMBH)

N_2	2.5 ppm
O_2	1.6 ppm
H_2O	1.2 ppm

with CO, CO_2, H_2 < 0.5 ppm

Hydrogen was occasionally used in small amounts (approximately 3% by volume) and was purified in a similar manner.

3.3.2. Crucible Material and Preparation

The crucibles were manufactured at the Max Planck Institute of electrolytic iron which was vacuum cast and machined to the dimensions indicated in Figure 3.3. It was necessary to deoxidize the crucible prior to use, in order to achieve low iron contents. This was

accomplished by maintaining the crucible in an argon -3% hydrogen mixture at 1450°C for approximately 24 hours.

3.3.3 Calcium Fluoride Preparation

The calcium fluoride employed was Merck Suprapur grade (typical residuals, Table 3.2) It was premelted in an argon -3% hydrogen atmosphere at 1450°C in a previously deoxidized iron crucible. The resulting material was colourless or, in some cases, clear with light hues of pink or green. A milky white colour normally indicated poor preparation (i.e. high iron contents). A "base" CaF_2 slag having approximately 0.2 wt% Fe was prepared by the addition of FeO. This base material was then added in varying amounts to pure calcium fluoride to obtain mixtures of the desired compositions.

Table 3.2

Typical CaF_2 Analysis (MERCK)

Pb < 5×10^{-5}%	Sr < 5×10^{-2}%
Cu < 5×10^{-5}%	Li < 5×10^{-4}%
Ni < 1×10^{-5}%	Na < 1×10^{-3}%
Cd < 5×10^{-5}%	K < 5×10^{-4}%
Mn < 5×10^{-5}%	

3.3.4 Electrode Construction

The basic form of the electrode follows the design of A. D. Graves et. al.[42] as modified by Prange[41] for the Fe-CaF_2 system. It is of coaxial design to minimize effects due to induction. The upper portion of the inner and outer electrodes was constructed of copper in order to eliminate the ferromagnetic effects encountered

at lower temperatures. The copper-iron junctions were screw-pressure fits at a level in the furnace representing about 900°C. The inner electrode (normally the anode) was of 1 mm diameter iron wire. The current pulse imposed on the electrode was supplied to the coaxial electrode externally in order to minimize its effect on the potential measurement. The current flowed between points BC in Figure 3.5 and the potential was read between AC. The outer electrode (normally the cathode) was constructed of iron with an inner diameter of 10 mm and an O.D. of 16 mm. It was not possible to employ a third reference electrode in the system while maintaining the coaxial geometry necessary for the minimization of inductance. However, there was only a very small error involved in taking the cathode as the reference electrode in this system. This is because the current densities at the cathode are far less than those at the anode, since its surface area was some 35 times greater.

3.3.5 Measurement of Electrode Area

In all experiments the electrode was lowered into the electrolyte 5 mm beyond initial contact after allowing for thermal expansion. However, the effective height was generally unkown due to wetting or climbing of the electrolyte. Following Prange[10] several electrodes were destructively tested by anodically dissolving a significant amount of the electrode. The effective heights were then measurable due to the length of the reduced electrode cross section.

3.3.6 Electronic Equipment

The galvanostatic pulses were generated by two Hewlett-Packard

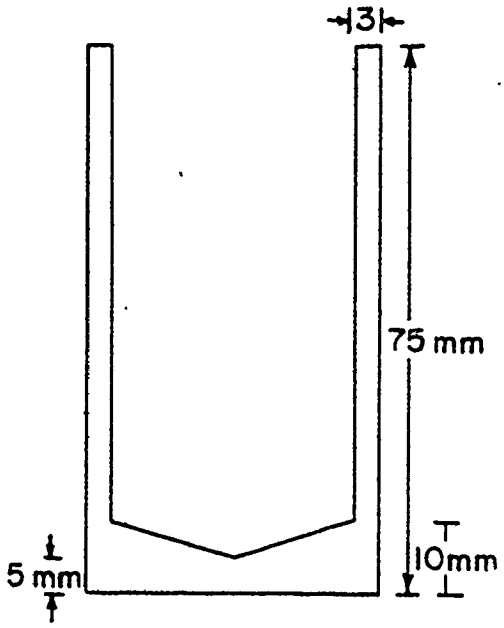

Figure 3.4: Iron Crucible Dimensions

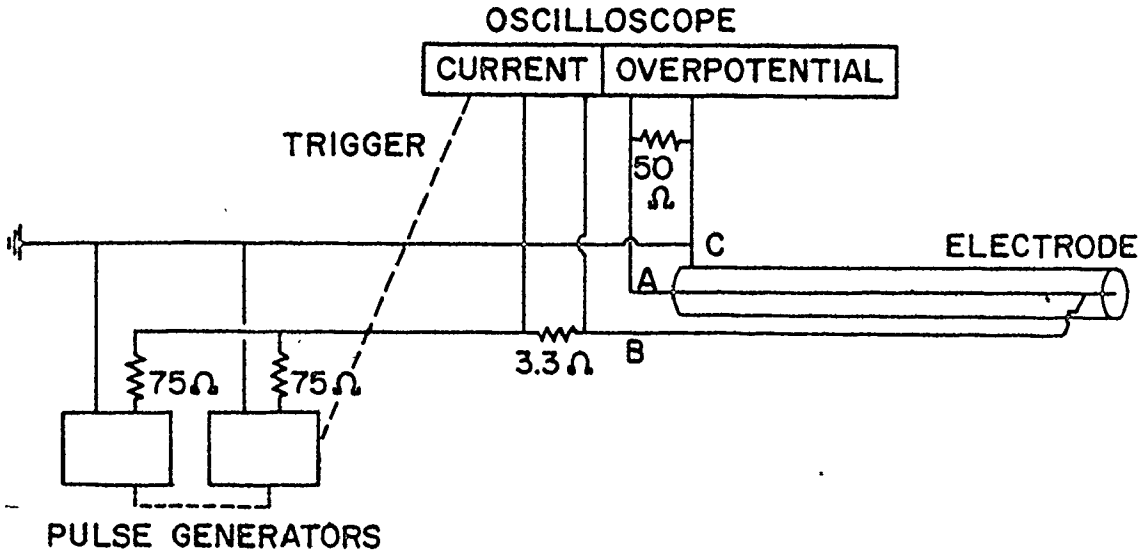

Figure 3.5: Circuit Diagram for the Double Pulse Measurement

model 214A pulse generators with rise times of approximately 20 ηsec. The first generator, when triggered manually, acted as the trigger for the second generator, which in turn triggered a Tektronix 7623 storage oscilloscope capable of single sweep operation (in conjunction with a Tektronix 7A13 differential comparator and 7B50 time base). The circuit diagram is given in Figure 3.5. The 50 Ω parallel resistance was employed to reduce "reflection" in the coaxial cables, and did not significantly affect the current measurements (cell resistance < .2Ω). The total cell current was measured as a potential drop over a 3.3Ω resistance.

3.3.7 Concentration Measurements

Polarographic measurements were made before and after each set of double pulse measurements. Five to ten potential curves for a variety of current densities were recorded on a millivolt chart-recorder in each case to obtain an average value. Current densities were normally in the range .025 to .5 ma/cm^2. The electrode was the same as that used for the double pulse measurements. However, the crucible, rather than the cathode, was taken as the reference for these measurements with the potential being measured between the anode and crucible.

Samples of CaF_2 for chemical analysis of total iron were taken from each run, with analysis being done by either atomic absorption or titration techniques. These concentrations were used in conjunction with the formula developed in Section 3.2.3 to determine a value k_m for use in the polarographic technique.

3.3.8 Double Pulse Measurements

Most of the measurements were made with t_1 in the range .8 to 3 μsec and with i_2 in the range 160-800 ma/cm^2. The higher current densities were necessary at the upper iron concentrations in order to obtain measurably large overpotentials.

The level slope criterion for a proper charging of the double layer requires some comment. In principle, there should be only one point at which the slope of the potential vs time curve tends towards zero at t_1, indicating proper charging. The tail should curve slightly up or down for slight over or under charging. In practice, the criterion can pose a difficult problem requiring subjective judgment. The oscilloscope trace immediatly following t_1, is obscured due to induction, so that judgments regarding zero slope are actually made .2 to .5 μsec after t_1. Furthermore, the curve does not change very quickly from positive to zero to negative slope. Rather, there is a range over which the region of zero slope simply increases in length. The double layer must be significantly overcharged before a trend towards a negative slope is observed thus compounding the problem of subjective error. The difficulty presumably arises due to the inability to observe the trace immediately following t_1.

Due to the considerations above the results could vary significantly (up to 30% in some cases), depending upon the approach to the zero slope (i.e. i_1, t_1, kept constant, adjust i_2, ... etc.). Through trial and error, the following method was chosen as the most accurate and reproducible for the experiments. For a particular set of data,

i_2 was held constant while a series of measurements was taken with t_1 in the range 3 to .8 μsec. For each measurement, t_1 was fixed and i_1 was slowly increased until the slope at t_1 just approached zero. Two to four such "sets" of information were obtained at each iron concentration at various values of i_2. All measurements were made at 1450°C (except for some CaF_2 - 10% CaO experiments -- see Section 3.3.9).

3.3.9 Experiments with CaF_2 - CaO Slags Containing 5% or 10% CaO

The slags were prepared in a consistent manner, with suprapur grade calcined $CaCO_3$ being added to premelted CaF_2. It proved impossible to achieve the very low iron contents in these systems. This is believed to be a result of the oxidation of some iron by the CaO (the size of the miscibility gap in the FeO - CaF_2 system is reduced by CaO). This is indicative of the very low Po_2 required to stabilize the low iron concentrations.

The primary objective of the work was to stabilize the oxygen concentration with respect to variations in iron content. The presence of the CaO also permitted an initial investigation of the effect of temperature. In a pure CaF_2 system, the working temperature range was constrained by the melting points of CaF_2 and iron. This did not permit a sufficiently large temperature span to measure an effect. However, the presence of an eutectic in the CaF_2 - CaO system increased the temperature range of liquid electrolyte, solid electrode to the point that some measurements at several different temperatures were attempted. The interpretation of the results was complicated by the fact that the electrolyte resistance and mass transfer coefficient

were also functions of temperature. This will be discussed in more detail in the next chapter. The temperature was measured with a type K thermocouple which had an unsheathed tip that was immersed to a depth of 5 mm in the CaF_2. It was necessary to make measurements quickly because the thermocouple degraded in the melt.

3.4 RESULTS AND DISCUSSION

3.4.1 Electrode Area

The results obtained for the destructively tested electrodes are summarized in Table 3.3. The areas determined in the CaF_2 - 10% CaO slags were significantly higher indicating a lower slag metal interfacial energy. The average value is taken to be 0.275 cm^2. The current density at the electrolyte gas interface was more sharply defined in the case of CaF_2 - CaO, as is indicated in Figure 3.6. For pure CaF_2, the variation in area is greater than in the case of CaF_2 - 10% CaO, with some indication that it may be dependent on $C_{Fe^{2+}}$.

Table 3.3

Electrodes Areas

Slag Type	$C(Fe^{2+})$ [wt%]	Electrode (cm^2) Area
CaF_2	.016	.168
CaF_2	.025	.193
CaF_2	.211	.209
CaF_2 - 10% CaO	.065	.275
CaF_2 - 10% CaO	.053	.278
CaF_2 - 10% CaO	N.A.	.271

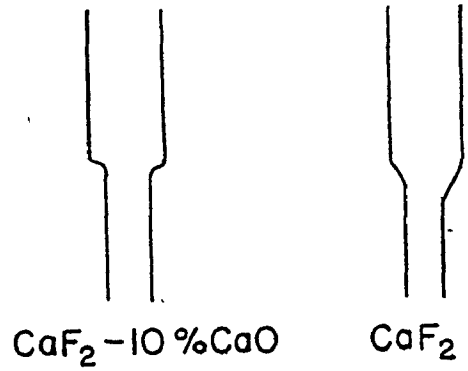

Figure 3.6: Dissolution of the Electode in Area Tests

3.4.2 The Mass Transfer Coefficient

The polarographic data may be treated with Equation (3.14) derived in Section 3.2.3.

The resulting data are summarized in Figure 3.7. The nature of the information and typical calculations for one data set are given in Appendix 1. As with the electrode areas, the apparent mass transfer coefficient may be a function of bulk concentration. However, the coefficient will be treated as constant $K_m = 2.82 \times 10^{-3}$ cm/sec since such a variation will not contribute significantly to the overall error.

In Section 3.2.3 it was noted that the equations are valid when the reaction involving the species of interest is the only one occurring. Under certain circumstances in this study, the assumption was not valid. In some of the early work, an argon 3% hydrogen atmosphere was used during the measurements. The polarographic concentrations

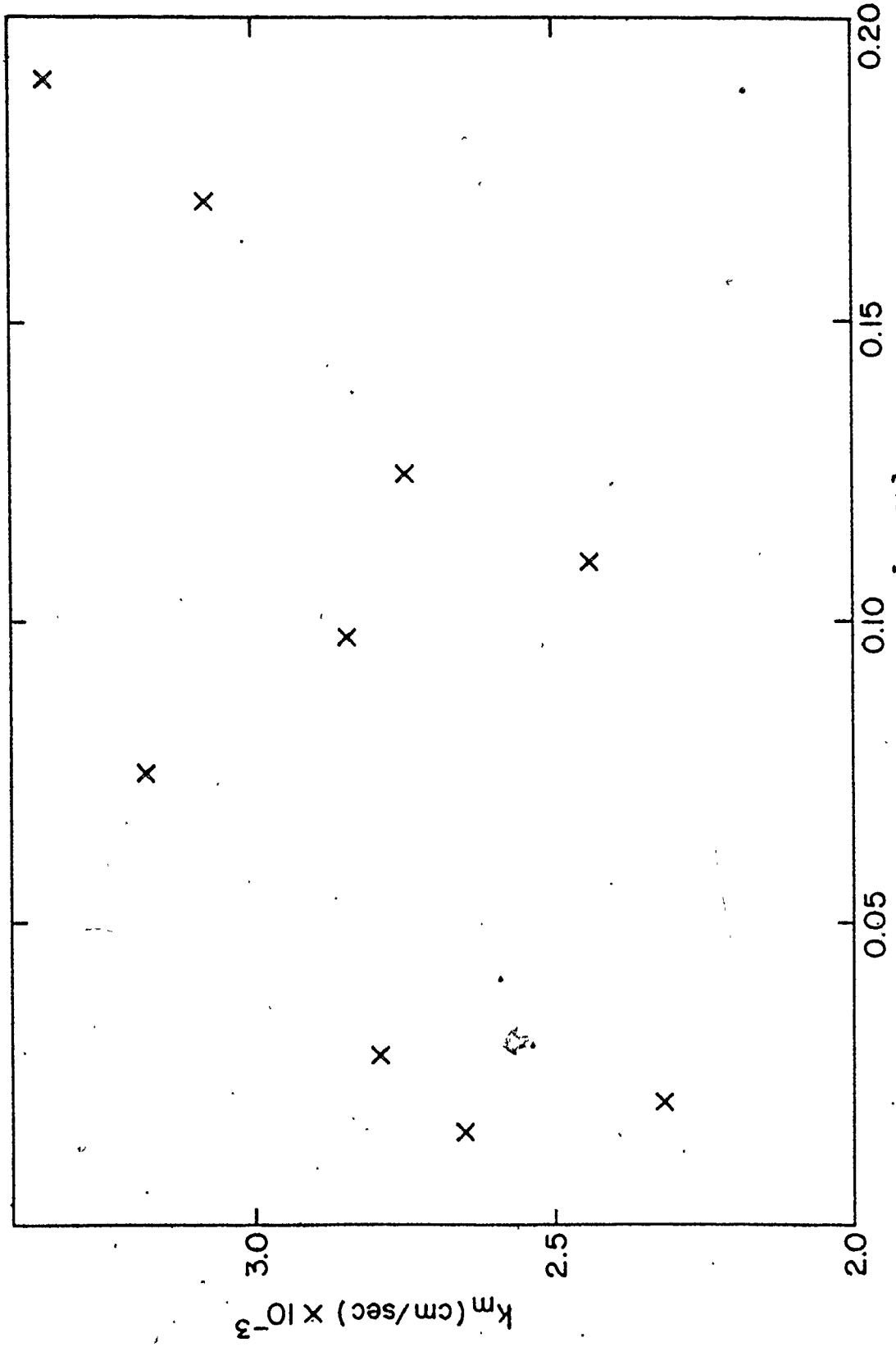

Figure 3.7: Mass Transfer Coefficient vs $C_{Fe^{2+}}$

obtained under these conditions were incorrect. It is believed that in addition to the iron reaction, the hydrogen dissolved in the anode was reacting (i.e. $H \rightarrow H^+ + e^-$) to give an anomalous potential. This conclusion was further substantiated by the observations of a "limiting current" pattern at the anode which would be consistent with a limiting hydrogen diffusion gradient within the anode. The use of hydrogen during double pulse measurements was discontinued. However, similar anomalies were noted during polarographic measurements in the CaF_2 - CaO melts and in the CaF_2 melts with extremely low iron contents. In these cases, an alternate method of determining the concentrations has been developed (Section 3.4.8).

3.4.3 Typical Potential vs Time Curves

The photos in Figure 8 represent typical voltage vs time traces for the double pulse technique. The short horizontal line in the lower left is the base or zero line prior to the beginning of the first pulse. In all photos, the vertical scale is 5 mv per large division and the horizontal scale is 1 μsec per large division. Figure 8a represents an undercharged interface at t_1 = 1.7 μsec since an upward slope is still evident. A portion of the higher potential during the initial high current charging step is just visible in the upper portion of the photo. This portion is completely off scale in the latter photos.

Figure 8b represents an overcharged condition at t_1 while 8c is properly charged--i.e. the slope is zero. Figure 8d also represents a properly charged condition, but with a shorter t_1 = 1.2 μsec.

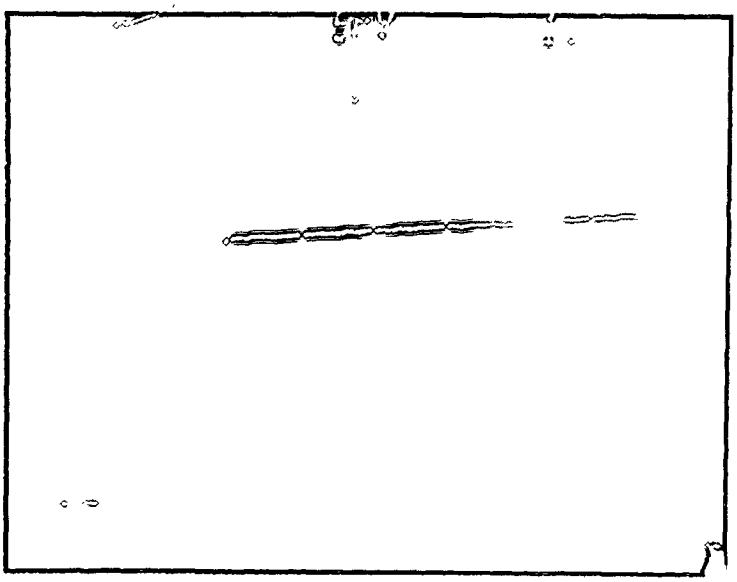

Figure 3.8a: Double Pulse Method - Undercharged Interface. The Horizontal Scale is 1 μsec per Large Division. The Vertical Scale is 5 mv per Large Division.

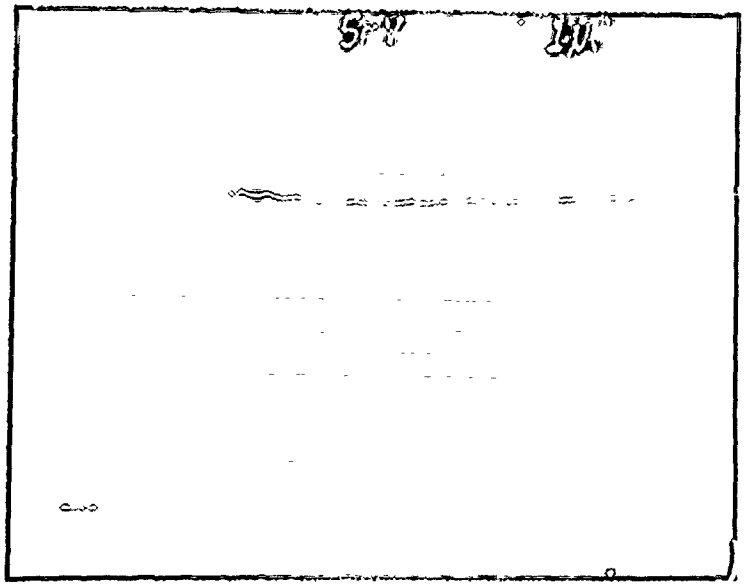

Figure 3.8b: Overcharged Interface

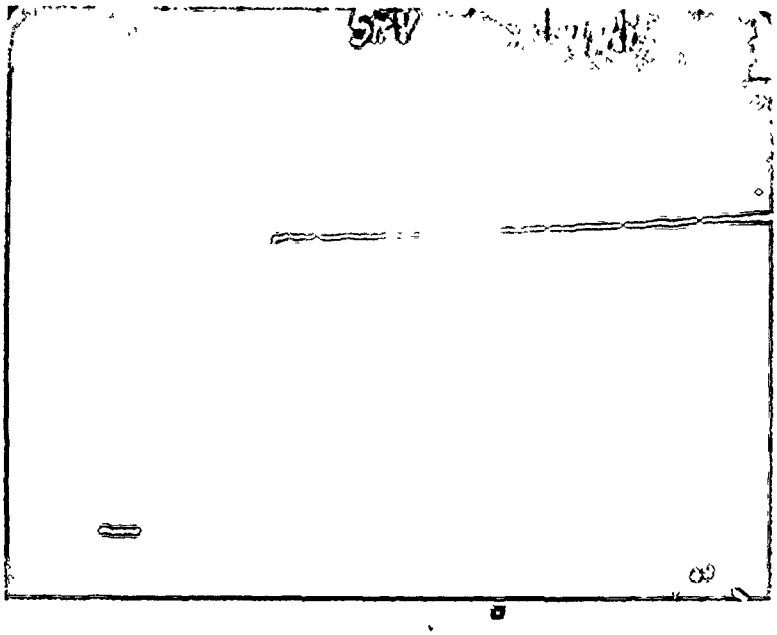

Figure 3.8c: Correctly Charged Interface
t_1 = 1.7 μsec

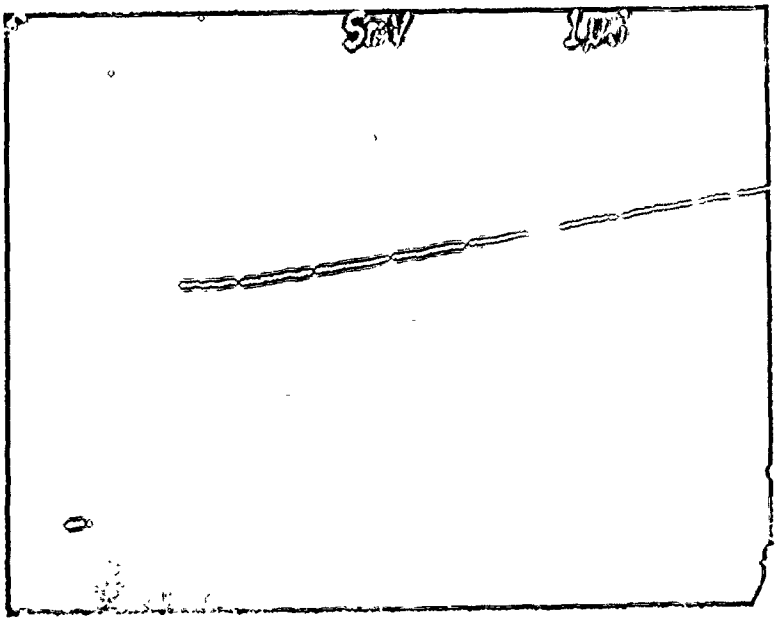

Figure 3.8d: Correctly Charged Interface
t_1 = 1.2 μsec

3.4.4 Typical Data - Overpotential vs $t_1^{\frac{1}{2}}$

Most of the important data are summarized in the plot of i_o vs $C_{Fe^{2+}}$ (Section 3.4.7). In this section, however, a number of typical double pulse data sets will be treated in more detail as an indication of the nature of the information obtained with this technique.

As discussed in Section 3.2.2, Matsuda et. al. showed that for sufficiently small t_1, the overpotential at t_1, $\eta_t=t_1$, should be a linear function $t_1^{\frac{1}{2}}$. Thus, Figures 3.9, 3.10 and 3.11 present data in the form of overpotential vs $t_1^{\frac{1}{2}}$. The significance of the term "sufficiently short times" will be discussed in Section 3.4.5.

The curves in Figures 3.9, 3.10 and 3.11 are all quite smooth but depart from linearity. At very short times they tend to level out and in some cases actually curve upwards again. The effect is particularly noticeable for times t_1 < 1 μsec. It is believed that this effect results from induction effects inherent in the electrode design and, to a lesser extent, from the response times in the electronic equipment. Consequently, the effect becomes more important at shorter t_1 when large currents i_{l1} are required to charge the double layer fully. This conclusion is qualitatively supported by work with an electrode having an inherently greater inductance in which this leveling off and upturning effect were observed with t_1 in the 3 to 5 μsec range. Consequently, data for t_1 less than .7 or .8 μsec were generally neglected.

This factor greatly increases the difficulty and error in extrapolation of the overpotential back to zero, as is required to eliminate the diffusion overpotential. The implications will be discussed in greater detail in Section 3.4.5.

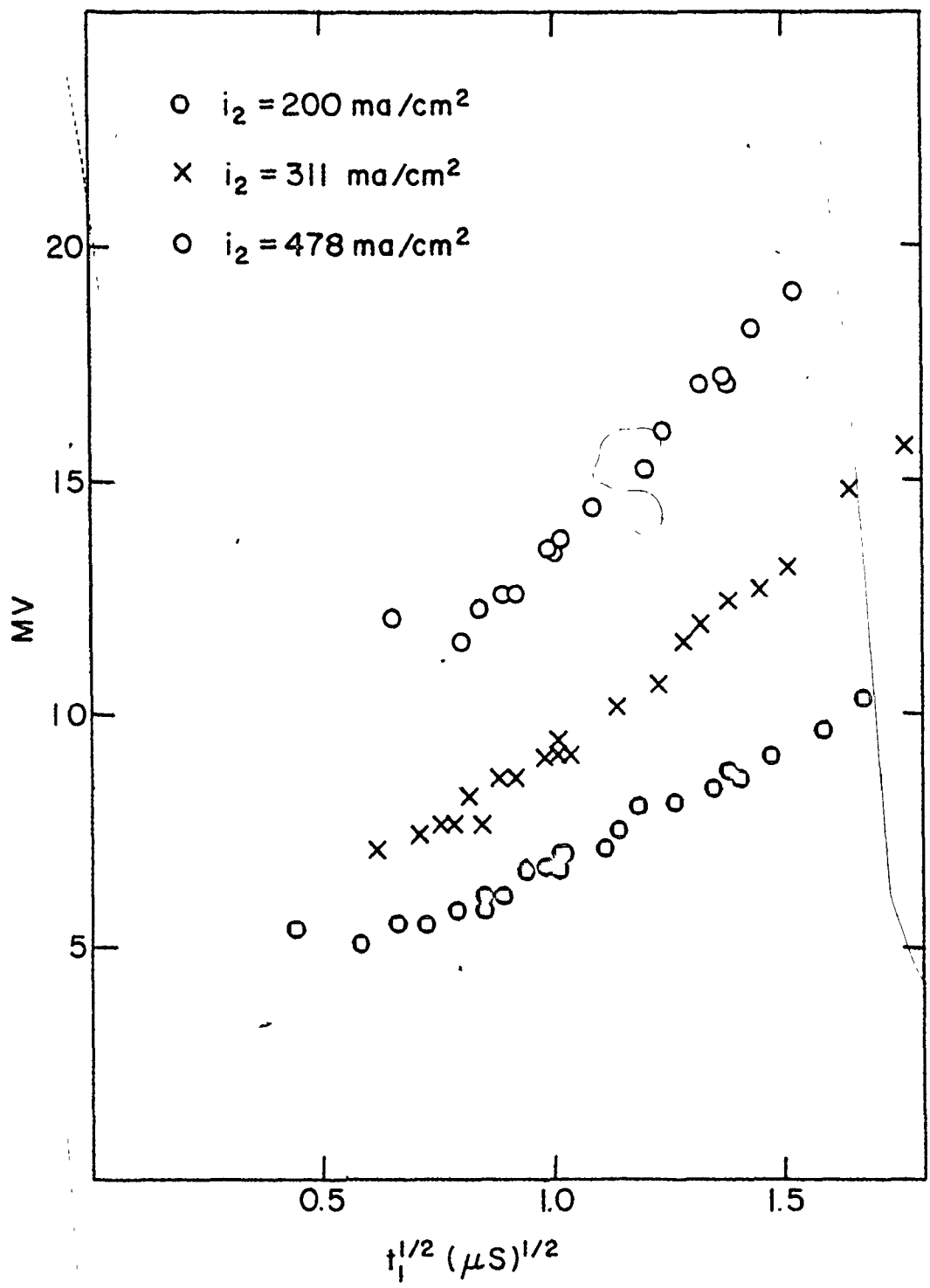

Figure 3.9: Overpotential vs $t_1^{\frac{1}{2}}$ - $C_{Fe^{2+}}$ = .0047 wt%

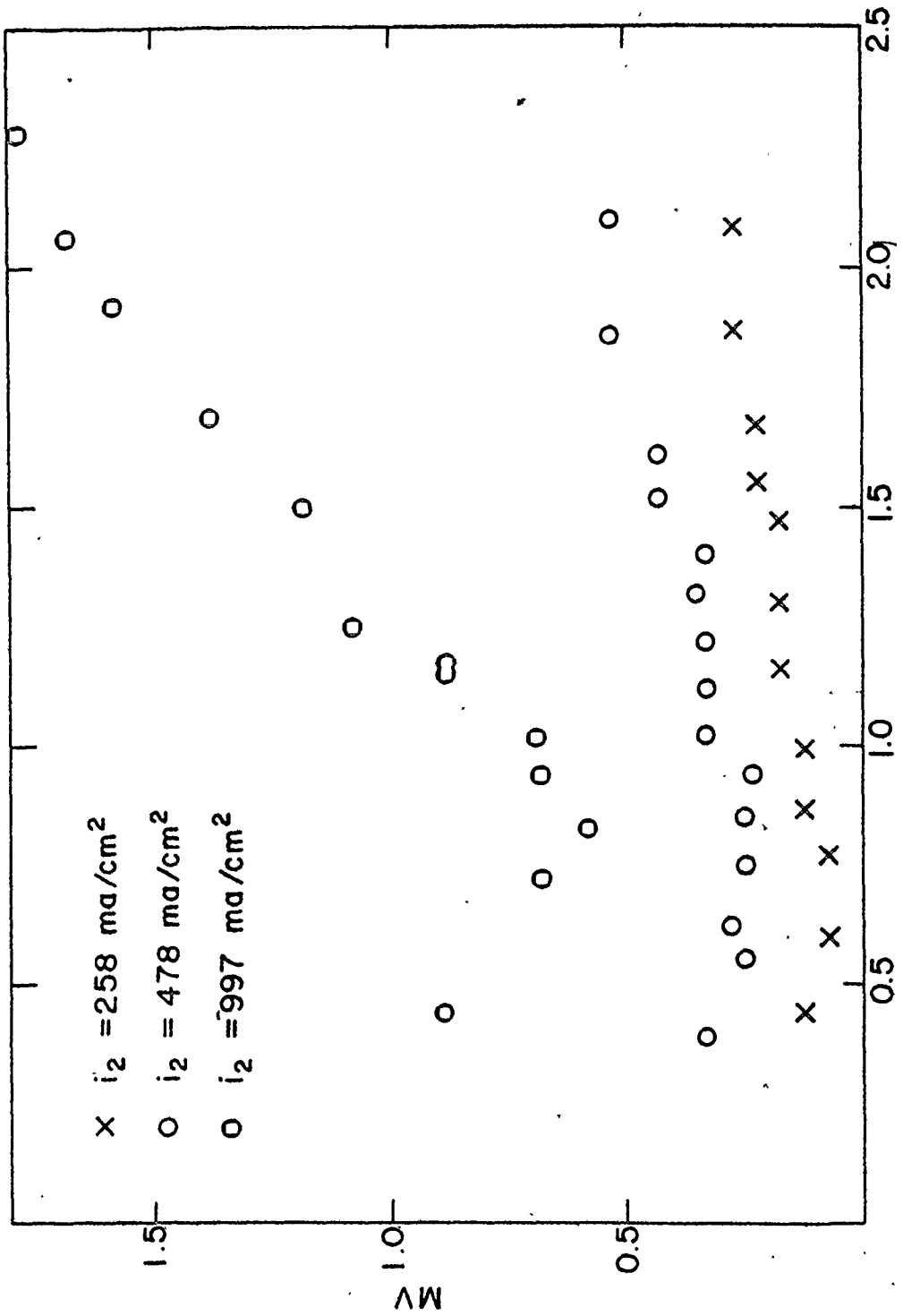

Figure 3.10: Overpotential vs $t_1^{\frac{1}{2}} - C_{Fe^{2+}} = .245$ wt%

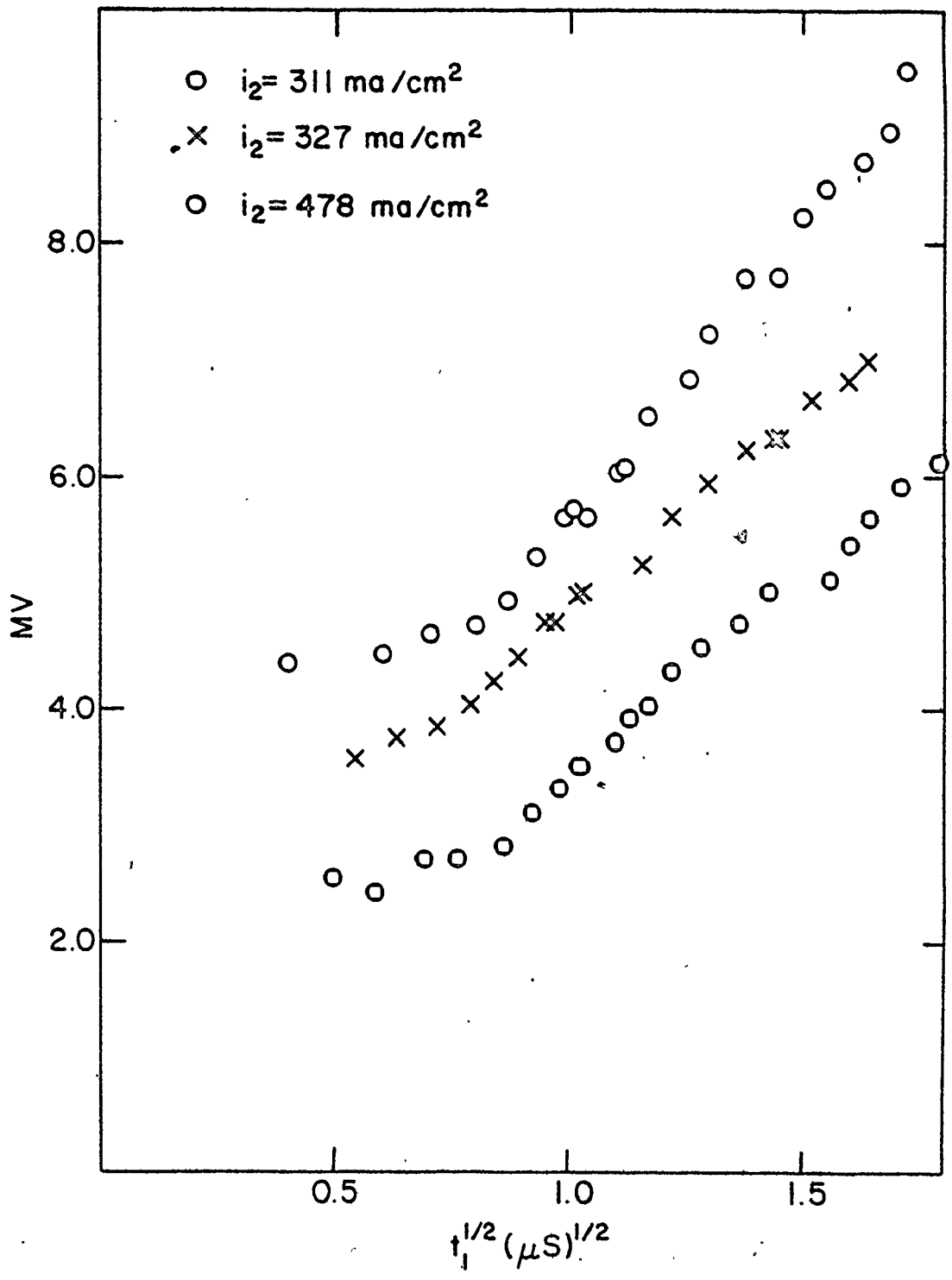

Figure 3.11: Overpotential vs $t_1^{\frac{1}{2}}$ - $C_{Fe^{2+}}$ = .010 wt%

The effect of bulk concentration on the development of the diffusion overpotential can be seen dramatically in comparing Figure 3.10 and 3.11. For equivalent currents i_2, the slope (mv/μsec$^{\frac{1}{2}}$) is approximately 1½ orders of magnitude greater for the lower concentration, which implies a greater correction necessary for the diffusion overpotential. On the other hand, the relative experimental errors involved in the determination of the overpotentials for high concentrations are greater due to the small overpotentials.

3.4.5 Overpotential as a Function of t_1

In Section 3.4.4, some typical plots of overpotential vs $t_1^{\frac{1}{2}}$ were presented and discussed. Matsuda, et. al., have suggested that the true ion exchange current density may be calculated by extrapolating $t_1^{\frac{1}{2}}$ to $t_1 = 0$ for sufficiently small t_1. It is necessary to examine what is meant by sufficiently small t_1. The second term in the series expansion is

$$\left(1 - \frac{9}{32}\right) \left\{\left(\frac{4}{3\pi^{\frac{1}{2}}}\right)\left(\frac{i_o}{ZF}\right)\left(\frac{1}{C_o' D^{\frac{1}{2}}}\right)\right\}^2 t_1. \qquad (3.15)$$

Note that the exchange current desnity i_o is squared in this term and does not cancel completely with the pre bracket factor RTi_2/ZFi_o, so that a numerical evaluation is not possible without prior knowledge of i_o. However, it is possible to estimate the relative magnitudes of the terms in $t_1^{\frac{1}{2}}$ and t_1 by choosing some typical values. The results are summarized in Table 3.4. In these examples, the second term is some 15 to 30% of the first and is therefore not negligible at t_1 = 1 μsec.

Table 3.4

Comparison of First and Second Terms in t_1 Expansion

$C_{Fe^{2+}}$ (mole/cm^3)	i_o (ma/cm^2)	$wt_1^{\frac{1}{2}}$ (t_1=1μs)	$(1-\frac{9\pi}{32})w^2t_1$	2/1
2.66×10^{-6}	8,523	2.49	.72	.23
1.31×10^{-5}	40,588	1.19	.16	.14
8.8×10^{-5}	241,104	2.13	.53	.25

Due to the interference of induction effects at the high currents necessary for very short t_1, it was not possible to conduct experiments in the range of t_1 = .05 to .1 μsec. This is the time interval that would be required if the second term were negligible. Since the experimental data are in the range of t_1 = 1 μsec, a nonlinear extrapolation in t_1 is required. The procedure for doing this will be discussed in Section 3.4.7.

3.4.6 Evaluation of the Electrolyte Resistance

A potential difference due to the electrical resistance of the CaF_2 electrolyte is associated with each experimental measurement. Although it is not directly related to the exchange current density, it must be accounted for properly in evaluation of i_o. With reference to Figure 3.2, there are two ways in which the electrolyte resistance R_{el} may be determined from the experimental data:

$$R_{el} = \eta_1/i_1, \qquad (3.16)$$

and $$R_{el} = (\eta_3 - \eta_2)/(i_1 - i_2).$$

These two resistance values were calculated for each data set

from an experiment and values of the mean and standard deviations determined. The two methods of computing R_{el} were in agreement. The second method of calculation might be subject to greater error since it depends on the difference between two experimentally measured quantities. This surmise was confirmed by the comparison of the standard deviations which were twice as large for the second method. Consequently, the first method was preferred and the values obtained from it are summarized in Table 3.5.

In Figure 3.12, the electrolyte resistance is plotted against the logarithm of the bulk iron concentration in the CaF_2. A linear fit shows a fairly clear trend to lower resistance at higher iron concentrations. There is no theoretical justification for expecting a straight line relationship in a logarithmic scale. It was simply chosen as a convenient way to present the data, in view of the experimental scatter.

It is not obvious why the electrolyte resistance should be a function of bulk iron concentration. It may be due to the effect of the iron ion on the electrical conductivity, or more probably due to a change in the electrode area. Table 3.3 indicates that the electrode area is probably a function of bulk iron concentration in the CaF_2 (a reflection of changes in interfacial tension). To compare the two effects: a 24% increase in electrode area is seen in the same composition range as is a 19% decrease in the electrolyte resistance.

Table 3.5

Data for CaF_2 Electrolyte

n	Extrapolated i_o (A/cm^2)	"i_o" at 1 μsec (A/cm^2)	Conc Fe in CaF_2 (moles/cm^2) x 10^{-5}	Double Layer Capacitance ($\mu F/cm^2$)	"Slope" W x 10^{-4} mole/(ma)(μsec)$^{\frac{1}{2}}$(cm)	Electrolyte Resistance (ohms)
4	160.4	97.5	12.1	4560	.044	.088
5	76.5	61.5	10.8	4562	.032	.090
10	44.9	27.1	4.09	1758	.138	.109
8	38.8	25.6	4.35	2147	.141	.110
15	45.5	23.2	3.20	1198	.225	.109
12	62.0	32.2	3.78	1447	.169	.109
17	16.5	7.27	.828	499	.690	.114
14	18.4	7.46	.785	494	.696	.111
16	4.12	1.69	.162	158	3.06	.123
13	4.23	1.80	.177	171	2.80	121
15	3.60	1.79	.198	181	2.51	120
23	5.96	2.21	.205	175	2.42	.119
21	9.01	2.55	.220	180	2.26	119
16	7.53	2.65	.242	208	2.06	.116
21	18.7	4.28	.363	255	1.38	.123
22	13.9	4.07	.355	234	1.41	121
24	15.5	4.05	.350	250	1.43	.119
24	14.5	4.51	.398	244	1.26	117
12	715	153	12.6	3038	.039	105
15	253	103	11.4	2269	.050	101
16	238	74.4	10.8	2573	.076	.104
14	502	48.1	4.93	1719	.078	094
9	429	68.9	5.27	1829	.080	.096
13	232	51.7	5.54	1863	.116	096
19	242	35.6	3.37	1389	164	094
18	355	52.9	4.37	1682	111	096
24	18.0	4.28	.363	300	1.32	.113
21	25.4	6.71	.626	354	.878	125
19	12.4	5.00	.437	346	1 04	.117
21	21.0	6.24	.566	393	920	118
19	28.4	12.6	1.39	538	.390	118
20	37.0	12.2	1.31	511	.458	125
14	6.71	2.12	.186	183	2.67	125
14	8.86	2.52	.215	193	2.31	124
14	8.36	3.20	.299	245	1.67	.114
17	9.92	3.26	.288	249	1 73	113
15	20.9	8 02	899	117	.66	111

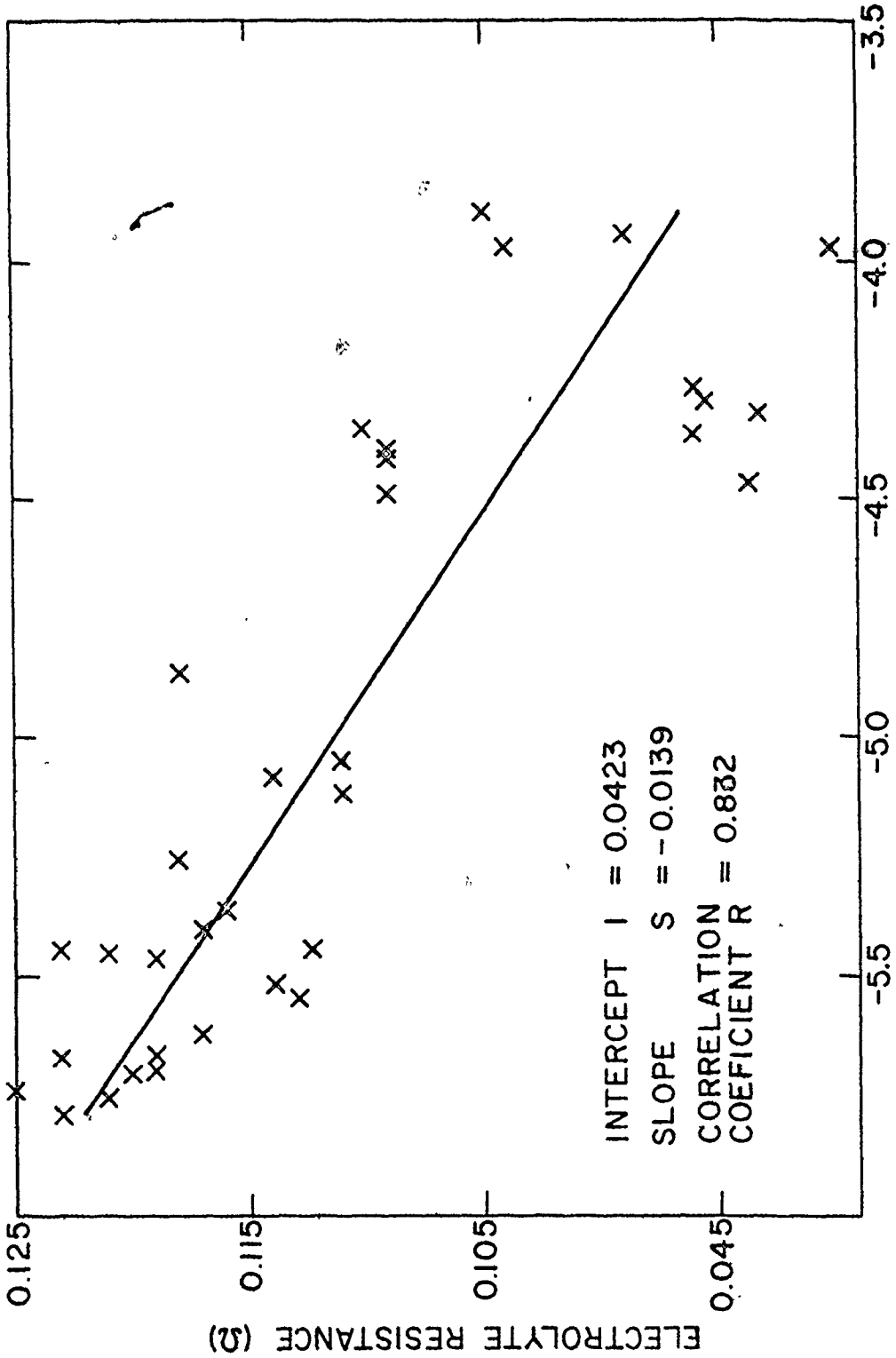

Figure 3.12: Electrolyte Resistance vs C_{Fe}^{2+}

Table 3.6

Data for 10% and 5% CaO in CaF_2

n	Extrapolated i_o (A/cm^2)	"i_o" at 1 μsec (A/cm^2)	Theoretical Concentration of Fe in Melt ($moles/cm^2$)x10^{-5}	Double Layer Capacitance ($\mu F/cm^2$)	"Slope" w x 10^{-4} $(mole/(ma)(\mu sec)^{\frac{1}{2}}(cm)$	Electrolyte Resistance (ohms)
21	235	40.0	5.49	1409	.148	.095
16	416	45.3	6.71	1355	.124	.094
14	67.7	28.4	4.45	1745	.179	.091
19	67.7	15.6	1.99	611	.382	.113
21	40.9	11.7	1.52	562	.494	.113
17	33.7	10.7	1.41	607	.531	.108
16	27.2	10.4	1.47	663	.509	.107
17	64.2	20.2	2.74	1030	.281	.092
16	58.0	18.7	2.54	905	.302	.093
16	133	22.5	2.91	887	.266	.098
18	48.9	17.5	2.47	1047	.310	.095
10	154	28.7	3.76	1486	.209	.095
7	34.9	16.3	2.60	1000	.295	.087
12	35.2	16.5	2.94	925	.263	.087
11	27.6	14.2	2.44	806	.314	.078
13	55.1	16.6	2.20	1471	.347	.089
13	36.1	14.0	1.99	1096	.381	.088
13	28.8	14.6	2.48	1055	.309	.087
12	36.8	16.7	2.63	1219	.292	.087
11*	11.2	5.76	.967	584	.768	.087
12*	11.6	5.83	.954	579	.778	.086
12*	10.3	5.53	.960	574	.774	.087
11*	13.1	6.12	.948	587	.783	.088
10*	9.35	5.70	1.16	587	.641	.088

*5% CaO

3.4.7 Extrapolation to $t_1 = 0$

It was established in Section 3.4.5 that a non-linear extrapolation was required. Examination of the equation

$$\eta_{t=t_1} = \frac{B}{i_o} + BWt_1^{\frac{1}{2}} + \left(1 - \frac{9\pi}{32}\right) BW^2 i_o t_1 \qquad (3.17)$$

with $B = \frac{RTi2}{ZF}$ and $W = \left(\frac{4}{3\pi^{\frac{1}{2}}}\right)\left(\frac{1}{ZF}\right)\left(\frac{1}{C_o' D^{\frac{1}{2}}}\right)^*$

shows that the extrapolation of this equation is complicated by the fact that i_o appears in both the denominator of the intercept and the numerator of the term in t_1.

The extrapolation was accomplished with a Levenberg-Marquardt type non-linear optimization algorithm. The experimental data were fitted to the equation by treating the "intercept" i_o and the "slope" W as the variables to be optimized. Proper convergence seems to be obtained in the analysis of each experiment. The resulting values of i_o from extrapolation and from the potential at 1 μsec, as well as values for W, are summarized in Table 3.5.

Can the accuracy of the data justify the added sophistication of this non-linear extrapolation? A comparison of the sums of squares of the residuals for a linear and non-linear fit showed that the non-linear fit was superior in almost all cases. This conclusion is significant in that the number of degrees of freedom for both extrapolations was two.

---

*The term with C_o is not required since this phase is pure iron.

3.4.8 An Alternate Approach to the Determination of Bulk Iron Concentrations in the CaF_2

The slope as defined by W in the previous section is inversely proportional to the bulk iron concentration. A plot of W vs $1/C_{Fe}$ is presented in Figure 3.13. On the basis of this correlation, the derived values of iron concentration were successfully applied whenever the standard polarographic technique failed: when hydrogren was present; in the experiments with very low iron contents; in the melts that contained CaO.

It is interesting to compare the empirically determined slope with that which may be evaluated theoretically:

Theory 7.8×10^{-10} mole/ma - cm - $(\mu sec)^{\frac{1}{2}}$

Experiment 4.8×10^{-10} mole/ma - cm - $(\mu sec)^{\frac{1}{2}}$

The agreement is as good as or better than that expected from the experimental accuracy of the concentration and diffusivity determinations. In addition to calibrating a reliable method for determining iron concentrations, the comparison further justifies the extrapolation procedure.

3.4.9 Exchange Current Densities as a Function of Bulk Concentrations

It is useful to relate the ion exchange current densities to the bulk concentrations of the reacting species in electrode and electrolyte. In the experiments, the iron concentration in the electrode remains constant, so that exchange current density may be related directly to the reactant concentration in the electrolyte. It is in this format that most of the experimental data will be presented.

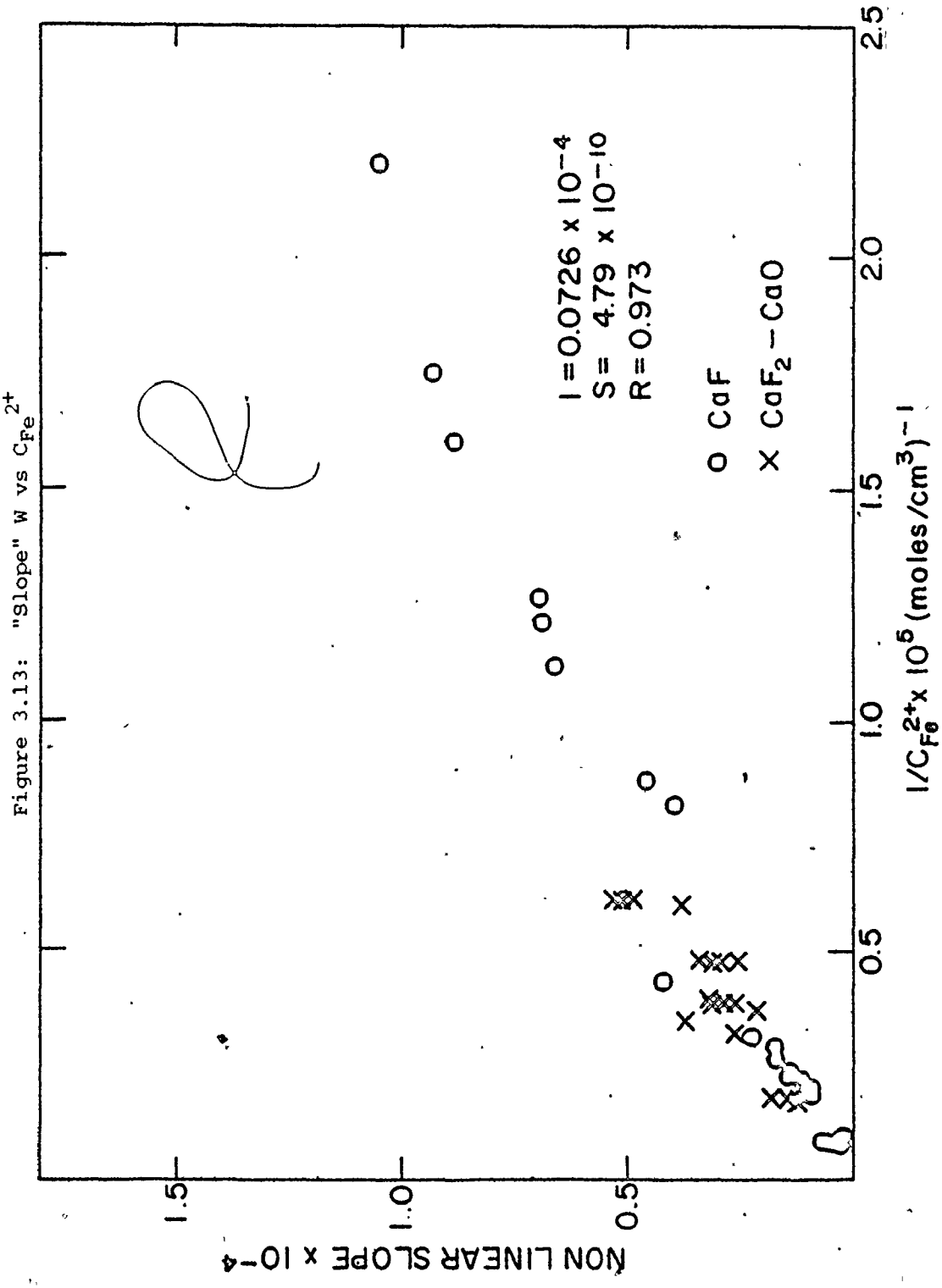

Figure 3.13: "Slope" W vs C_{Fe}^{2+}

The development of the equation necessary for the determination of the transfer coefficient and the standard heterogeneous rate constant is given.

Recall that the exchange current density is defined by the relations

$$i_o = ZFk_o'C' \exp\left\{-\left({}_oE_a't + ZF\Delta\phi_{eq}\right)/RT\right\}$$
$$= ZFk_oC \exp\left\{-\left({}_oE_a - (1-\alpha)ZF\Delta\phi_{eq}\right)/RT\right\}. \qquad (3.5b)$$

The concentrations C and C' can be expressed in terms of $\Delta\phi_{eq}$

$$\frac{k'c'}{kc} = \exp\left\{\left(\alpha ZF\Delta\phi_{eq} + (1-\alpha)\, ZF\Delta\phi_{eq}\right)/RT\right\}$$
$$= \exp\left\{ZF\Delta\phi_{eq}/RT\right\} \qquad (3.18)$$

with $k = k_o \exp\left(-{}_oE_a/RT\right)$ and $k' = k_o' \exp\left(-{}_oE_a'/RT\right)$

This may be substituted into equation 3.5b to give

$$i_o = ZFkC\left(\frac{k'c'}{kc}\right)^{(1-\alpha)} = ZF(kc)^{\alpha}(k'c')^{(1-\alpha)} \qquad (3.19)$$

With the assumption that k_o, k_o', ${}_oE_a$, and ${}_oE_a'$ are independent of the concentrations C and C' (see Chapter 5), the leading terms may be grouped in a constant Y, such that

$$Y = ZF\, C^{\alpha} k'\left(\frac{k}{k'}\right)^{\alpha}. \qquad (3.20)$$

The exchange current density may be expressed as

$$i_o = YC'^{(1-\alpha)}$$

or alternatively

$$\log i_o = \log Y + (1-\alpha) \log C'. \qquad (3.21)$$

Thus, log i_o may be plotted against log C' to determine α and Y.

Figure 3.14 is a plot of exchange current density (evaluated at t_1 = 1 μsec) vs iron concentration in the electrolyte. This represents the data obtained with CaF_2 melts over a wide range of iron contents. The data may be represented by a straight line, although this cannot be considered to be particularly strong evidence in support of the theory. In any event, it is possible to determine an apparent transfer coefficient and standard heterogeneous rate constant. This will be done in Section 3.4.10. The difference between the results of Prange, and those of the current study is believed to be due to a difference in choosing the zero slope criterion in the measurements.

Figure 3.15 compares the exchange current densities for t_1 = 1 μsec (Figure 3.14) with those obtained using the non-linear extrapolation to t_1 = 0. The scatter in the latter is much greater, as would be expected in any extrapolation. However, the slope is nearly identical to that in Figure 3.14. The extrapolation procedure increases the estimate of i_o by about a factor of three. Thus the extrapolation is quite important. In other words, there is a significant concentration overpotential at 1 μsec.

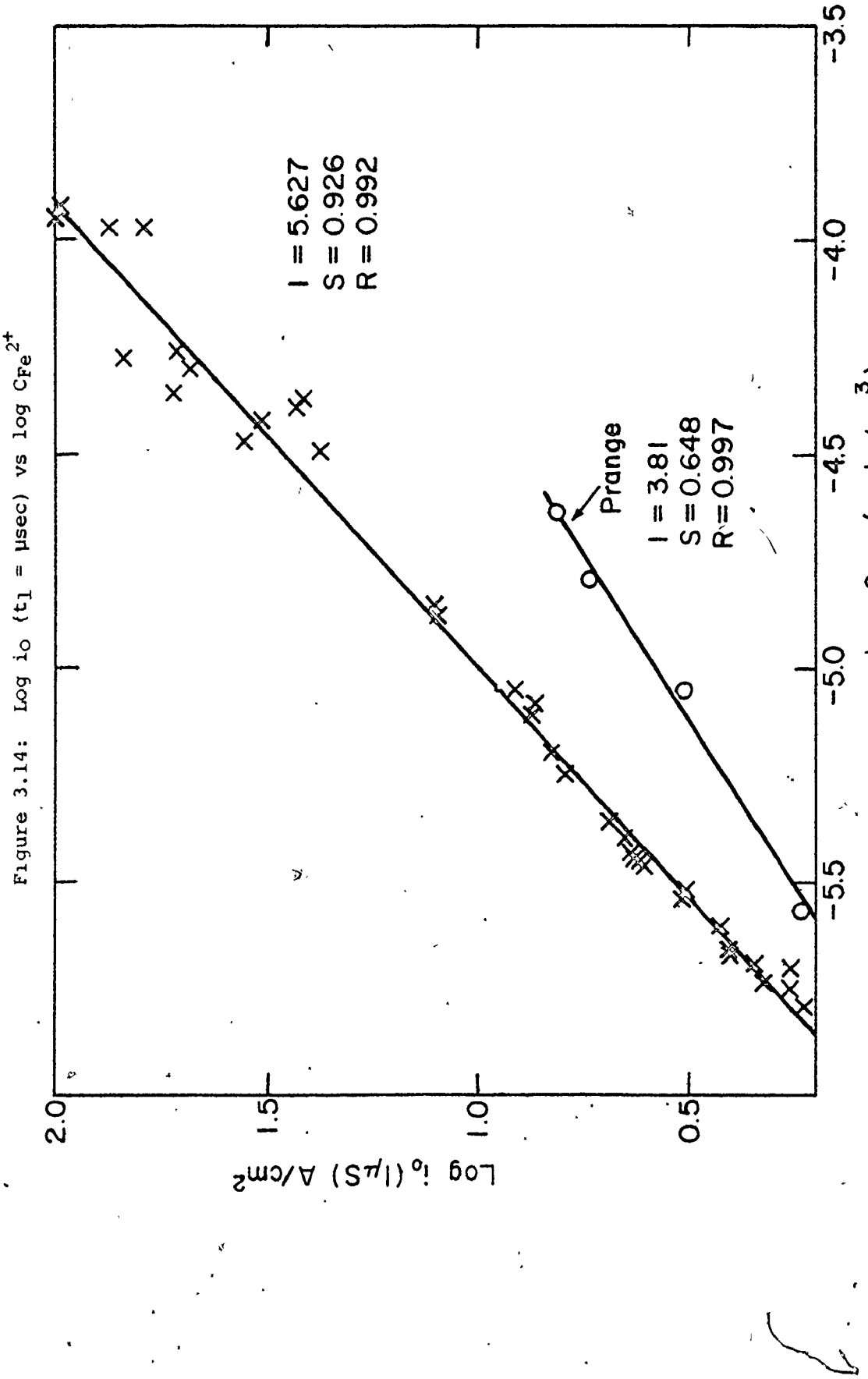

Figure 3.14: Log i_o (t_1 = μsec) vs log $C_{Fe^{2+}}$

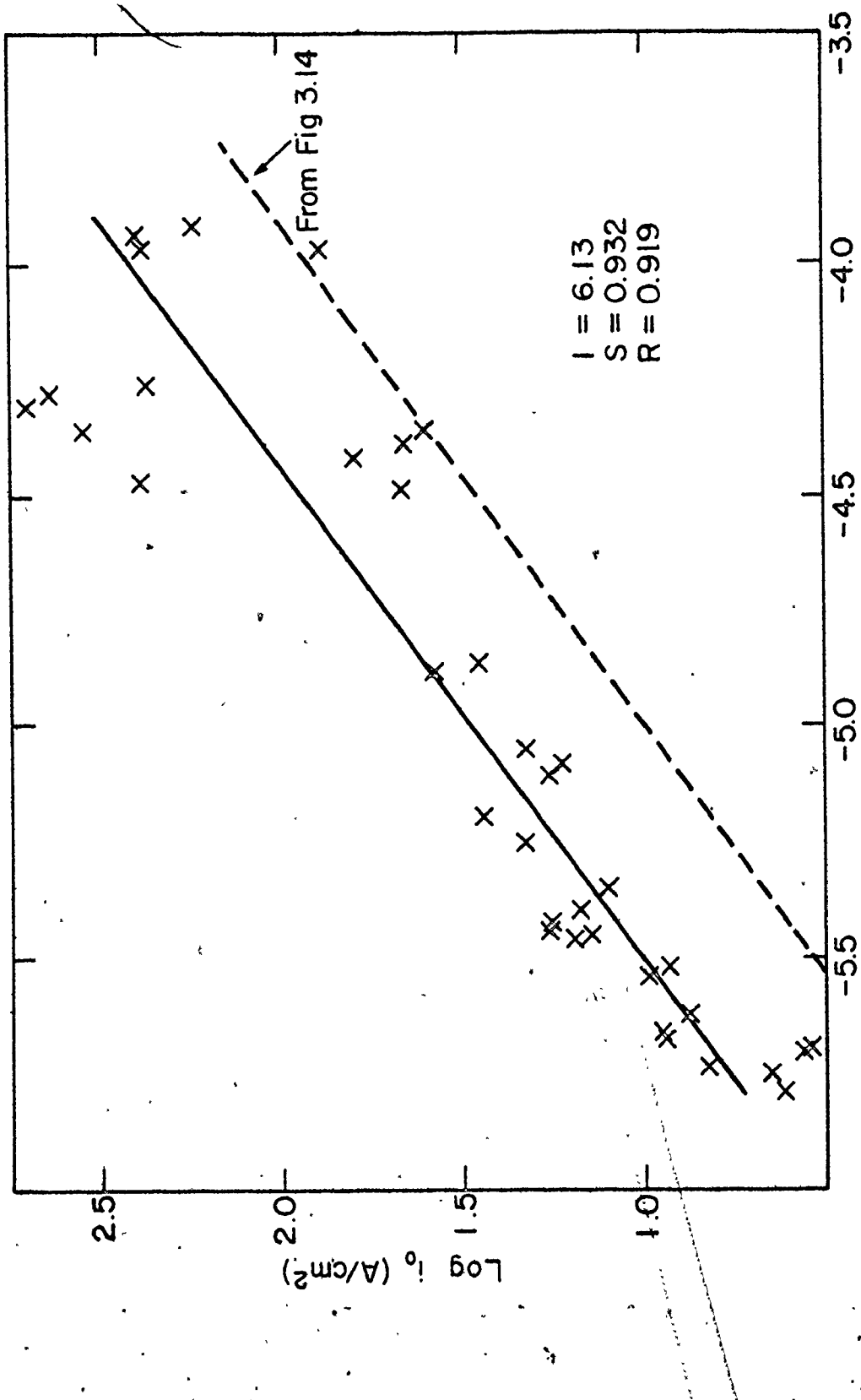

Figure 3.15: Log i_o (extrapolated) vs log C_{Fe}^{2+}

Figure 3.16 compares the exchange current densities (evaluated at t_1 = 1 μsec) for CaF_2 - CaO melts with that for the case of "pure" CaF_2 (Figure 3.14). These measurements were generally harder to make and were in an iron concentration range which gave less accurate results. This is reflected in the greater degree of scatter. Although the best linear fit lies slightly below that of Figure 3.14, the difference does not appear to be statistically significant. The exchange current densities should be considered essentially the same. This is a little suprising since it is clear that slag-electrode interfacial tension is very different for the CaF_2 - CaO case, as evidenced by the changes in electrode surface area (i.e. meniscus) and the general electrode and crucible behaviour. Figure 3.17 shows a similar plot comparing extrapolated exchange currents for CaO containing melts with the best fit from Figure 3.15.

3.4.10 Calculation of the Transfer Coefficient and Standard Rate Constant

Following Bauer,[43] $\Delta\phi_{eq}$ may be written

$$\Delta\phi_{eq} = \frac{RT}{ZF}\left\{\ln\left(\frac{k'}{k}\right) + \ln\left(\frac{C'}{C}\right)\right\} \qquad (3.22)$$

The formal standard potential $\Delta\phi^{o}_{eq}$ can be defined at C = C' such that

$$\Delta\phi_{eq} = \Delta\phi^{o}_{eq} + \frac{RT}{ZF}\ln\left(\frac{C'}{C}\right) \text{with } \Delta\phi^{o}_{eq} = \frac{RT}{ZF}\ln\left(\frac{k'}{k}\right) \qquad (3.23)$$

If one adopts the convention that the formal standard potential is the reference potential (i.e. $\Delta\phi^{o}_{eq}$ = 0), k = k' and, k', the standard heterogeneous rate constant, may be determined from $Y = ZFk'C^{\alpha}$.

From Figure 3.15, apparent values for the two variables which characterize the exchange current density i_o may be calculated. The values obtained are

"transfer coefficient" $(1 - \alpha) = .932$

"standard rate constant" $k' = 8.03$

It is important to emphasize that, although the parameters α and k are of value in recording kinetic data, it is really the exchange current density which is indicative of the reaction rates at equilibrium for a specified concentration. This will be discussed in more detail in Chapter 5.

3.4.11 The Double Layer Capacitance

There are two methods for calculating the interfacial capacitance:

$$C_{DL} = i_1 t_1/(\eta_1 - \eta_3), \qquad (3.24)$$

and $$C_{DL} = i_1 t_1/(\eta_2 - i_2 R_{el}).$$

The second method generally gave slightly higher capacitance values and larger standard deviations. In principle a dependence of measured C_{DL} on t_1 is expected since i_1 has a small Faradaic component. However, no such trend was seen in the data. Since the correction is expected to be small in any case, it is ignored. The results from the application of the first method are summarized in Table 3.5.

As with the exchange current densities, the capacitance is clearly a strong function of bulk iron concentration. Figure 3.18 shows a plot of this capacitance as a function of concentration.

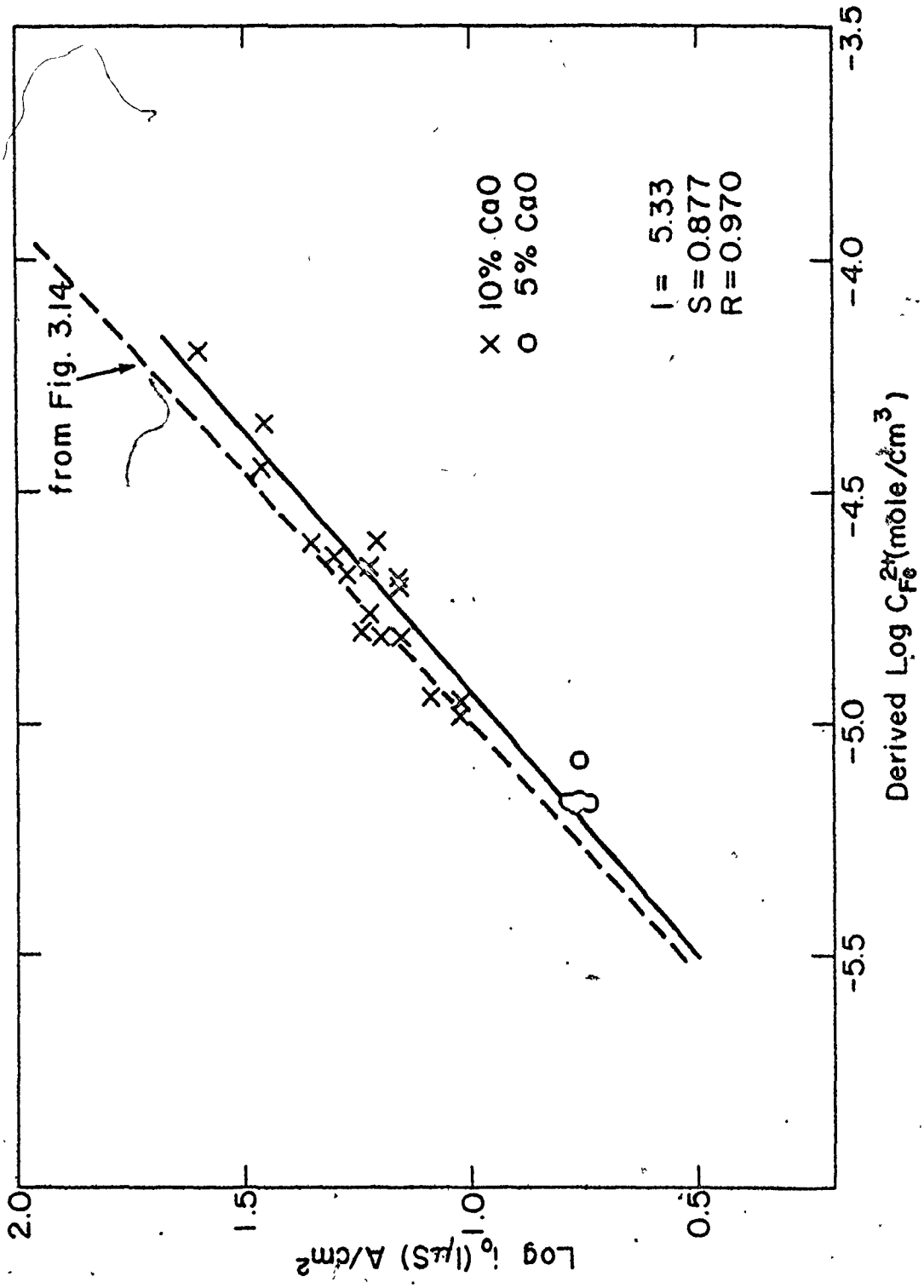

Figure 3.16: Log i_o (t_1 = 1 μsec) vs log C_{Fe}^{2+} for CaF_2 - CaO melts

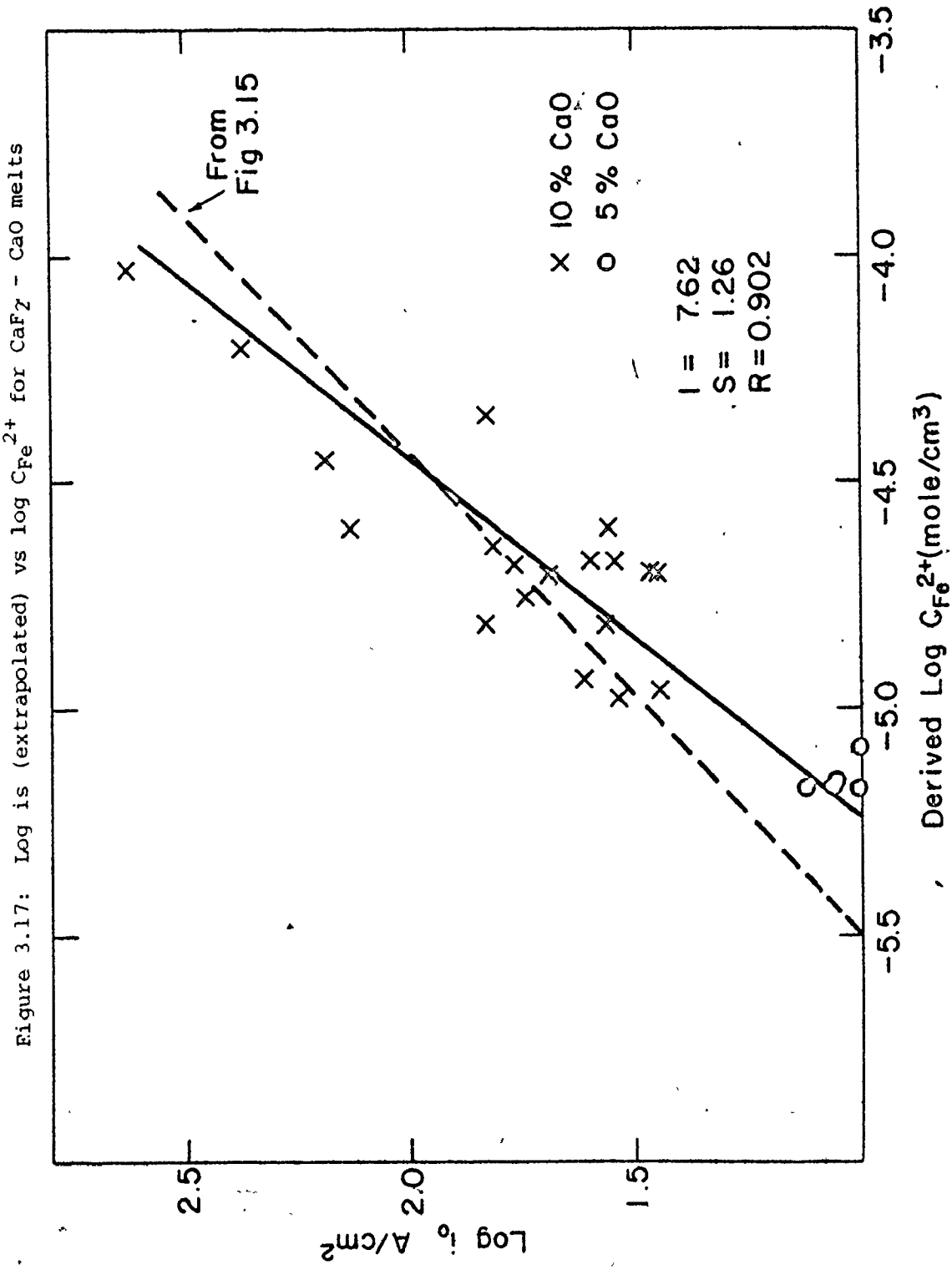

Figure 3.17: Log is (extrapolated) vs log C_{Fe}^{2+} for CaF_2 - CaO melts

It represents strong evidence to suggest that the nature of the Fe/CaF_2 interface changes significantly with iron concentration. The implications of such a conclusion will be discussed further in Chapter 5.

Figure 3.19 compares the data for CaO containing slags with the results of Figure 3.18. No significant difference is apparent.

3.4.12 Temperature Dependence of the Exchange Current Density

Some preliminary work was done at temperatures other than 1450°C in order to study the effect of temperature on the exchange current density. Pure CaF_2 was not suitable for such experiments because the possible temperatures were constrained in a relatively narrow range between the melting points of CaF_2 and iron. However, the presence of an eutectic in the CaF_2 - CaO system lowered the melting point by some 50°C, so that some preliminary temperature dependence measurements could be made in these melts.

Measurements were made within the temperature range 1380°C to 1450°C and the results are presented in an Arrhenius type plot in Figure 3.20. The apparent activation energy of 9 Kcal/mole obviously has a large uncertainty associated with it.

3.4.13 Comparison of Predicted and Actual Single Pulse Curves

Berzins and Delahay[35] presented a theoretical expression for the single pulse galvanostatic method in terms of $C^{\prime}_{Fe}$, D_O, i_o and C_{DL}. Thus, another check on the experimental double pulse data is provided by calculating a theoretical curve for a single pulse measurement using data obtained with the double pulse technique and

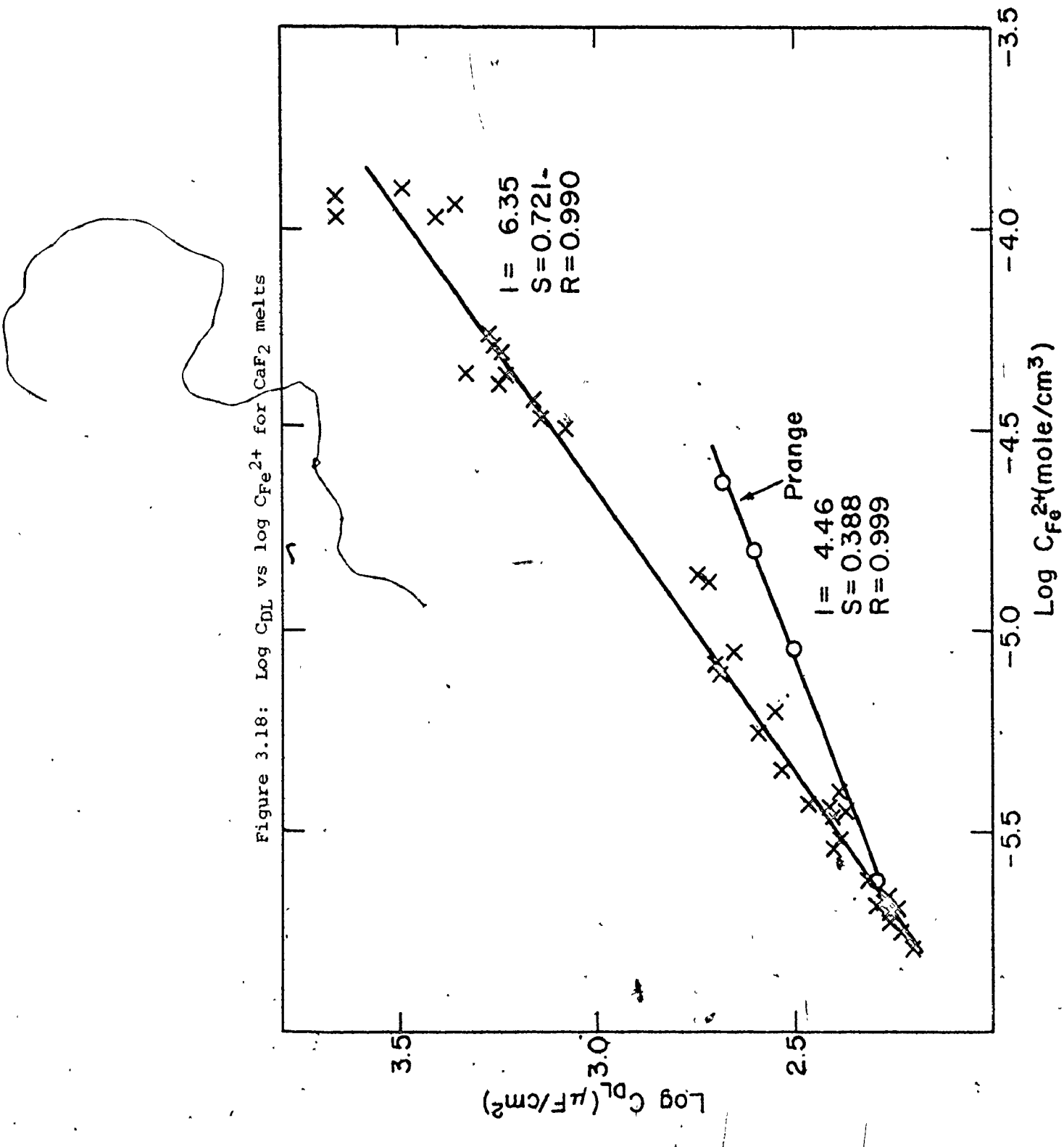

Figure 3.18: Log C_{DL} vs log C_{Fe}^{2+} for CaF_2 melts

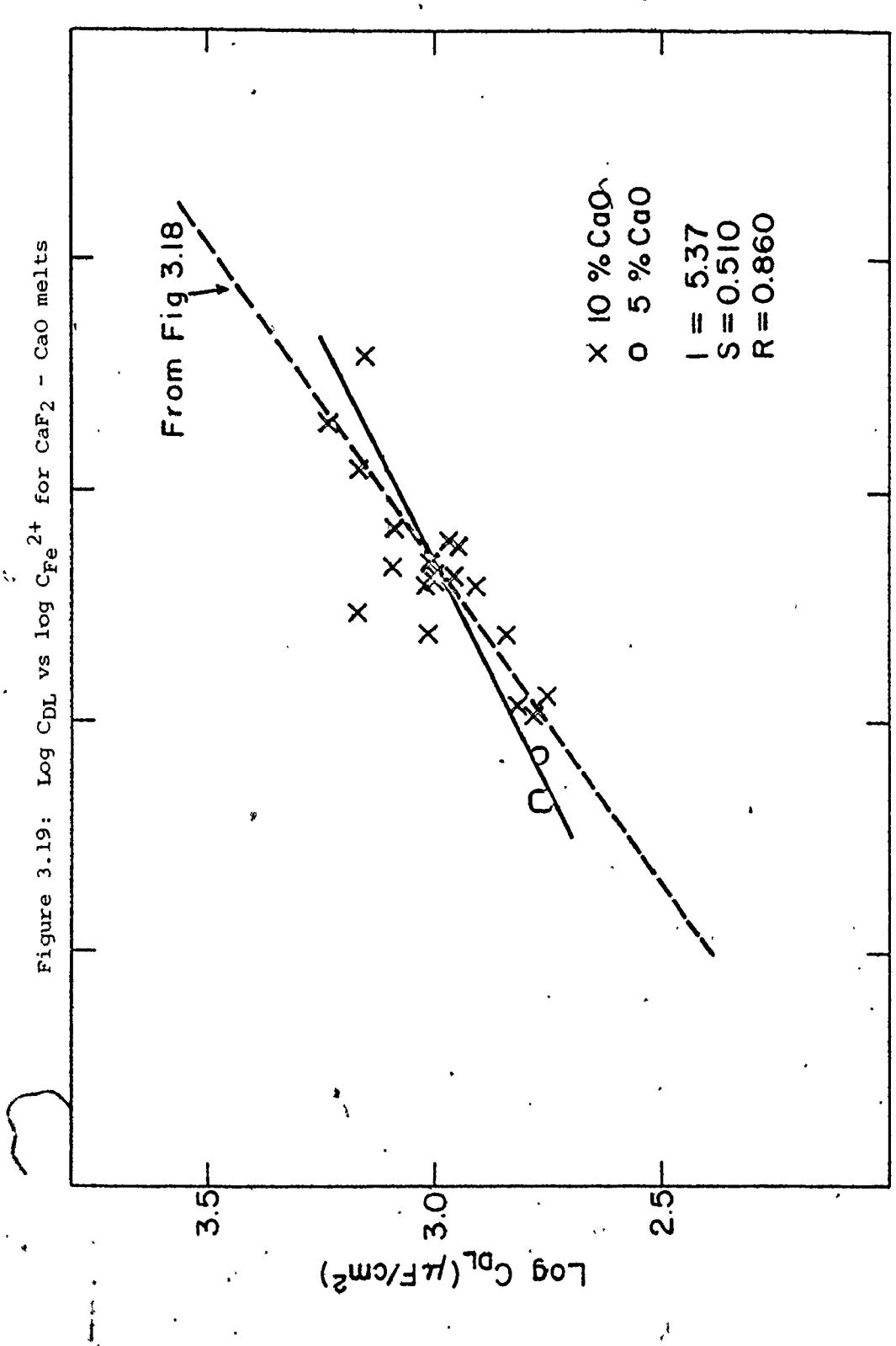

Figure 3.19: Log C_{DL} vs log C_{Fe}^{2+} for CaF_2 - CaO melts

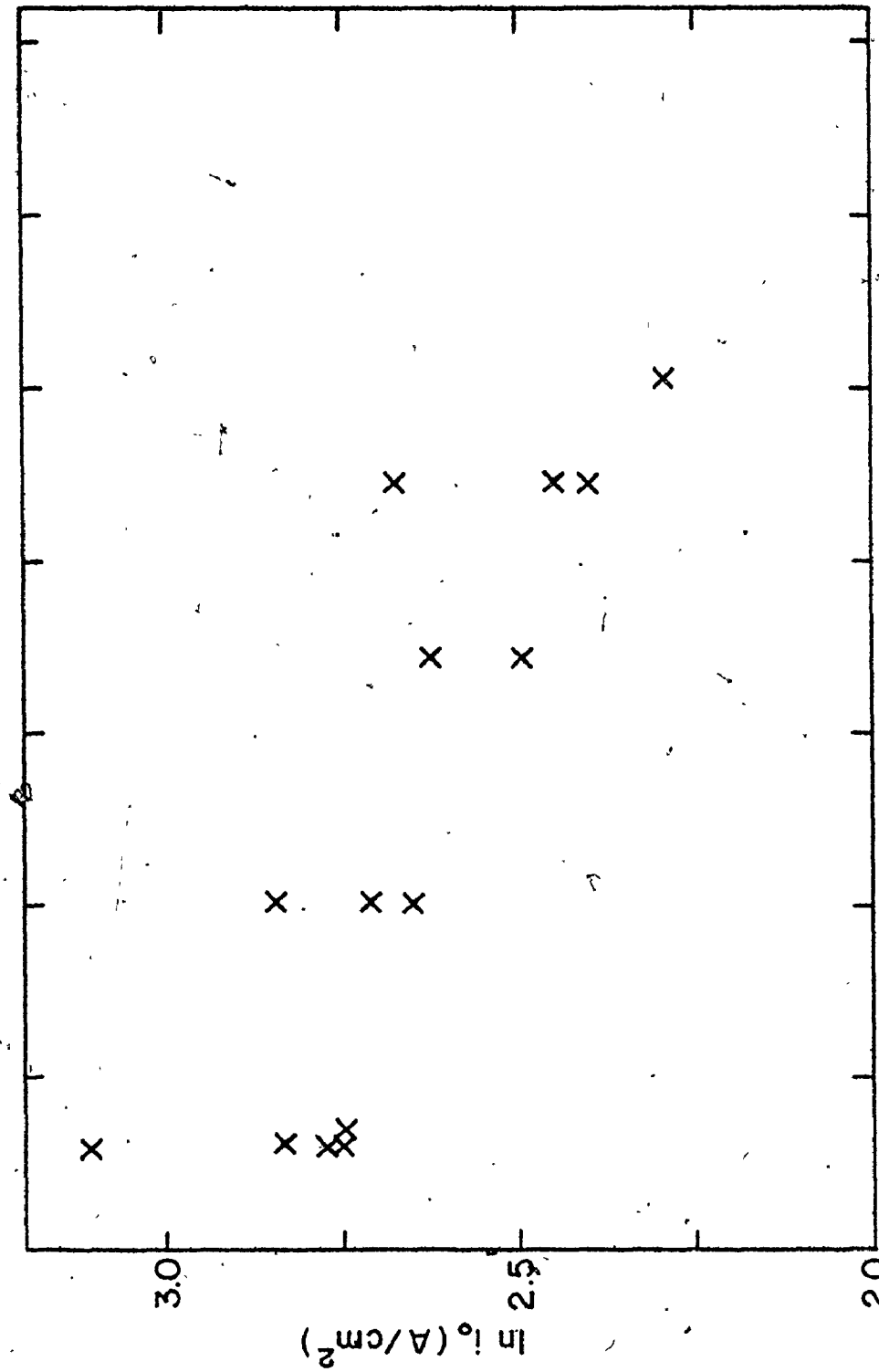

Figure 3.20: Exchange Current Density vs Slag Temperature

comparing with an experimentally measured single pulse curve. A series of photos were taken of a single pulse event in a range of voltages and times in order to obtain the data summarized in Figure 3.21.

The agreement between the theoretical and experimental curves is quite good, although conclusions should be drawn with caution. The theoretical equation is strongly dependent on the double layer capacitance, but relatively insensitive to the ion exchange current density. A calculation in which the exchange current density was doubled resulted in an almost imperceptible change in the theoretical curve.

Figure 3.21: Comparison of Theoretical and Experimental Curves for the Single Pulse Method

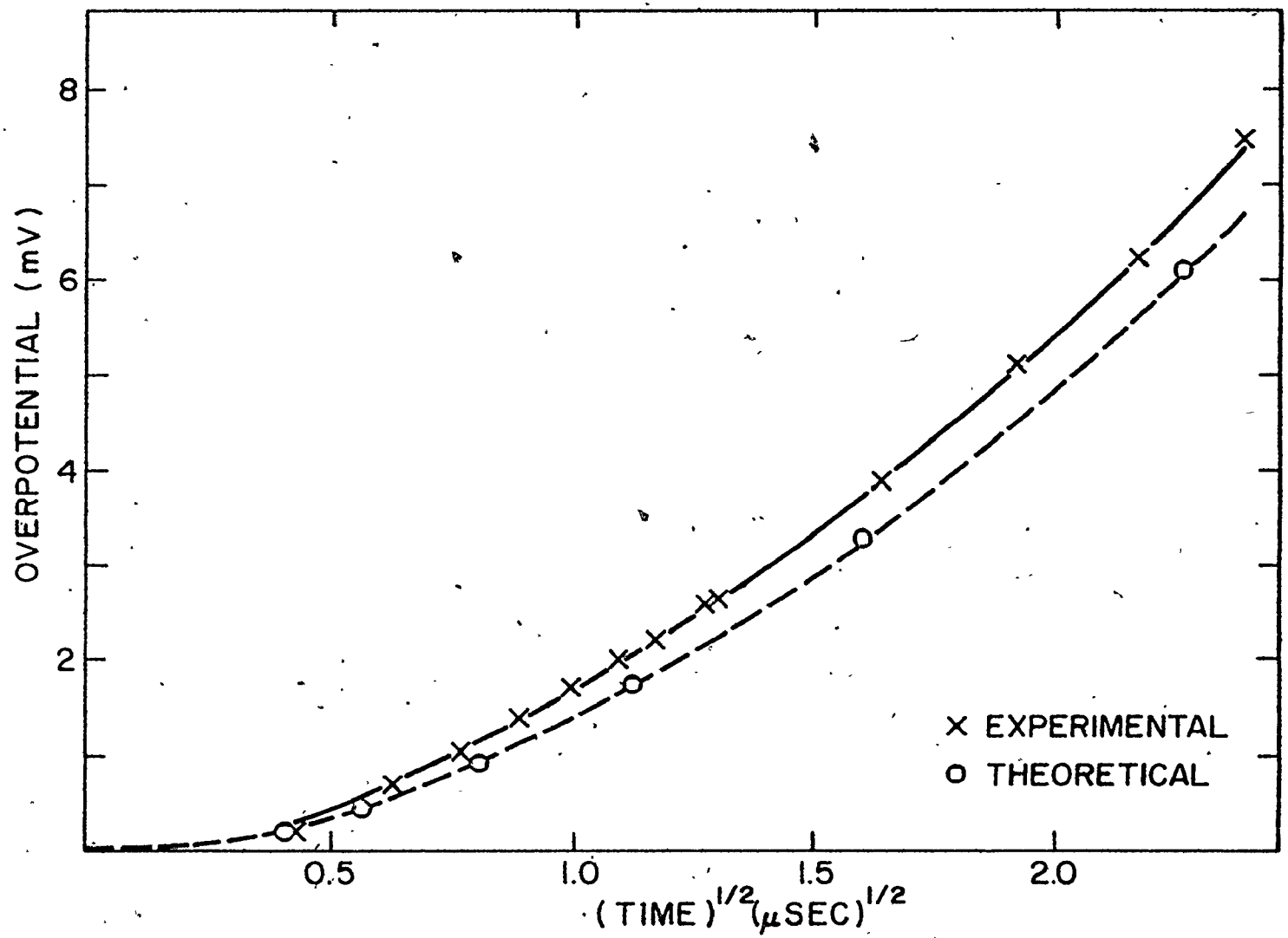

CHAPTER 4: SLAG/METAL INTERFACIAL REACTIONS

- CHEMICAL APPROACH

4.1 INTRODUCTION

Some of the advantages of an electrochemical approach to interfacial reaction kinetics are clear. A large volume of accurate data can be produced in a short period of time with relatively simple experimental procedures. However, considerable analysis of this data is necessary in order to calculate useful kinetic parameters from the experimentally measured transient potentials and currents. The theoretical treatments necessary for this analysis were developed primarily for electrochemical reactions in aqueous solutions. There is no evidence that such an approach is directly applicable in high temperature molten salt or slag systems, although in the absence of evidence to the contrary, this basic assumption was made in the previous chapter.

Due to the central importance of such an assumption to the proper interpretation of the electrochemical data, it is desireable to consider an alternate experimental approach which could lead to an independent order of magnitude confirmation of the kinetic data. Consequently the so called chemical approach to this problem was undertaken.

In these experiments pure FeO was separated from CaF_2 by an iron foil. Progress of the reaction was monitored through the use of oxide markers in the foil.

4.2 THEORY

In chapter 2, a phenomenological approach has been used in conjunction with postulates and approximations in order to relate diffusion fluxes to concentration gradients. In both metallic and ionic diffusion,

the interdiffusivity matrix for concentration gradients was expressed in terms of tracer diffusivities and thermodynamic activity data. The validity of the approach was based on the assumption that fundamental coupling was negligible. That is, it was assumed that to a good approximation, all of the mechanisms and physical information necessary to describe the system were carried by the tracer diffusivity data.

Lu[31] has postulated that a similar phenomenological approach may generate a reasonable first approximation to multicomponent slag/metal interfacial reactions. The development is directly analogous to that for ionic diffusion, with two exceptions. The driving forces for interfacial reactions are electrochemical potential differences instead of gradients, and a choice of reference frame is not required. Fluxes J_i are replaced by reaction rates R_i, and chemical reaction rate constants k_i from the mass action law replace tracer diffusivities.

It will be shown that the approach makes an assumption equivalent to a diagonalized mobility matrix in the lattice fixed frame. That is, fundamental coupling is assumed to be negligible. In the absence of the need to choose a reference frame, charge balance is the only remaining coupling mechanism. Directly analogous to diffusion, it is implicit in the above that to a good approximation, all of the mechanistic and physical information required by the system is contained in the rate constants measured by independent single reaction experiments.

Interfacial slag/metal reactions are considered to be concurrent anodic and cathodic reactions of the form

$$M_1 \rightleftarrows M_i^{z_i+} + z_1 e^- . \qquad (4.1)$$

Several basic assumptions are made:

(a) The slag phase is purely ionic (i.e., no free electrons), and the metal phase is truly metallic,

(b) The reaction takes place at a narrow interface, since the phases are completely immiscible,

(c) There is no net transfer of charge across the interface,

(d) All reactions as written are of first order,

(e) The transient period prior to the establishment of a quasi-steady state field is very short and can be neglected.

In order to express the reaction rate equation in the conventional manner comprising forward backward and net rates, it is useful to define an absolute electrochemical activity $\bar{a}_i$ such that

$$\bar{a}_i = \exp\ (u_i + z_i F\phi/RT) = a_i \exp\ (z_i F\phi/RT) \qquad (4.2)$$

The definition is a simple extension of the concept of absolute activities, as defined by Guggenheim[34] as $\mu_i = RT\ln a_i$.

It is postulated that a modified form of the law of mass action is applicable for such elementary charge transfer steps, so that:

$$R = \vec{R} - \overleftarrow{R} = \vec{k}^*\bar{a} - \overleftarrow{k}^*\bar{a}'a_e^{z_i} \qquad (4.3)$$

Expanding and manipulating the result, one has:

$$R = \vec{k}^* a \exp\ (z_i F\phi/RT) \left\{ 1 - \frac{\overleftarrow{k}^* a' a_e^{z_i} \exp\ (z_i F\phi'/RT)}{\vec{k}^* a \exp\ (z_i F\phi/RT)} \right\},$$

$$= \vec{k}^* a \exp\ (z_i F\ /RT) \left\{ 1 - \frac{\overleftarrow{k}^* a' a_e^{z_i}}{\vec{k}^* a} \exp\ (-zF\Delta\phi/RT) \right\} \qquad (4.4)$$

where $\phi - \phi' = \Delta\phi$

The meaning of the term in the curly brackets is quite straight forward but is best clarified when dealing with a specific set of reactions.

However, the pre-bracket term, and in particular the factor exp $(z_i F\phi/RT)$ requires further explication. It has been observed previously that the splitting of an electrochemical potential into chemical and electrical portions involves one degree of arbitrariness since most chemical bonds are electrical in nature. In keeping with the convention chosen for ionic diffusion, it is convenient to consider only electrical forces relating to the charge balance constraint in the electrical term, with all other effects being taken in as part of the chemical term. Under these circumstances, $|\phi|$ must be less than or equal to $|\Delta\phi|$ which represents the total effect of the charge balance constraint. In fact it is possible to write

$$\phi = (1-\alpha)\Delta\phi \quad \text{with } 0 \leq \alpha \leq 1. \tag{4.5}$$

The choice of the symbol α is not accidental. In fact, its meaning is quite similar to that of a symmetry factor[44] assigned to it in the traditional electrochemical theory. In both cases, it is indicative of the relative amount of the electrical potential difference attributed to each phase.

In this chapter, charge transfer reactions of the form

$$\begin{aligned} Fe &\rightarrow Fe^{2+} + 2\bar{e} \\ O + 2\bar{e} &\rightarrow O^{2-} \end{aligned} \tag{4.6}$$

are important so that the solution of the two rate equations

$$\begin{aligned} R_{Fe} &= \vec{k}^*_{Fe}\, \bar{a}_{Fe} - \overleftarrow{k}^*_{Fe}\, \bar{a}'_{Fe} \\ R_O &= \vec{k}^*_O\, \bar{a}_O - \overleftarrow{k}^*_O\, \bar{a}'_O \end{aligned} \tag{4.7}$$

subject to the charge balance constraint is of particular interest. The detailed calculations are somewhat lengthy and are left to Appendix 2, although the final results are summarized below,

$$R_{Fe} = b_{Fe}\frac{A}{RT}\left\{1 + \frac{b_0 - b_{Fe}}{b_0 + b_{Fe}}\right\}\left(1 - \frac{A}{2RT}\right)$$

$$R_0 = b_0\frac{A}{RT}\left\{1 - \frac{b_0 - b_{Fe}}{b_0 + b_{Fe}}\right\}\left(1 - \frac{A}{2RT}\right) \qquad (4.8)$$

where $b_{Fe} = \vec{k}_{Fe}C_{Fe}$, $b_0 = \vec{k}_0 C_0 (a_e^-)^2$

and A is the chemical affinity, defined by $A = \mu - \mu' = \frac{C_{FeO}}{K_{eq}C_{Fe}C_0}$ with K_{eq} being the equilibrium constant for the reaction $Fe + 0 \rightarrow FeO$

4.3 EXPERIMENTAL DESIGN AND PROCEDURE

4.3.1 General Considerations

In the electrochemical experiments, an externally applied electrical potential was used to drive the anodic dissolution of iron. In the "chemically driven" experiments an oxygen potential gradient, (i.e. FeO activity gradient) was viewed as an equivalent chemical driving force for iron dissolution.

The basic principles of the approach are illustrated schematically in Figure 4.1 in which liquid iron oxide ($a_{FeO} = 1$) is separated from liquid calcium fluoride ($a_{FeO} << 1$) by a solid iron foil. The overall reactions might be summarized in the following way:

a) $FeO \rightarrow Fe + (O)_{Fe}$ at interface 1

b) Diffusion of oxygen through the foil to interface 2

c) $Fe + (O)_{Fe} \rightarrow (FeO)_{CaF_2}$ at interface 2

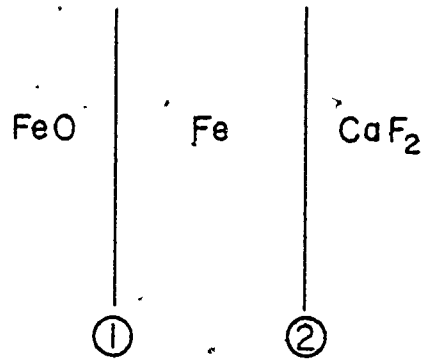

Figure 4.1: Schematic Diagram of the Experimental Principle

These reactions might be alternatively expressed in an electrochemical format involving simultaneous anodic and cathodic steps. The overall kinetics should then be analysed in terms of the relative contribution of each of the following steps:

(1) $(Fe^{2+})_{FeO} + 2e^- \rightarrow (Fe)_{Fe\ foil}$

$(O^{2-})_{FeO} \rightarrow (O)_{Fe\ foil} + 2e^-$ } at interface 1

(2) Diffusion of oxygen along its activity gradient in the foil

(3) $(Fe)_{Fe\ foil} \rightarrow (Fe^{2+})_{CaF_2} + 2e^-$

$(O)_{Fe\ foil} + 2e^- \rightarrow (O^{2-})_{CaF_2}$ } at interface 2

(4) Diffusion of Fe^{2+}, O^{2-} away from interface into bulk CaF_2

Thus the overall kinetics can be divided into two coupled interfacial reaction steps and two diffusion/transport steps. Transport in the iron oxide is not considered since it can be treated as a single component system in equilibrium with the iron. The kinetics

of the interfacial reactions are related to the nature of the interface. However, the rate of oxygen transport through the foil is related to its diffusivity and foil thickness while transport away from interface 2 is related to the FeO diffusivity in CaF_2 and the stirring conditions at the interface. Consequently the relative contributions of the transport steps to the overall kinetics of the process can in principle be changed through appropriate choices and variations in foil thickness and stirring conditions.

4.3.2 Design and Manufacture of the Rotating Crucible Containing FeO

The experimental criteria were met with a rotating iron crucible whose basic configuration and dimensions are given in Figure 4.2. Several (normally 6) 1 mm diameter "windows" of thin iron foil were made in the crucible by drilling holes through to the central hole and then covering these holes with an iron foil of an appropriate thickness. Normally 2 foils of differing thickness were used in a single crucible in order to obtain a direct evaluation of the effect of foil thickness on the reaction rate. The foil was held tightly against the crucible with selective spot welding around the edges. A firm bond at the foil/crucible interface was then achieved with a diffusive welding process in which the crucible was held in a controlled H_2/H_2O atmosphere at 1000°C for a period of about 12 hours.

Three methods of monitoring the overall reaction kinetics were attempted. Initially, the measurement of the change in the iron content in the calcium fluoride on a continuous basis with the polarographic technique was proposed. Platinum alloyed as a marker in the original foil was also tried. The use of finely dispersed oxide markers in the iron foil was found to be the most effective. These markers were

created in the foil by internally oxidizing an Fe - 0.4 wt% aluminum alloy foil in a controlled atmosphere ($P_{H_2}/P_{H_2O} \simeq 15$) at 1000°C for approximately 12 hours prior to welding them to the crucible. The alloy was melted in an argon arc furnace from 99.95% Fe and 99.99% Al, both from A. D. McKay. It was subsequently cold rolled to the desired foil thickness (.05 to .2 mm) in a Stanat 2-high mill prior to being internally oxidized. The internal oxidation and welding steps were carried out in a Kanthal resistance furnace. In both cases the atmosphere consisted of an argon-30% Hydrogen ultra high purity mixture (99.999%) bubbling through a column of distilled deionized water at approximately 150 ml/min. Samples from most foils were mounted and polished to check for an acceptable distribution and size of the oxides. An Fe-2 wt% Pt - 0.4 wt.% Al foil was prepared in a similar manner.

4.3.3 Experimental Design and Procedure

The overall schematic presentation of the experimental apparatus is found in Figure 4.3. The CaF_2 containing crucible was machined from Ferrovac E grade iron. The use of a flat alumina disc was necessary as a guide to prevent the rotating crucible from contacting the outer crucible. The outer crucible was held in a molybdenum wire cage in order that it could be raised and removed without cooling the molybdenum resistance furnace below 1250°C.

The rotating iron crucible was supported in the lower furnace with an 998 recrystallized alumina tube. It was held with an alumina locking pin and wrapped with iron wire to prevent slippage of the pin during rotation. The supporting tube and rotating electrode could be raised and lowered through a "Cajon" O ring seal and could be

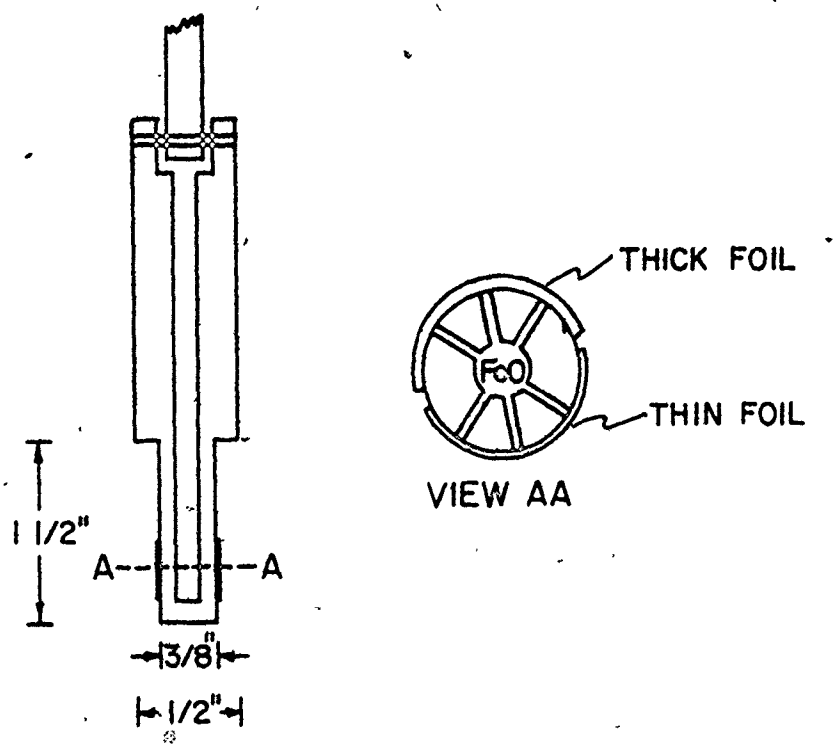

Figure 4.2: Design of the Rotating Crucible

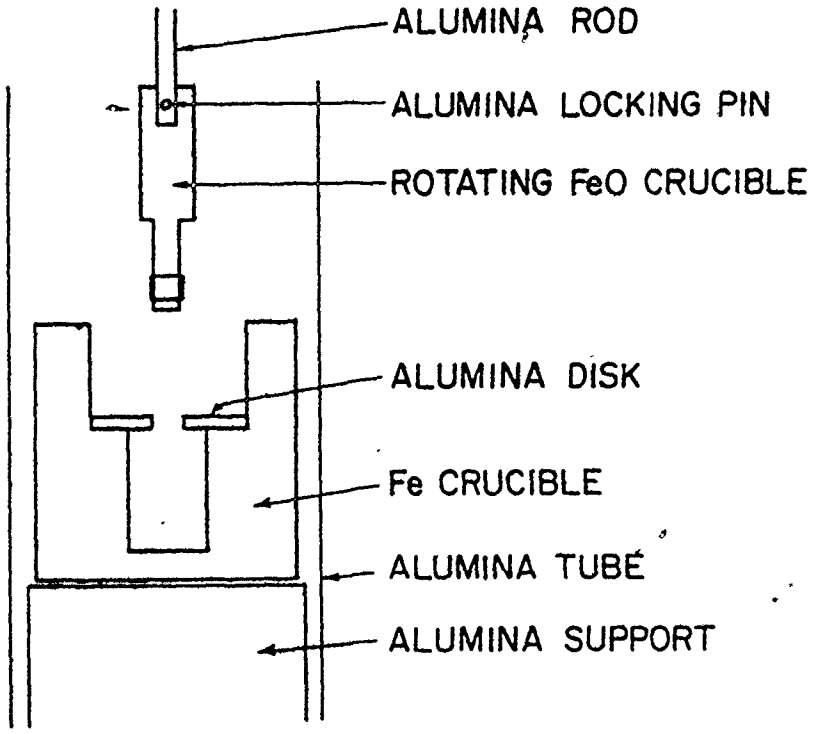

Figure 4.3: Design of the Experimental Apparatus

removed from the furnace through an air lock while still maintaining an inert atmosphere in the furnace.

The basic furnace atmosphere was maintained with argon (UHP grade) which was deoxidized by passing it over zirconium turnings at 600°C. Approximately 5% Hydrogen (UHP grade) was added to the argon when a reducing atmosphere was required (e.g. during the melting of CaF_2).

FeO for the rotating electrode was prepared by melting Fe_2O_3 (99.9%) in a Ferrovac E crucible under an inert atmosphere. It was then ground to minus 80 mesh to insure proper penetration of the oxide powder through the 1 mm holes to contact the foil window.

When the CaF_2 melt had stabilized at a temperature of 1430°C (see next section) the rotating crucible was lowered 1 cm into the CaF_2 melt (prepared as in the electrochemical experiments - Chapter 3) and rotation at 60 rpm commenced immediately. The crucible was raised from the melt after a predetermined time (normally 15, 30 or 45 minutes) and removed from the furnace in preparation for another run. The rotating crucibles were then sectioned and polished for metallographic analysis.

4.3.4 Measurement of CaF_2 Temperatures

The CaF_2 temperature was initially measured with a bare wire type-R Platinum-Rhodium thermocouple inserted directly in the melt. The thermocouple deteriorated rapidly after a period of about 30 minutes but reliable and reproducible measurements could be obtained during the initial period. In order to investigate the effect on temperature of the insertion of the rotating crucible into the CaF_2 melt a "mock crucible" containing a type-R thermocouple was constructed

(Figure 4.4) and inserted into the melt in the same way as a normal crucible. The temperature approached within 1°C of its final value after a period of 2 minutes in the melt. The temperatures of the two methods agreed to within 5°C. The "mock crucible" measurements were taken as more representative of the true interfacial temperature.

4.3.5 Chemical Analysis of CaF_2 for Fe

Samples of approximately 1 gm were taken periodically from the CaF_2 for analysis. Often some CaF_2 would adhere to the bottom of the rotating crucible. These were also analysed for iron content. The weighed samples were first held briefly in hot dilute HCl in order to remove any presence of metallic iron on the surface introduced through handling or contact with the iron crucibles. Each sample was then dissolved in 5 ml of concentrated perchloric acid and boiled to dryness. The residue was then redissolved in 5 ml of concentrated HCl and diluted to 25 ml with distilled deionized water prior to analysis for iron with atomic absorption.

4.4 RESULTS

4.4.1 The Nature of the Data

The oxide markers serve to indicate the location of the original foil/FeO interface. The diffusion of oxygen through the foil is expected to proceed under a strong chemical potential gradient, while the iron clearly does not experience an equivalent gradient. Consequently one would expect the iron from the deposition reaction to accumulate as a relatively inclusion free layer at the FeO/foil

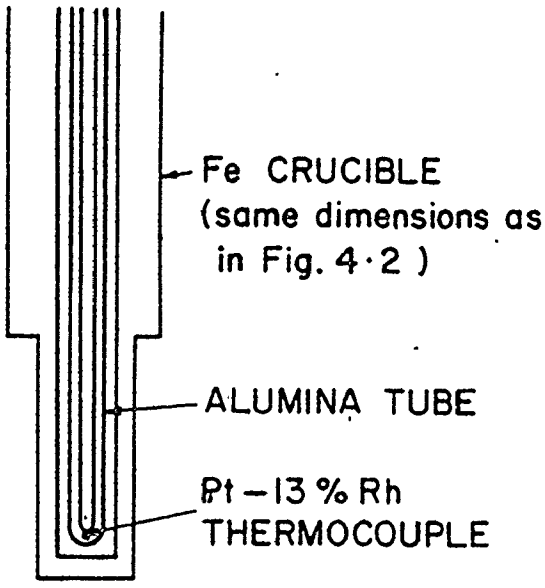

Figure 4.4: Design of the "Mock Crucible" for Temperature Measurement

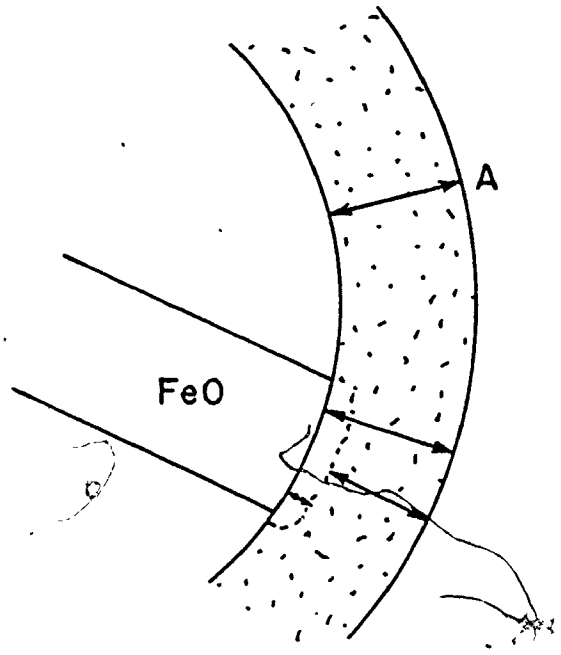

Figure 4.5: Measurement of the Foil

interface. The oxygen should then act to dissolve the iron anodically at the foil/CaF_2 interface. One would therefore expect from a mass balance that the total foil thickness would remain approximately constant with time, although the inclusion bearing portion (original foil) should thin and the inclusion free layer thicken with time. The rate of this thickening process serves as a measure of the overall reaction rate.

4.4.2 Sample Preparation and Measurement

After reaction, the rotating electrodes were sectioned through the windows, mounted and polished for metallographic analysis. A light 10 second etch in Nital 2% was used to highlight the inclusions.

Foil thickness was measured on an optical microscope with a previously calibrated Reichert vernier eyepiece to an accuracy of .002 mm or better.

Referring to Figure 4.5, four basic measurements are considered important. Location A indicates the unreacted or original foil thickness at some distance from the window. At the window the foil thickness can be divided into inclusion bearing (original foil) and inclusion free ("cathodic" deposition) regions. The total thickness at the window is clearly the sum of these.

Figures 4.6a, 4.6b and 4.6c indicate photos from a typical sequence of experiments of 10, 20 and 30 minute durations. The separation into inclusion bearing and inclusion free regions is clearly visible. From such sequences of experiments, rate information may be determined, as discussed in the next section. The metallographic results are summarized in Table 4.1 in terms of mean values and standard deviations for each sample.

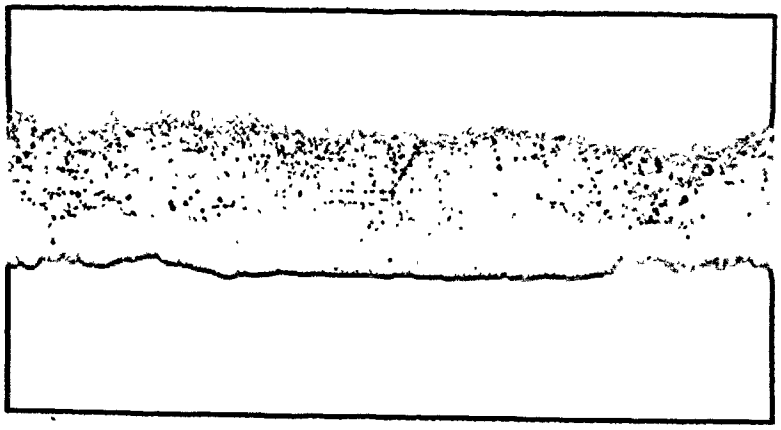

4.6a: Reaction Time 15 minutes

4.6b: Reaction Time 30 minutes

4.6c: Reaction Time 45 minutes

Figure 4.6: Typical Metallographs of Reacted Pellets (300×)

Table 4.1: Metallographic Data for Iron Foils

Sample	Reaction Time (min)	Unreacted Foil Thickness (mm)			Inclusion Bearing Thickness (mm)		Total Window Thickness (mm)		Inclusion Free Thickness (mm)		
		$\bar{x}$	σ_{n-1}	n	$\bar{x}$	σ_{n-1}	$\bar{x}$	σ_{n-1}	$\bar{x}$	σ_{n-1}	n
5	30	.0893	.0041	18	.0900	.0021	.1134	.0032	.0234	.0020	13
6	20	.0925	.0022	14	.0894	.0021	.1081	.0031	.0187	.0015	15
7	10	.0899	.0046	17	.0903	.0037	.1054	.0071	.0151	.0043	18
8	50	.0936	.0030	20	.0919	.0009	.1260	.0013	.0341	.0007	8
9	30	.0884	.0032	16	.0832	.0015	.1110	.0026	.0278	.0030	8
10	45	.0864	.0039	11	.0728	.0021	.1033	.0022	.0305	.0021	11
12	30	.0917	.0020	10	.0920	.0015	.1245	.0053	.0325	.0044	7
13	45	.0742	.0034	13	.0702	.0018	.1147	.0025	.0445	.0032	9
14	15	.0888	.0031	11	.0837	.0019	.1042	.0035	.0205	.0020	11
15*	30	.0942	.0031	13	.0882	.0009	.1134	.0018	.0252	.0012	15
16	45	.0887	.0047	14	.0759	.0014	.1145	.0019	.0386	.0015	21
17	30	.0946	.0054	12	.0825	.0018	.1111	.0025	.0286	.0018	14
18	15	.0789	.0081	13	.0617	.0015	.0839	.0015	.0232	.0009	13
24	30	.0698	.0029	9	.0625	.0014	.1018	.0043	.0392	.0036	17
26	15	.0757	.0022	12	.0765	.0022	.0938	.0023	.0174	.0013	19
28	15	.1516	.0073	9	.1446	.0067	.1772	.0169	.0326	.0109	9
28	45	.0631	.0036	8	.0646	.0015	.1053	.0043	.0407	.0046	10
30	30	.1534	.0050	7	.1527	.0013	.1707	.0016	.0180	.0017	7
30	30	.0599	.0015	5	.0550	.0017	.0789	.0046	.0238	.0034	10
32	15	.1453	.0054	9	.1393	.0018	.1519	.0024	.0126	.0012	10
32	15	.0570	.0046	9	.0582	.0022	.0787	.0041	.0205	.0027	12
29	45	.1465	.0058	8	.1307	.0107	.1609	.0192	.0287	.0091	10
29	45	.0568	.0033	8	.0553	.0030	.0838	.0079	.0285	.0051	9
31	30	.1408	.0060	5	.1329	.0062	.1489	.0057	.0160	.0019	6
31	30	.0620	.0065	5	.0590	.0040	.0775	.0067	.0186	.0028	8
33	15	.1542	.0026	11	.1486	.0036	.1619	.0036	.0133	.0009	9
33	15	.0543	.0039	7	.0558	.0016	.0784	.0022	.0226**	.0008	10
37	45	.1400	.0047	5	.1432	.0023	.1708	.0066	.0275	.0057	17
37	45	.0651	.0031	5	.0650	.0024	.1163	.0057	.0513**	.0044	14
38	30	.1410	.0028	6	.1384	.0030	.1603	.0076	.0219	.0069	13
38	30	.0604	.0066	9	.0623	.0021	.0828	.0024	.0205	.0018	18
39	15	.1433	.0068	7	.1404	.0014	.1561	.0025	.0157	.0023	16
39	15	.0600	.0031	10	.0594	.0019	.0718	.0015	.0124	.0010	18

*Sample 15 no rotation in CaF_2

4.4.3 Calculation of Rate Information

A preliminary examination of Table 4.1 indicates that the anticipated mass balance is not preserved. That is, the thinning of the inclusion bearing foil is much less than the growth of the inclusion free region. This observation will be discussed in the Section 4.5.1. For the present, it is sufficient to mention that the growth of the inclusion free region will be taken in the analysis for determination of the reaction rate.

For each sequence of experiments, representing a range of reaction times, the average inclusion free thicknesses were plotted against time. Under certain circumstances (discussed in Section 4.5.4) the reaction may be considered linear with time after some initial period. Thus the slope of a best linear fit will give the growth rate of the inclusion free region in mm of iron per minute, as illustrated in Figure 4.7.

This growth rate is readily converted to an oxygen flux per cm^2 taking the density of iron as 0.141 moles/cm^3 and $FeO_{(l)}$ as 50.7 mole % O at 1430°C. The results are summarized in Table 4.2, along with the corresponding results of the chemical analysis for iron in calcium fluoride.

4.4.4 Measurement and Analysis for Platinum Bearing Foils

The platinum in the foil was originally intended as a marker to augment or replace the oxides. The original concern (although not substantiated by experiment) was that the oxide markers would interact significantly with the oxygen flux through the foil. In this respect, the platinum was felt to be more "inert". In fact the

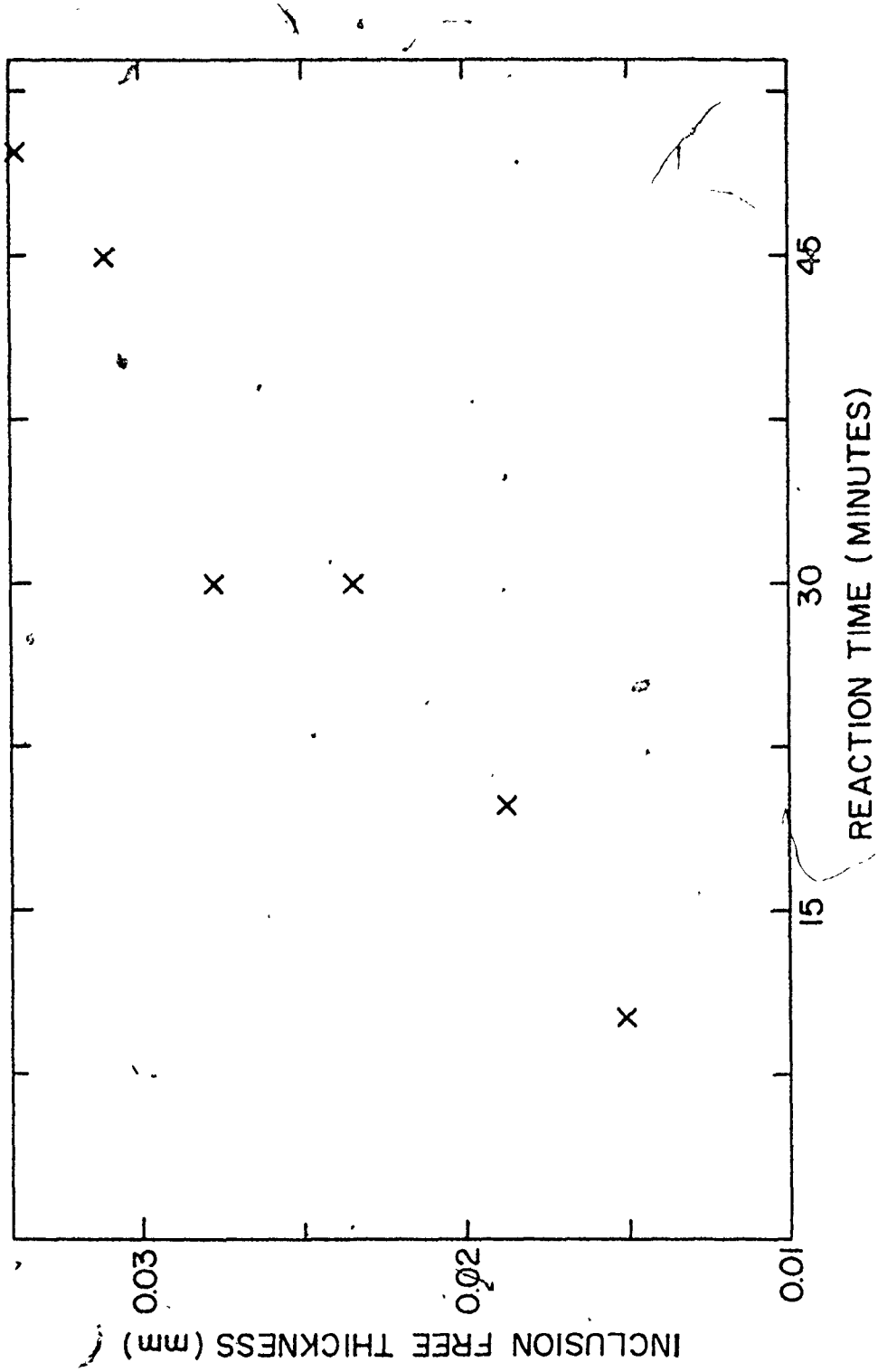

Figure 4.7: Typical Growth Rate for the Iron Foil

Table 4.2

Data for the growth rates in the iron foils

Samples	wt% Fe in CaF_2	Reaction Rate Moles O/cm^2 -min	Correlation Coefficient	Intercept
5, 6, 7, 8, 9, 10	.0124	6.82×10^{-6}	.97	.0105
12, 13, 14	.0193	1.16×10^{-5}	1.0	.0085
16, 17, 18	.0193	7.40×10^{-6}	.98	.0147
24, 26	.0198	2.10×10^{-5} (1.4×10^{-5})*	-	-.0044
28, 30, 32 Thick	.0068	9.72×10^{-6}	.97	.0011
Thin		9.72×10^{-6}	.98	.0081
29, 31, 33 Thick	.0067	7.40×10^{-6}	.94	.0039
Thin		9.57×10^{-6}	-	.0012
37, 38, 39 Thick	.0082	5.66×10^{-6}	1.0	.0099
Thin		7.83×10^{-6}	-	.0043
All Samples	.011	8.0×10^{-6}	.78	.0085

* Corrected for a more reasonable intercept

Table 4.3

Metallographic Data for Iron -2% Platinum Foils

Sample	Time (min)	Unreacted Foil Thickness (mm)			Total Window Thickness (mm)			$\bar{\Delta x}$ (mm)
		$\bar{x}$	σ_{n-1}	n	$\bar{x}$	σ_{n-1}	n	
19	30	.1804	.0026	5	.2924	.0096	6	.1120
20	30	.0973	.0035	7	.2211	.0116	8	.1238
21	30	.1243	.0009	5	.2480	.0140	5	.1237
34	20	.1781	.0065	8	.2584	.0148	8	.0803
34	20	.0996	.0063	10	.1954	.0138	10	.0958
35	10	.1782	.0018	6	.2306	.0127	10	.0524
35	10	.0996	.0022	9	.1464	.0090	6	.0468
36	5	.1892	.0081	4	.2147	.0068	7	.0255
36	5	.0976	.0026	7	.1331	.0079	11	.0358

Reaction Rate 5.20×10^{-5} moles O/cm^2-min

Correlation Coefficient 0.987

Intercept 0.014

diffusion of platinum was too great for its use as a marker under these experimental conditions. However, the results were none the less surprising and are summarized in Table 4.3.

4.5 DISCUSSION

The ultimate objective of this work is an order of magnitude estimate of the Fe/CaF_2 interfacial kinetics in order to compare with that obtained from the electrochemical data. However, several factors must be considered in order to extract this kinetic information. The causes and implications of the apparent mass balance discrepancy must be considered. Furthermore, the influence of the transport steps must be analysed and quantified before the interfacial kinetics may be properly interpreted.

4.5.1 Mass Balance

If the actual reaction process were properly represented by that presented in the previous section, a mass balance should exist in which the overall foil thickness is independent of time. That is, the growth of the inclusion free region should exactly compensate the thinning of the inclusion bearing region. It is clear from Table 4.1 that this is not the case. The growth is 5 to 10 times that of the thinning ($\bar{x}$ = .004 mm in 30 min, σ_{n-1} = .005 for thinning). Most foils do show some thinning although some actually show a slight growth, which is reflected in the large σ_{n-1}. One important factor which bears on this problem is the uniformity of the initial foil thickness. Although many precautions were taken to optimize the

uniformity of thickness, some fluctuations were unavoidable. Thus while the data for foil growth inherently compensates for this fluctuation in foil thickness, the thinning data which is dependent on comparing averages from window and non-window regions of the foil does not. This is reflected in the generally lower σ_{n-1} values for the inclusion free thicknesses. While this consideration can account for the relatively larger scatter in the thinning, it cannot explain the significantly smaller average rate of thinning. It is necessary to conclude that the postulated reactions involving an intimate coupling of iron and oxygen are not completely correct.

It is therefore necessary to consider what the oxygen might be doing that the iron is not.

The straight forward transient effect of saturating the foil with oxygen would only account for a .0003 mm iron growth.

It is possible that the oxygen is reacting in some manner not related to the presence of CaF_2, i.e. through some gaseous reaction, or simply by reaction and growth of the oxide inclusions. In order to investigate this possibility, one rotating crucible was held at temperature, without insertion in the CaF_2 melt, for a period of 30 minutes. A typical photo from the resulting sample is shown in Figure 4.8. The foil is markedly different from those in Figure 4.6. No clear inclusion free region has developed. The foil is dominated by the agglomeration and growth of large inclusions near the FeO interface. These experimental results, coupled with the observation that no significant difference in size and distribution of inclusions was noted between window and non-window foil locations in the normal

300X

Figure 4.8: Metallograph of a Foil Reacted for 30 minutes without Contacting CaF_2

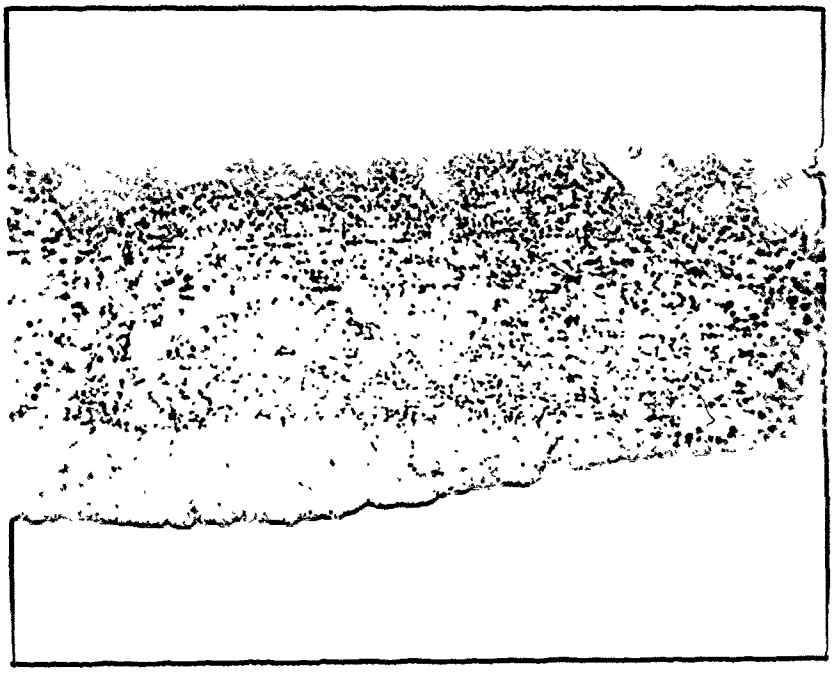

Figure 4.11: Sample 38 - Transition from Normal to Extraordinary Growth of the Inclusion Free Zone

experiments would suggest that the formation and growth of the inclusion free region is strongly related to the presence and action of the CaF_2.

Some understanding of this mass balance problem can be obtained from the CaF_2 phase diagram in Figure 4.9. Whether or not, in fact, a miscibility gap exists in this system is relatively unimportant. The important conclusion is that some finite amount of calcium metal is soluable in CaF_2. There is considerable circumstantial evidence to suggest that a significant amount of calcium metal was in fact dissolved in the CaF_2 used in both the chemical and electrochemical experiments. The strongest evidence is the poor iron yield realized in FeO/CaF_2 additions to the CaF_2.

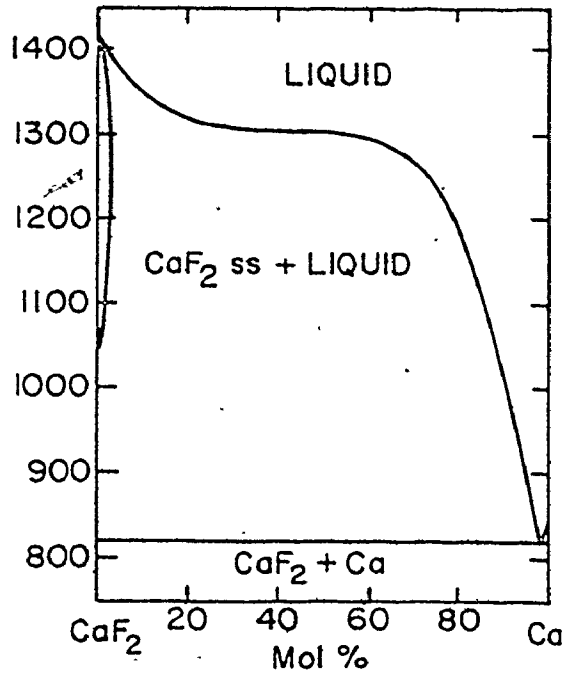

Figure 4.9: Phase Diagram for Ca - CaF_2

In both the electrochemical and chemical experiments master CaF_2 slags containing about 0.2 wt% Fe (as FeO) were produced and added in predetermined quantities to increase the iron content of the working melts. The achieved iron yields were rarely above 80% of the theoretical calculation, and often far worse. In a typical example, 2.85 gms of CaF_2 - 0.19 wt% Fe was added to 45 gms of a .004 wt% melt. The theoretical yield would give a .012 wt% Fe melt. The actual was .008 wt%, a 50% yield. The yields generally became poorer with low initial iron in the melt. This suggests that the iron cations were being reduced by calcium in the melt. On some occasions, evidence for this reduction of iron was observed in the form of metallic iron which nucleated and grew while floating on the CaF_2 surface through a surface tension effect.

The initial experimental design was based on a semicontinuous polarographic measurement of bulk iron content in the CaF_2 during the rotation of the crucible. The method was abandoned in favour of the foil marker approach after repeated failure to detect significant changes in bulk iron concentration in spite of evidence that the desired reaction was proceeding to some extent. The rotating crucibles in these experiments had as many as 24 windows in an effort to achieve rather large macroscopic changes. In spite of the fact that no net changes in bulk iron concentration were detected in the CaF_2 during these experiments, a considerable amount of "plating out" of iron on the crucible walls and electrodes was observed. This is taken as further evidence of reduction of the iron by calcium.

Thus, it seems reasonable to conclude that the mass balance

discrepancy is related to the reducing power of soluble calcium in the CaF_2. At least two mechanisms are possible. The simplest would involve direct oxidation of the calcium at the foil interface. The alternative is a two step process in which the iron is anodically dissolved by the oxygen as previously proposed but is then more or less immediately reduced by the calcium. There is no direct evidence for either mechanism although the latter seems more consistent with the plating out effect seen in some of the experiments (Appendix 3).

In either case the growth of the inclusion free region at the FeO/foil interface appears to be a valid indicator of the overall kinetics of the process.

4.5.2 Transport in the Calcium Fluoride

Most species in most non-polymer liquids have relatively constant diffusivities of order 10^{-5} cm^2/sec. Iron was determined to have a diffusivity of 2.5×10^{-5} cm^2/sec in CaF_2 with the electrochemical method.[41] Thus it is the stirring condition at or near the foil/CaF_2 interface which will have a strong and changeable influence on the resistive contribution of this step to the overall reaction.

Taking a typical value for kinematic viscosity for bivalent molten salts as about .006 cm^2/sec,[17] one can calculate a Taylor*

---

*The Taylor[44] number for concentric cylinders is defined by

$$Ta = Re^2 \left(\frac{r_o - r_i}{r_1} \right) \qquad (4.9)$$

where Reynolds number $Re = \left(\frac{r_o - r_1}{r_1} \right) \frac{\Omega}{\nu}$

inner radius r_i rotation speed Ω radians/min
outer radius r_o kinematic viscosity ν

number of approximately 5 x 10^4 for this system. This is well above the upper limit for laminar flow although somewhat less than that for fully developed turbulent flow. Nevertheless, it is clear that there will be a significant velocity component perpendicular to the rotating crucible at some small distance from the crucible which will greatly enhance the mass transfer rate.

It is not possible to calculate an explicit mass transfer coefficient for this system, nor is it necessary. It is sufficient to know whether or not this transport step offers a significant or negligible resistance to the overall reaction. Some feel for its significance is obtained from sample 15, which was not rotated (i.e. under the influence of natural convection only). The mean inclusion free thickness in sample 15 was .0252 mm after 30 minutes which compares with a range of .0234 to .0392 mm growth in five similar 30 minute experiments in which the crucibles were rotated. This result is informative in as much as it indicates that although the transport through CaF_2 step is perhaps an important kinetic consideration, it is far from the dominant one.

A simple model (Figure 4.10a) is proposed to further analyze this problem. It is assumed for the moment that during the time interval between the passage of the trailing edge of previous window and the leading edge of the window under consideration (0.1 sec), the interfacial concentrations have the opportunity to approach those of the bulk value. If transport in the CaF_2 is important, a concentration profile will develop in which the leading edge of the window will be

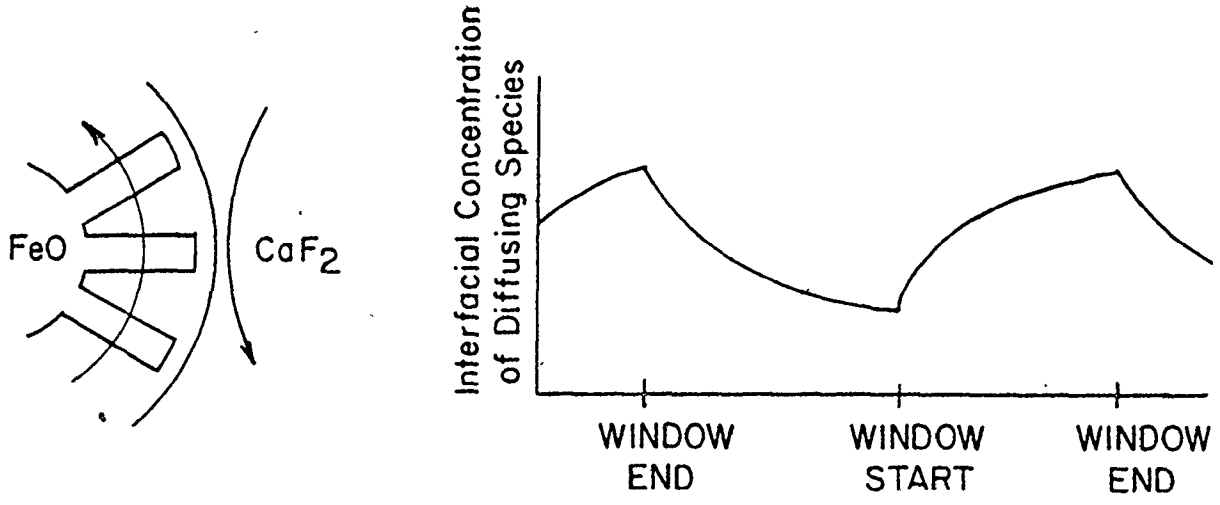

Figure 4.10: Model for the Analysis of the Influence of Electrolyte Diffusion on the Reaction

in contact with a significantly lower interfacial concentration of diffusing species than the trailing edge (Figure 4.10b). Under such circumstances, the trailing edge would experience a significantly lower driving force for the reaction, with a smaller growth rate for the inclusion free region of the trailing edge as a direct consequence. Although fluctuations in the inclusion free thickness did occur (see σ_{n-1}, Table 4.1), no systematic deviation from leading to trailing edge of the window was seen in the data.

Finally, it will be noted from Table 4.3 that the presence of platinum in the foil led to a dramatic increase in the reaction rate. Such an observation is inconsistent with the hypothesis that transport in the CaF_2 offers significant resistance to the overall reaction.

Thus on the basis of this discussion it seems reasonable to assert that within the scope and accuracy of these experiments,

transport in the CaF_2 had a negligible influence on the overall kinetics.

4.5.3 Oxygen Transport in the Iron Foil

Unlike transport in a liquid which involves diffusion and convection, transport in a solid is a strictly diffusive process which can be treated directly. To the accuracy with which oxygen diffusivity and solubility for δ-iron are known, a limiting steady state oxygen flux can be calculated. This limiting value will occur when the overall rate is completely controlled by oxygen diffusion in the foil. Under these conditions chemical equilibrium will exist at both FeO/foil and foil/CaF_2 interfaces. The oxygen concentration may be taken as the solubility limit at the FeO foil interface and negligible at the foil/CaF_2 interface. Taking D_O = 3.76 x 10^{-5} cm^2/sec[45] and (O) = .063 at %[46] at 1430°C one can calculate:

$\bar{J_O}$ = 2.2 x 10^{-5} moles O/cm^2-min for foil .006 cm thick

J_O = 9.1 x 10^{-6} moles O/cm^2-min for foil .015 cm thick

A comparison with the rates in Table 4.2 shows this theoretical diffusion limiting rate to be close to but larger than those measured.

It is possible under a quasi-steady state assumption to estimate the diffusion related influence on the calculated interfacial reaction rate constant with a simple model (details in Appendix 4). Using the oxygen diffusivity and solubility data, it is shown in Appendix 5 that for the thin foils, 35% of the total oxygen driving force is consumed by the diffusion process and 65% by the interfacial reaction

in order to maintain the quasi steady state. It is also possible to estimate that the overall rate with the thick foil would be about 65% of that in the thin foil. In three double thickness experiments, the corresponding values are found to be 72, 78 and 100%.

However, at best this model must be considered semi-quantitative. In view of the scatter in the experimental data it is certainly not clear whether or not the difference seen between the thick and thin foil rates is statistically significant. Secondly, errors in oxygen diffusivity and solubility data could have an important influence on the calculation. The important conclusion which may be drawn, however, is that the influence of oxygen transport in the foil, is not overwhelming. That is to say, a significant portion of the information content of the overall experimental rate is due to the nature of the interfacial reaction kinetics.

4.5.4 Interfacial Kinetics - Assumptions

Having established the relative importance of the major transport steps, it is possible to properly consider the interfacial kinetics. In order to preserve the clarity of the discussion, a number of simplifying assumptions will be made initially.

1.) The overall reaction is assumed to be controlled entirely by the interfacial process and transport offers no resistance to the overall reaction. It is unlikely that this approximation is precisely correct but the previous section suggests that such an assumption would lead to an underestimation of the interfacial parameter by somewhat less than a factor of two.

2.) The interfacial reactions consist of two anodic and two cathodic steps at two interfaces. The rate limiting step may be any one or any combination of these. It is assumed that the important step is the $O + 2e^- \rightarrow O^{2-}$ reaction at the foil/CaF_2 interface.

3.) It is assumed that the rate of the reverse reaction $O^{2-} \rightarrow O + 2e^-$ is negligible.

In calculating the oxygen flux rates which are summarized in Table 4.2, a linear growth with time has been assumed. The conditions under which such an assumption is valid must be discussed. Obviously there is an initial transient period in which an oxygen gradient develops in the foil. In terms of foil growth, however, this was shown to be one to two orders of magnitude smaller than the effects measured and can be ignored. Furthermore, the bulk CaF_2 concentrations do not change measurably during the experiment (as determined in the polarographic tests). In fact, even if there were a full mass balance (i.e. all iron goes into CaF_2 with oxygen) which clearly overstates the case, the bulk concentration would typically change from .012 to .015 wt% Fe during a 30 minute experiment, a relatively small change. In addition, the net rate has been assumed independent of foil thickness, and the FeO remains unchanged during the experiment. Thus on the basis of these assumptions one would predict a true steady state situation in which a linear growth rate would be anticipated. It is interesting to point out that even if the effect of changing foil thickness were considered by introducing a root time dependence, the dependence would correspond to some time interval greater than zero

because of the finite initial foil thickness. Thus even such a correction would lead to near linear kinetics.

If the rate were truly linear throughout the range of experimental times, the intercept thickness at time zero should be approximately zero. This is not the case. In fact the intercept centres closer to .01 mm, with considerable variation. The reason for this tendency to a non zero intercept is not clear. It appears to be rather random in nature and it is suspected that this may reflect the initial condition or prior history of the iron oxide or foil. Or it may simply represent iron which comes out of the iron oxide upon cooling.

One final comment with respect to the basic data is necessary. One two occasions (marked ** in Table 4.1) the foils appeared to exhibit an extraordinary growth. In sample 38 (Figure 4.11, refer to page 110) the foil appeared to go suddenly from normal to extraordinary thickening within one window. The reasons for this are not clear, although it is interesting to note that all three instances occurred in the later experiments. Although no such records were kept, it is possible and in fact likely that these foils originated within the same "batch". Thus one might speculate that some contamination occurred which resulted in an acceleration effect similar to that noted in the platinum foils.

4.5.5 Interfacial Kinetics - Net Oxygen Flux

Figure 4.12 shows the oxygen flux plotted against bulk iron concentration in CaF_2. Although there is a very slight upward trend in rate with concentration, the concentration range is relatively small and the scatter large. Thus it seems unreasonable to draw any

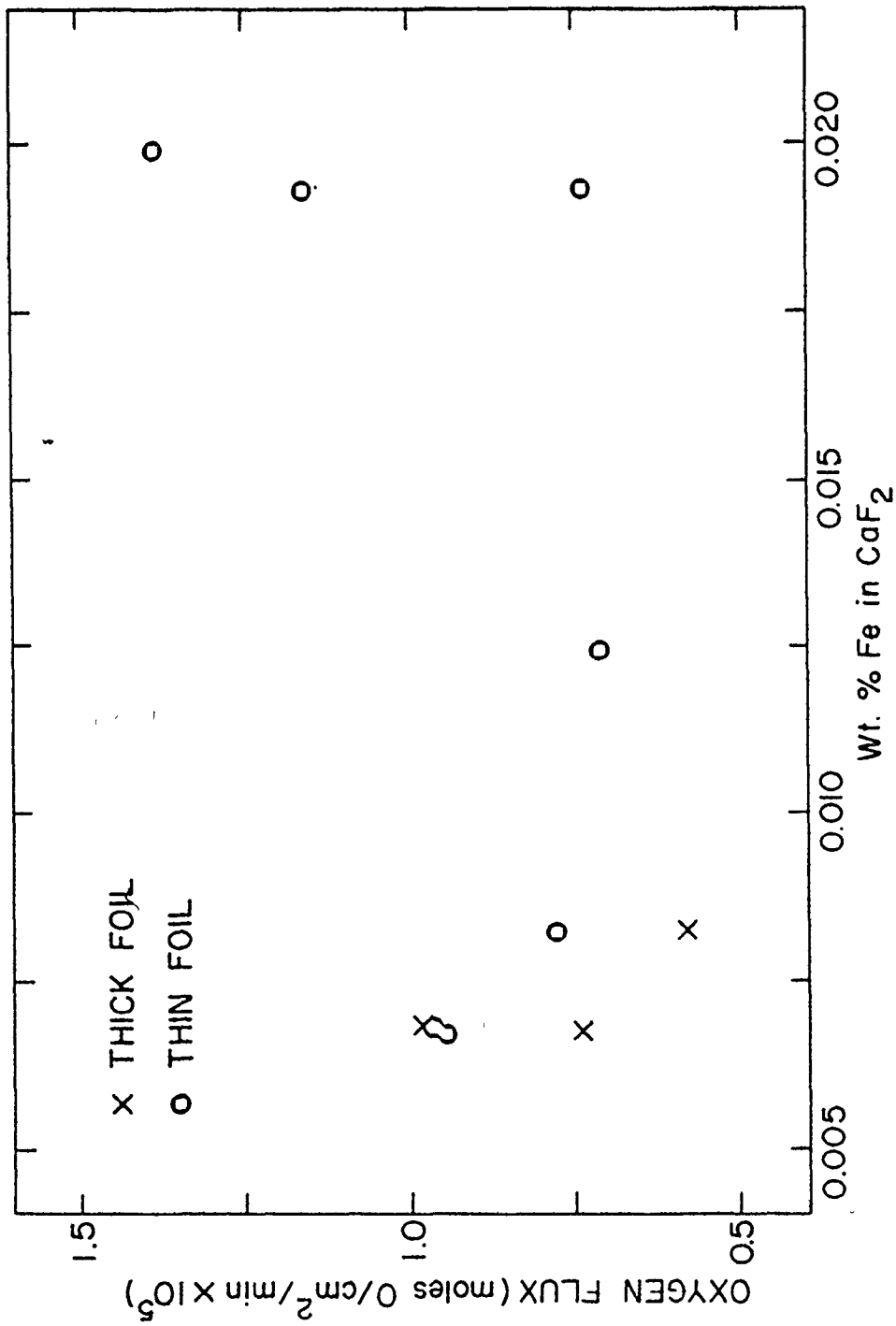

Figure 4.12: Oxygen Flux as a Function of Bulk Iron Concentration

conclusions on the concentration dependence.

In the absence of any clearcut trend with concentration, all of the data in Table 4.1 were plotted against reaction time without regard for foil thickness or iron concentration. This resulted in a slope of 8.0×10^{-6} moles of oxygen/cm^2-min, an intercept of .0085 mm iron, and a correlation coefficient of .776. A mean concentration was taken as .011 wt% Fe in CaF_2. These values will be used as representative kinetic parameters in the balance of this report.

4.5.6 Interfacial Forward Rate Constant

In the absence of a significant reverse reaction the kinetic expression may be represented by the simple equation $R_{net} = \vec{R} = \vec{k}C_O$. The assumption that no appreciable diffusion resistance occurs is equivalent to assuming oxygen saturation (i.e. equilibrium with FeO) at the foil/CaF_2 interface. Thus with $R_{net} = 8 \times 10^{-6}/60 = 1.3 \times 10^{-7}$ moles O/cm^2-sec and $C_O = 6 \times 10^{-5}$ moles O/cm^3, the forward rate constant for $(O) + 2e^- \rightarrow (O^{2-})$ may be evaluated directly as 2.2×10^{-3} cm/sec.

4.5.7 Rate of Reverse Reaction - Approximate Calculation

The implications of the assumption regarding the significance of the back reaction should be examined. Normally tracer work is required to investigate this problem. Alternatively, one can use kinetic data from two bulk concentrations to calculate the relative effect of the back reaction if the rate constants can be assumed constant over this concentration range. However, the electrochemical evidence suggests these constants to be strong functions of concentration, so

this approach is unlikely to be useful. One can, however, gain a feel for this problem with a simple model, which is detailed in Appendix 5. We see that the hypothetical oxygen concentration in the foil which is in equilibrium with the CaF_2 melt may be estimated as 6×10^{-9} moles/cm^3. Thus, at equilibrium, the forward rate R = (2.2×10^{-3}) (6×10^{-9}) = 1.3×10^{-11} moles O/cm^2-sec which is equal to the back reaction rate. This back reaction rate is dependent only on the CaF_2 phase and not on the actual forward rate. Hence it is concluded that under the experimental conditions, the back reaction is some four orders of magnitude slower and can be ignored.

4.5.8 The Rate Controlling Interfacial Reaction

The only assumption which remains to be discussed is that regarding the nature of the slow interfacial reaction. The term "slow reaction" is meant to suggest the reaction which proceeds in series with other reactions or transport steps and offers a significantly greater resistance to the overall reaction. By direct analogy with the electrical circuit, this reaction step will consume the greatest portion of the overall voltage drop or in this case driving force. In Section 4.3.1 a sequence of four electrochemical reactions were suggested to represent the reactions at the interfaces.

1.) $Fe^{2+} + 2e^- \rightarrow Fe$
2.) $O^{2-} \rightarrow O + 2e^-$
} at FeO/foil interface

3.) $Fe \rightarrow Fe^{2+} + 2e^-$
4.) $O + 2e^- \rightarrow O^{2-}$
} at CaF_2/foil interface

In addition to the above mentioned anodic and cathodic reaction steps,

the oxidation of calcium to Ca^{2+} has also been postulated. The kinetics of this reaction should be controlled by the transport in the CaF_2. This transport step offers a negligible contribution to the overall reaction resistance (Section 4.5.2), so that the calcium oxidation reaction need not be considered within the context of the rate controlling interfacial step.

It was assumed in 4.5.4 that the oxygen transfer at the CaF_2/foil interface (i.e. 4) was the important reaction. Clearly the experimental design was based on the ability to satisfactorily separate transport rates and interfacial kinetics. It is not possible to distinguish explicitly between the proposed rate controlling steps at the interfaces. However, it is possible to gain some feel for the probable slow steps and the errors involved.

In Section 4.2, the true oxygen flux was expressed in terms of b_O and b_{Fe}. It has been noted that most species in most liquid systems have diffusivities of order 10^{-5} cm^2/sec. If one accepts the analogous premise which has some basis in experience that all elements at a given interface will have kinetic parameters within a range of an order of magnitude or so, one could speculate that iron at the CaF_2/foil interface might have a forward rate constant $\vec{k}_{Fe}$ of order 10^{-3}. This implies that $b_{Fe} >> b_O$ due to the large difference in surface concentrations. Thus the charge balance correction factor becomes

$$\left\{1 + \frac{b_{Fe} - b_O}{b_{Fe} + b_2}\right\} \approx 2 \qquad (4.10)$$

so that the measured value of b_O would be twice that of the true value. Although it may be reasonable to assume that $\vec{k}_{Fe} \approx 10^{-3}$,

it is important to consider the numerical consequences of the possibility that the kinetics of the iron reaction is dominant at the CaF_2/foil interface. With such an assumption it is possible to calculate

$$\vec{k}_{Fe} = 1.3 \times 10^{-7}/0.141 = 9.2 \times 10^{-7} \text{ cm/sec.}$$

Furthermore, it is necessary that $b_O >> b_{Fe}$, so that $Ro >> 1.3 \times 10^{-7}$, which implies that $\vec{k}_O >> 2.2 \times 10^{-3}$ cm/sec.

If in fact, $b_O >> b_{Fe}$, all of the same arguments and conclusions hold with the exception that $\vec{k}_{Fe}$ rather than $\vec{k}_O$ is to be evaluated from the experimental data. However, it is rather unreasonable to expect that $\vec{k}_O$ is some five orders of magnitude greater than $\vec{k}_{Fe}$. Thus it is unlikely that the kinetics of the iron dissolution reaction is important in controlling the overall rate. Since the iron deposition (reaction 1) should have a similar influence on the kinetics of the FeO/foil interface, it seems reasonable to relate the overall kinetics to the rates of the oxygen reaction.

The problem may be analysed in the manner illustrated in Figure 4.13 which used the approach developed in Appendix 5. Either both oxygen reactions offer about the same resistance to the overall reaction or their resistive contributions are significantly different. If, as has been assumed in the previous sections, oxygen transfer at the CaF_2/foil interface offers a far higher resistance to the overall reaction than any other step, it will be considered as the rate controlling step (Figure 4.13a). There is some evidence to suggest that this may in fact be the case. It is possible that phases which are more "comfortable" together (as manifested by lower

interfacial tensions, etc.) would offer less resistance and inherently faster interfacial kinetics (see also Section 4.5.9). This tendency is indicated in the electrochemical data. Using the wetting characteristics as a guide, the FeO is clearly more comfortable with iron than is the low iron containing CaF_2.

If, as is represented in Figure 4.13b, the oxygen transfer at the FeO/foil interface was rate limiting, an identical situation would exist in terms of calculation of the forward rate, influence of back reaction rate, etc. The only difference, of course, is that the kinetic information would be pertinent to oxygen transfer at the FeO/foil rather than the CaF_2/foil interface.

Consider now the final possibility--that the resistive contributions from both interfaces are about equal (Figure 4.13c). In this case the driving force or concentration is only half that originally anticipated. This circumstance would lead to an underestimation of the kinetic parameter by a factor of two.

Summarizing, the best estimate for the oxygen reaction rate constant $\vec{k}_O$ at the CaF_2/foil interface is 2.2×10^{-3} cm/sec. This could be overestimated by as much as a factor of two or underestimated by as much as a factor of four, depending on the relative kinetics of the interfacial reactions and the oxygen transport in the foil (Figure 4.13d).

4.5.9 Interfacial Kinetics - Platinum Containing Foils

A comparison of the data in Figures 4.2 and 4.3 indicates that the alloy foil containing 2 wt% platinum exhibits a reaction rate more than six times that of the normal foil. This is indeed a very surprising

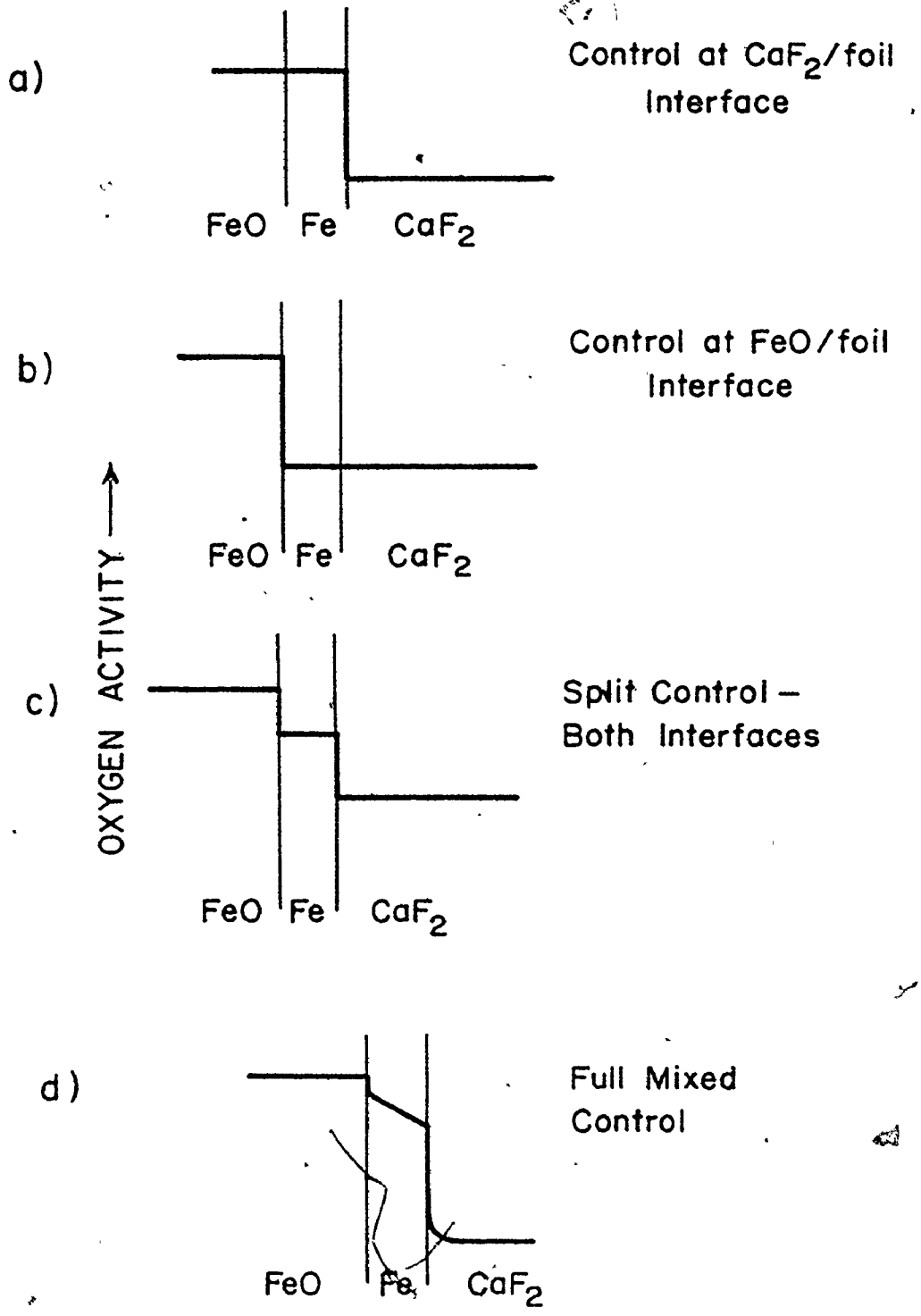

Figure 4.13: Possible Oxygen Activity Distributions for the Reaction Mechanisms

result since the platinum was originally intended as an inert marker. As previously stated, the platinum should not accelerate the transport in the CaF_2 and must, therefore act to increase the oxygen diffusivity in the foil, or the interfacial reaction rate, or both. In the absence of information on oxygen diffusivity in this alloy, any further discussion would be highly speculative. However, the absence of any clear dependence of rate on foil thickness, and the near linear kinetics in the range of 5 to 30 minutes would indicate that a significant portion of the rate increase is probably due to a catalytic effect at the CaF_2/foil interface.

Preliminary electron microprobe traverses of the foil failed to show an inflection point in the platinum concentration which could be used to estimate the original foil interface, indicating that the interdiffusivity was too great for the purposes of a marker. These experiments shed some light on one final question. Since any catalytic effect of platinum is clearly at the CaF_2/foil interface, it suggests that the rate controlling interfacial step in the pure foil occurs there, rather than at the FeO/foil interface (i.e. Figure 4.13a in preference to 4.13b).

Clearly, far more detailed work must be done on this system before definitive conclusions may be drawn. However the effect of a relatively small amount of platinum in the foil is both interesting, and dramatic.

CHAPTER 5: DISCUSSION - COMPARISON OF THE CHEMICAL AND ELECTROCHEMICAL EXPERIMENTAL APPROACHES

In Chapter 3, ion exchange current densities in amperes/cm^2 obtained with a double pulse electrochemical technique have been presented graphically as a function of iron concentration in the CaF_2. In Chapter 4, the chemical approach based on a rotating iron crucible has permitted the calculation of a rate constant for oxygen transfer at the iron/CaF_2 interface in units of cm/sec. The comparison of these two approaches (both the models and the experimental data) is a primary objective of this chapter. Once a reliable estimate for the kinetic parameters of the interfacial reaction has been obtained, a comparison with the mass transport information is possible. A prediction of the most likely rate control regime (i.e. transport, mixed etc.) can then be made.

Since the nature and application of chemical and electrochemical kinetic information is normally quite different, it is necessary to consider on what basis, if any, that it may be compared. With respect to basic information content, such a comparison is encouraging. The ion exchange current density in the electrochemical theory carries information on the flux at the metal/electrolyte interface under dynamic equilibrium conditions. The forward rate constant, multiplied by the equilibrium interfacial concentration has a similar role in the chemical formalism.

5.1 THE THEORY OF THE ELECTROCHEMICAL KINETICS - A REEXAMINATION

Prior to a comparison with the chemically derived data, it is necessary to reconsider the classical electrochemical approach which

is outlined in Chapter 3. In the application of this theory to aqueous solutions, it is necessary (and normally reasonable) to assume that, to a good approximation within the time frame of the experiment, only one chemical species reacts at the interface. In contrast, oxygen is clearly present and able to react in this Fe/CaF_2 system.

Both the theoretical and experimental implications of a second reacting species are significant, particularly in reference to the concept of equilibrium. There exists one additional degree of freedom in the system. If only one species (e.g. iron) is able to transfer at the interface, it is always possible to impose a potential difference at that interface so that no reaction occurs. There is no ambiguity in determining this equilibrium condition since current must pass through the external circuit in order for the reaction to proceed. With the exchange durrent density being defined by Equation 3.5b, knowledge of i_o as a function of $\Delta\phi_{eq}$ will permit determination of the fundamental parameters (α, etc.). It is possible to uniquely relate $\Delta\phi_{eq}$ to C'_{Fe} when iron is the only species which reacts (Equation 3.18), so that knowledge of i_o as a function of C'_{Fe} is sufficient.

If oxygen is also able to transfer at the interface, the relation between $\Delta\phi_{eq}$ and C'_{Fe} is no longer unique. Furthermore, the absence of an external current cannot be used as a criteria for the existance of equilibrium at the interface. Even when the external current is zero, coupled reactions may proceed at the interface until equilibrium is reached. This will occur when a_{FeO} (as defined by the presence of pure iron and the partial pressure of oxygen) is uniform through-

out the system.

In addition, the derivation leading to Equation 3.21 requires that k_o, k'_o, α, ${}_oE_a$, and ${}_oE'_a$ remain independent of interfacial concentrations. This assumption may not be reasonable in the Fe/CaF_2 system. The surface active nature of oxygen is well known. Furthermore, the nature of the Fe/CaF_2 interface changes significantly with C'_{Fe}, as is indicated by the changing interfacial tension and interfacial charging characteristics (capacitance - see Section 5.6).

This discussion leads one to the necessary if somewhat negative conclusion that no simple theoretical relationship exists in this system between the exchange current density and the so called fundamental parameters. The values of α and k' calculated in Section 3.4.10 are valuable as empirical, but not theoretical parameters.

In Chapter 3 the possibility of an oxygen reaction at the interface was not considered in the interpretation of the double pulse data. The results from the initial experiments, in which an argon -5% hydrogen gas mixture was used, indicate that the effect of the oxygen reaction on the actual double pulse measurement is probably negligible. In terms of the effect of hydrogen, two time frames were evident. The influence of hydrogen was evident in the longer time frame of milliseconds or seconds. The polarographic technique, for instance, was clearly influenced by the presence of hydrogen. However, the agreement between values of i_o obtained with and without the flow of hydrogen indicates that it had a negligible effect on the double pulse measurement. The same is probably true of the oxygen.

Put in another way, the oxygen is expected to have a significant

influence on the nature of the Fe/CaF_2 interface. However the electrical double pulse may be thought of as an almost instantaneous transient probe which is capable of exploring the response of iron to the nature of that interface, without altering it significantly.

5.2 COMPARISON OF THE MATHEMATICAL MODELS FOR THE ELECTROCHEMICAL AND CHEMICAL APPROACHES

Following Lu,[31] the electrochemical expression

$$i_F = i_o \left\{ \exp\left(-\alpha ZF\eta_t/RT\right) - \exp\left((1-\alpha)\ ZF\eta_t/RT\right) \right\} \qquad (3.5a)$$

and the chemical expression (derived from Equation A.10)

$$R_{Fe} = \vec{k}_{Fe}\, C_{Fe} \exp\left((1-\alpha)\ ZF\Delta\phi/RT\right) \left\{ 1 - \exp\left[-\ (A + ZF\Delta\phi)/RT\right] \right\} \qquad (5.1)$$

are shown to be identical. The electrical portion of the driving force is split into two parts, such that

$$\Delta\phi = \Delta\phi_{eq} + \eta_t \quad \text{and} \quad A + ZF\Delta\phi_{eq} = 0. \qquad (5.2)$$

By factoring out $\exp\left(-(1-\alpha)\ ZF\eta_t/RT\right)$ from Equation 5.1, one obtains

$$R_{Fe} = \vec{k}_{Fe}\, C_{Fe} \exp\left(-(1-\alpha)\ A/RT\right) \left\{ \exp\left((1-\alpha)\ ZF\eta_t/RT\right) - \exp\left(-\alpha\ ZF\eta_t/RT\right) \right\}. \qquad (5.3)$$

Noting that $i_F = -ZFR_{Fe}$, the relation

$$i_o = ZF\vec{k}_{Fe}\, C_{Fe} \exp\left(-(1 - \alpha)\, A/RT\right) \qquad (5.4)$$

is obtained by inspection. The linearized chemical approach is a valid approximation only near equilibrium (i.e. $A << RT$) so that the factor $\exp\left((1 - \alpha)\, A/RT\right)$ can be ignored. The forward constant, k_{Fe} can then be related to i_o in the following way

$$\vec{k}_{Fe} = i_o/ZFC_{Fe} \qquad (5.5)$$

This equation permits the calculation of a value of $\vec{k}_{Fe}$ from the ion exchange current density in Chapter 3 which may then be compared with the value of $\vec{k}_o$ determined in Chapter 4. Equation 5.5 could have been derived directly from the linearized forms of the electrochemical and chemical formalisms.

Equation 5.4 might have been expressed in the form

$$i_o = ZF\, \vec{k}_{Fe}\, C_{Fe} \exp\left((1 - \alpha)\, ZF\Delta\phi_{eq}/RT\right). \qquad (5.6)$$

The comparison of Equations 5.6 and 3.5b could lead to the conclusion that

$$\vec{k} = k_o \exp\left(-{}_oE_a/RT\right), \qquad (5.7)$$

which would be a more general relationship than Equation 5.5, which requires $A << RT$ (i.e. $ZF\Delta\phi_{eq} << RT$). However, $\Delta\phi_{eq}$ is not normally defined the same way in the two formalisms. Furthermore the difficulty in evaluating true values for α, $k_o \exp\left(-{}_oE_a/RT\right)$, etc. has been discussed in Section 5.1. Consequently, the comparison of data in Section 5.3 will be limited to the use of Equation 5.5.

Although the chemical and electrochemical approaches are shown to be mathematically equivalent one major conceptual difference exists. The electrochemical formalism considers the potential difference at the interface as a force which modifies the shape of the energy barrier and hence affects the rate constants (Figure 3.1). The chemical formalism assumes that the field alters the effective concentrations through an electrochemical activity. The final result is clearly the same since any kinetic expression is a product of these two factors.

5.3 COMPARISON OF THE ELECTROCHEMICAL AND CHEMICAL DATA

The basic compatability of the respective mathematical models was demonstrated in Section 5.2. Within an acceptable error, it was possible to verify the validity of the assumptions (summarized in Section 4.5.4) necessary for the interpretation of the data from the rotating crucible experiments. However, in Chapter 3 it was necessary to assume the general applicability of the model for the double pulse method in the Fe/CaF_2 system in order to interpret the transient voltage response. In particular, the following was assumed:

1.) the existance of an interfacial charging process which could by approximated by a constant capacitance,

2.) the existance of a charge transfer potential which could be attributed to one reacting species (e.g. iron),

3.) the applicability of the functional dependence for the concentration overpotential determined by Matsuda, et. al.[37]

The inability to verify these assumptions motivated the rotating crucible

experiments in order that independently measured experimental data could be compared. Although the electrochemical data is available over a range of concentrations, the rotating crucible data is assumed valid only at .011 wt% Fe, so that comparison of the rate constants is possible at only one point.

Evaluation of i_o from Figure 3.15 at C'_{Fe} = .011 wt% Fe as 16.3 amperes/cm^2 gives (with Equation 5.5)

$$\vec{k}_{Fe} = 16.3/(2)\ (96{,}500)\ (.141) = 0.6 \times 10^{-3} \text{ cm/sec.}$$

It is now possible to compare the rate information obtained from the two approaches.

Electrochemical Approach: $\vec{k}_{Fe} = 0.6 \times 10^{-3}$ cm/sec.

Chemical Approach: $\vec{k}_o = 2.2 \times 10^{-3}$ cm/sec.

Since the rate constant derived from the electrochemical data is associated with iron while the rate constant obtained from the foil/marker experiments is for oxygen, a numerical comparison is not as conclusive as might be hoped. Nevertheless, the agreement of the independent experimental approaches is very encouraging in terms of the accuracy of the measurements and the validity of the necessary assumptions. In this respect, the approach persued in Chapter 4 has successfully substantiated the order of magnitude estimates of kinetic information obtained with the double pulse electrochemical technique.

It is important to recognize that i_o is a strongly increasing function of C'_{Fe}. This implies that the rate constants are not in fact constant, but are also strong functions of bulk iron concentra-

tion in the CaF_2. Consequently the chemical rate equations may only be approximated as linear relationships over narrow ranges of concentration. For application to broader ranges of concentration, solutions to systems of non-linear equations must be obtained.

5.4 PREDICTION OF THE RATE CONTROLLING REGIME

Prediction is possible once reliable information on the interfacial reaction rate constants and mass transfer coefficients is available for a particular system. Following the approach of Yamada,[3] a modified Sherwood number is used. Since the rate constants and mass transfer coefficients may be thought of as conductivities in the electrical circuit analogy (Chapter 1), their relative magnitudes will determine the importance of each possible rate controlling step. The modified Sherwood number is defined in the following way:

$$Sh = \vec{k}/km$$

Yamada has discussed three control regimes according to the value of the Sherwood number:

$Sh < 0.1$	Interfacial Reaction Control
$0.1 < Sh < 10$	Mixed Control
$Sh > 10$	Transport Control

For this Fe/CaF_2 system, $\vec{k}$ is taken as approximately 1×10^{-3} cm/sec. In Section 3.4.2, k_m for the unstirred CaF_2 was found to be 2.8×10^{-3} cm/sec. (i.e. with $D \approx 2.5 \times 10^{-5}$, the "boundary layer thickness" is

10^{-2} cm). Thus Sh ≈ .36, even though the interfacial reactions proceed quite quickly. This is well within the mixed control regime, although tending towards reaction control. If the reaction rate constants measured in the Fe/CaF_2 system are indicative of those in more complex metallurgical systems, the influence of interfacial rates on the overall reaction kinetics may be greater than is normally supposed.

5.5 INTERFACIAL CHARGING IN THE Fe/CaF_2 SYSTEM

In Chapter 3, the interfacial charging process was attributed to an electrical double layer capacitance without further comment. The double layer in aqueous solutions is understood to result from the alignment of water depoles, solvated, and absorbed ions. The nature of the metal/electrolyte interface is not well understood in medium and high temperature molten salt systems. However it has been suggested that the double layer structure becomes more compact with increasing temperature.[42] Goto[47] has suggested that the term electrical double layer, as it is normally construed in aqueous systems, may be misleading in the case of a molten salt or slag electrolyte. Until the phenomena is more fully understood, it may be better described as interfacial charging, or as an interfacial capacitance.

Figures 3.18 and 3.19 show a clear and significant increase in this interfacial capacitance with the concentration of iron in the CaF_2 electrolyte. The increasing iron concentration is presumably accompanied by a greater concentration of oxygen ions in the electrolyte. It is possible that the observed change in the interfacial

capacitance is simply due to the changes that these elements bring about in the electrolyte, and the added flexibility (in terms of charge distributions and interactions) which is possible. It is possible that these same factors influence the interfacial kinetics in a similar manner.

It is clear that a far more intense study of this interfacial charging phenomena is necessary, although the manner in which this might be accomplished is not obvious. For a proper theoretical interpretation of the double layer charging and its relation to surface tension (and the zero charge potential) it is necessary to assume that the interface is ideally polarizable[48] (maintaining constant temperature and composition). The exchange current densities in this and other molten salt systems indicate that they more closely approximate ideally reversible, rather than ideally polarizable interfaces. In spite of efforts to make conventional measurements of variations in capacitance with the potential applied to the interface,[42] Prange[41] has pointed out that this may not be possible. Any attempt to apply a potential difference to the interface will result in a electrochemical reaction and build up of a diffusion potential until a steady state is reached. Consequently the potential difference will occur, not at the interface as intended but over the resulting diffusion gradient. If this is the case, the resulting data will show the relationship between interfacial capacitance and interfacial concentration, rather than the potential difference as intended.

CHAPTER 6: CONCLUSIONS

1.) A phenomenological framework which takes account of fundamental coupling is necessary for the proper description of ionic diffusion.

2.) The double pulse galvanostatic technique is suitable for the measurement of ion exchange current densities in the Fe/CaF_2 system at 1450°C when a non-linear extrapolation is used.

3.) The exchange current density and the interfacial capacitance are strongly increasing functions of iron concentration in the CaF_2.

4.) A theoretical model of slag/metal reactions based on chemical kinetics has been modified and successfully compared with the electrochemical theory.

5.) An independent experimental approach based on an internally oxidized iron foil has confirmed the kinetic data obtained with the double pulse technique.

6.) Mixed control of the reaction kinetics at the Fe/CaF_2 interface is predicted in the absence of mechanical stirring.

7.) The presence of 2 wt% platinum in the internally oxidized iron foil increased the reaction rate by more than a factor of 6.

APPENDIX 1

Calculation of the Mass Transfer Coefficient

Current and steady state potential data for a typical experiment are listed in Table A.1. Figure A.1 is a plot of i/ZFC_o' vs $\exp\left(\frac{ZF}{RT}\eta_{AR}\right) - 1$ where the bulk concentration C' has been determined by chemical analysis to be 0.097 wt%. Because the bulk concentration is drifting slowly with time, only the last set of current vs potential data is used for each experiment to determine k_m values, although such measurements were made before and after each set of double pulse measurements.

The valance has been assumed to be 2, which may be reasonable for such low iron contents. The slope in Figure A.1 should then correspond with k_{m_1} which is evaluated as 2.9×10^{-3} cm/sec for these data.

Table A.1

Typical Polarographic Data

i (ma/cm^2)	η_{AR} (mv)
.105	.305
.153	.46
.188	.55
.213	.635
.228	.68
.259	.75
.259	.76
.259	.77

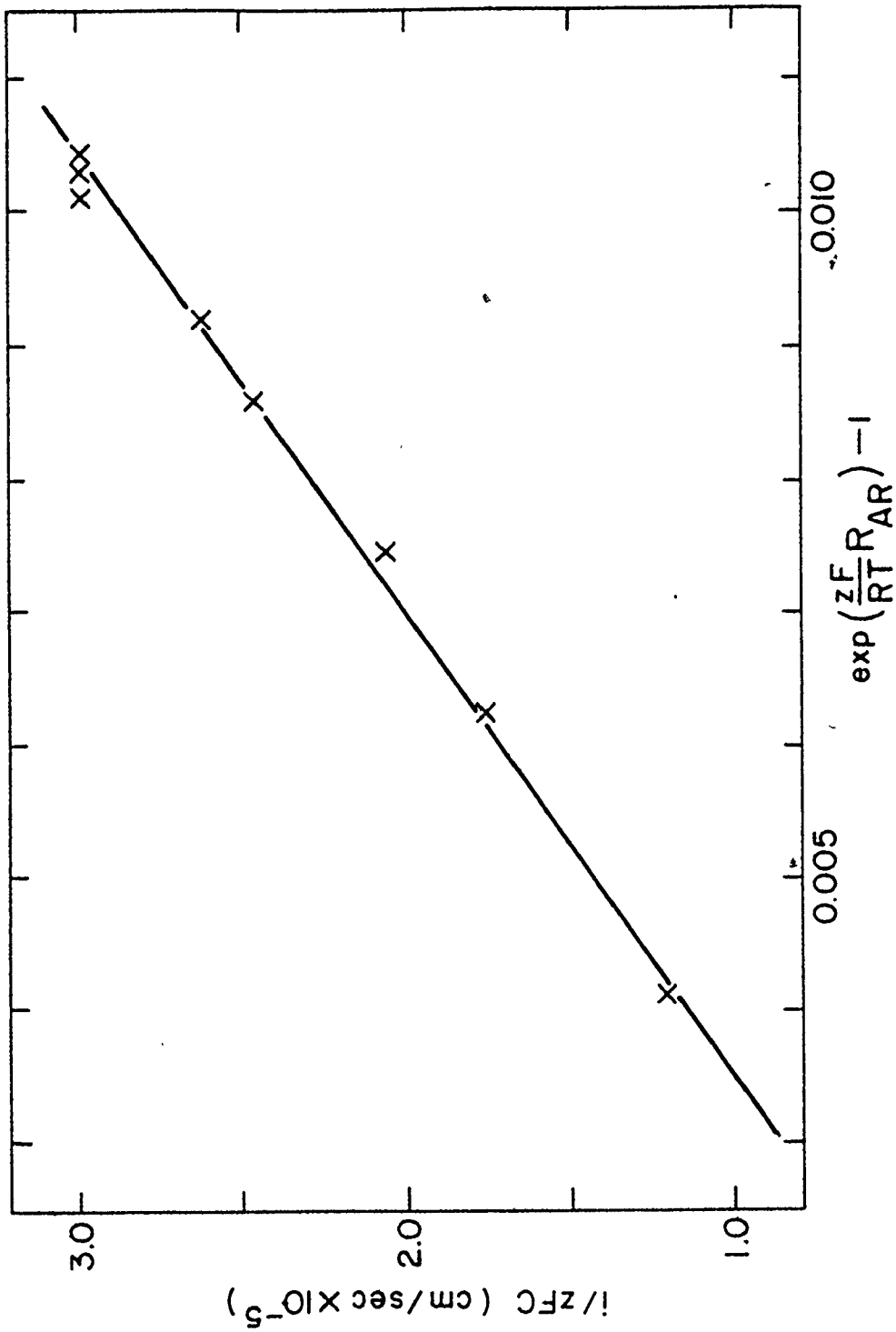

Figure A.1: Determination of k_m, the Mass Transfer Coefficient

APPENDIX 2

Reaction Kinetics for Simultaneous Anodic and Cathodic Interfacial Reactions

It is often convenient to consider simultaneous anodic and cathodic reactions, as has been done frequently in this work. However, such systems of equations must ultimately be combined in such a manner as to result in electrically neutral components in order that they be useful. This is particularly true when one wishes to consider the driving forces and final equilibrium conditions in a reacting system, which are discussed below.

Consider the reactions

$$\begin{aligned} &Fe \rightarrow Fe^{2+} + 2e^- \\ &O + 2e^- \rightarrow O^{2-} \end{aligned} \qquad (A.1)$$

When electroneutrality conditions hold, these two electrochemical reactions are equivalent to

$$Fe + [O] \rightarrow (FeO), \qquad (A.2)$$

for which the equilibrium constant may be written

$$K_{eq} = \frac{C_{FeO}}{C_{Fe}C_O}. \qquad (A.3)$$

This equilibrium constraint is fully defined as written.

It is also possible to write equilibrium relations for each of the electrochemical relations although they are not unambiguously defined

$$K_{Fe}^{eq} = \frac{C'_{Fe}\,(a_e^-)^2}{C_{Fe}} \qquad K_O^{eq} = \frac{C'_O}{C_O(a_e^-)^2} \,. \tag{A.4}$$

Therefore $(a_e^-)^2$, the activity of electrons in the metallic phase may be written as

$$(a_e^-)^2 = \frac{C'_O}{C_O K_O^{eq}} = \frac{K_{Fe}^{eq} C_{Fe}}{C'_{Fe}} \,, \tag{A.5}$$

and substituted into the preceding equation to give

$$K_{Fe}^{eq} K_O^{eq} = \frac{C'_{Fe} C'_O}{C_{Fe} C_O} = \frac{C_{FeO}}{C_{Fe} C_O} \tag{A.6}$$

which results in the relation $K_{Fe}^{eq} K_O^{eq} = K_{eq}$.

Consider now the kinetic equations**

$$\begin{aligned} R_{Fe} &= \vec{k}_{Fe} C_{Fe} \exp(2F\phi/RT) - \overleftarrow{k}_{Fe} C'_{Fe} (a_e^-)^2 \exp(2F\phi'/RT) \\ R_O &= \vec{k}_O C_O (a_e^-)^2 \exp(-2F\phi/RT) - \overleftarrow{k}_O C'_O \exp(-2F\phi' RT) \,. \end{aligned} \tag{A.7}$$

**In these equations, $k_{Fe} C_{Fe}$ replaces $k^*_{Fe} a_{Fe}$. Either concentrations or activities may be used in these elementary rate expressions, depending on whether or not the thermodynamic information is included or excluded from the rate constants and equilibrium constants.

By considering the limiting case of kinetic equilibrium when $R_{Fe} = 0$ and $R_O = 0$, it is possible to show that

$$\frac{\vec{k}_{Fe}}{\overleftarrow{k}_{Fe}} \exp\ (2F\Delta\phi/RT) = \frac{C'_{Fe}(a_e^-)^2}{C_{Fe}} = K_{Fe}^{eq}$$

$$\frac{\vec{k}_O}{\overleftarrow{k}_O} \exp\ (-2F\Delta\phi/RT) = \frac{C'_O}{C_O(a_e^-)^2} = K_O^{eq} \qquad (A.8)$$

$$\frac{k_O k_{Fe}}{k_O k_{Fe}} = K_{eq}. \qquad (A.9)$$

The rate equations may then be manipulated to give

$$R_{Fe} = \vec{k}_{Fe} C_{Fe} \exp\left(2F(1-\alpha)\,\Delta\phi/RT\right) \left\{1 - \frac{C_{FeO}}{K_{eq} C_{Fe} C_O} \exp\ (-2F\Delta\phi/RT)\right\}$$

$$R_O = \vec{k}_O C_O (a_e^-)^2 \exp\left(-2F(1-\alpha)\,\Delta\phi/RT\right) \left\{1 - \frac{C_{FeO}}{K_{eq} C_{Fe} C_O} \exp\ (2F\Delta\phi/RT)\right\}. \qquad (A.10)$$

However, it is noted that

$$\frac{C_{FeO}}{K_{eq} C_{Fe} C_O} = \exp\ (-A/RT), \qquad (A.11)$$

where A is the chemical affinity (or "driving force") as defined by Prigogine.

It is convenient to make the following substitutions

$$k_{Fe} C_{Fe} = b_{Fe},\ \frac{A}{RT} = p,\ \frac{2F\Delta\phi}{RT} = X,\ k_O C_O (a_e^-)^2 = b_O\ .$$

For small deviations from equilibrium in the reaction zone, $p \ll 1$, and consequently $X \ll 1$. It is possible to expand the exponential function, neglecting all terms beyond 2nd order. Then

$$\exp(X) = 1 + X + \tfrac{1}{2}X^2. \tag{A.12}$$

In this manner, one obtains the following kinetic relationships:

$$\begin{aligned} R_{Fe} &= b_{Fe}(p + X)\left\{1 - \tfrac{1}{2}(p + X) + (1 - \alpha)X\right\} \\ R_O &= b_O(p - X)\left\{1 - \tfrac{1}{2}(p - X) - (1 - \alpha)X\right\}. \end{aligned} \tag{A.13}$$

The constraint of no net flux of charge implies that $R_{Fe} - R_O = 0$ for all reaction time. These two equations can then be solved for X, the field in terms of b_{Fe}, b_O, and p. In order to obtain a simple and physically clear solution, α will be taken as $\frac{1}{2}$ since a more complex quadratic equation otherwise results in clouding of the physical content. Thus

$$b_{Fe}(p + X)(1 - \tfrac{1}{2}p) - b_O(p - X)(1 - \tfrac{1}{2}p) = 0. \tag{A.14}$$

But $p \ll 1$ so that $(1 - \frac{1}{2}p) \neq 0$. Hence the relation

$$b_{Fe}(p + X) - b_O(p - X) = 0 \tag{A.15}$$

may be solved for X to give

$$X = \left(\frac{b_O - b_{Fe}}{b_O + b_{Fe}}\right)p$$

$$R_{Fe} = b_{Fe}p \left\{1 + \frac{b_O - b_{Fe}}{b_O + b_{Fe}}\right\} (1 - \tfrac{1}{2}p)$$

$$R_O = b_O p \left\{1 - \frac{b_O - b_{Fe}}{b_O + b_{Fe}}\right\} (1 - \tfrac{1}{2}p) \; . \qquad \text{(A.16)}$$

In examining the expression for R_{Fe}, the term $b_{Fe}p$ can be considered the "natural rate" for iron, while the term in the curly brackets is a charge coupling correction to the rate arising from the charge balance constraint. The term $(1 - \frac{1}{2}p)$ is a second order correction which arises from the $\exp\left\{2F\ (1 - \alpha)\ \Delta\phi/RT\right\}$ term in the original expression when $\alpha = \frac{1}{2}$.

If the reverse reactions are negligible, it is possible to develop a similar set of relations, starting from

$$R_{Fe} = b_{Fe} \exp\left\{(1 - \alpha)X\right\}$$

$$R_O = b_O \exp\left\{-(1 - \alpha)X\right\} \qquad \text{(A.17)}$$

to give, when $\exp\left\{(1 - \alpha)X\right\}$ is linearized:

$$R_{Fe} = b_{Fe} \left\{1 + \frac{b_O - b_{Fe}}{b_O + b_{Fe}}\right\}$$

$$R_O = b_O \left\{1 - \frac{b_O - b_{Fe}}{b_O + b_{Fe}}\right\} . \qquad \text{(A.18)}$$

However, it is not always clear that $\exp\left\{(1 - \alpha)X\right\}$ can be properly linearized, since X may be large. Under these circumstances, the following relationships are applicable

$$R_O = b_O \left(\frac{b_{Fe}}{b_O}\right)^{\frac{1}{2}}, \qquad R_{Fe} = b_{Fe} \left(\frac{b_O}{b_{Fe}}\right)^{\frac{1}{2}} . \qquad \text{(A.19)}$$

APPENDIX 3

Some Evidence of Plating Out of Iron During the Rotating Crucible Experiments

Two possible reaction mechanisms at the foil/FeO interface have been suggested in Section 4.5.1. The first may be written

$$[O]_{foil} + 2e^- \rightarrow (O^{2-})_{CaF_2}$$

$$(Ca)_{CaF_2} \rightarrow (Ca^{2+})_{CaF_2} + 2e^-.$$

The second mechanism may be written

$$[O]_{foil} + 2e^- \rightarrow (O^{2-})_{CaF_2}$$

$$[Fe]_{foil} \rightarrow (Fe^{2+})_{CaF_2},$$

followed by

$$(Ca)_{CaF_2} + (Fe^{2+})_{CaF_2} \rightarrow (Ca^{2+})_{CaF_2} + [Fe]_{foil}.$$

The end result of both proposed mechanisms is identical, although iron may be thought of as a catalyst in the second case.

Although most of the iron should be reduced quickly and plate out on the foil again, some could escape and plate out elsewhere in the system. In the early rotating electrode experiments, in which a polarographic electrode was inserted into the melt, growth of the polarographic electrode was noted even though it was located 2 cm

distant from the rotating crucible (Figure A.2). This plating out may be taken as evidence of iron ions present in the CaF_2 which are later reduced. This suggests that the second of the proposed reaction mechanisms may be important.

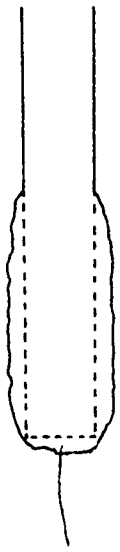

Figure A.2: Growth of Polarographic Electrode During Rotating Crucible Experiments

APPENDIX 4

Distribution of A Driving Force Among Reactions in Series

For any kinetic phenomena operating in a linear regime the flux may be expressed as the product of a driving force and a constant (i.e. mass transfer coefficient, reaction rate constant, etc.). Ohm's law is of this type, relating the current to a voltage and conductivity. If a known voltage difference is applied to resistances in series, then the portion of that overall voltage difference which appears over each individual resistance may be calculated under the steady state condition that the current flux through each resistance is equal.

An analogous calculation is possible under quasi steady state conditions in a reacting system. Consider the FeO/foil, CaF_2 system with the following assumptions:

1.) Equilibrium conditions prevail at the FeO/foil interface.

2.) No significant concentration gradient exists in the CaF_2 phase.

3.) The rate of the reverse reaction at the CaF_2/foil interface is negligible.

It is then possible to construct a diagram showing the oxygen concentration as a function of location (Figure A.3a). Since all of the concentrations of interest are in the iron foil, a plot of oxygen activity vs location is conceptually equivalent. Oxygen concentrations in moles/cm^3 will be used in the numerical calculations. However it proves to be easier to sketch activities in order to illustrate

the concepts since one need not be concerned with equilibrium constants for the interfacial reactions (Figure A.3b). In Figure 14a, C_2 is equal to the oxygen solubility in iron at 1430°C, i.e. 6.02×10^{-5} moles/cm^3. The diffusive flux may be written as

$$J_{dif} = \frac{Do}{\delta} (C_2 - C_3) \tag{A.20}$$

and the reaction flux at the CaF_2/foil interface may be written as

$$\vec{J}_{Rx} = \vec{k}C_3. \tag{A.21}$$

Under quasi-steady state, $J_{dif} = \vec{J}_{Rx}$. The overall flux from Table 2 is typically 8×10^{-6} moles O/cm^2-min, so we may estimate C_3 as follows:

$$8 \times 10^{-6} = \frac{Do}{\delta} (C_2 - C_3) = (3.76 \times 10^{-5}) \cdot (6.02 \times 10^{-5} - C_3) \ (60)/(.006) \tag{A.22}$$

$$\therefore \ C_3 = 3.9 \times 10^{-5} \text{ moles O/cm}^3.$$

Consequently, k may be estimated as follows:

$$8 \times 10^{-6} = \vec{k} \ (3.9 \times 10^{-5}) \ (60) \tag{A.23}$$

$$\vec{k} = 3.4 \times 10^{-3} \text{ cm/sec}$$

It is interesting to note that $(3.9 \times 10^{-5}/6.02 \times 10^{-5}) \times 100 = 65\%$ of the total driving force (oxygen concentration difference) is "consumed" by the interfacial reaction, with the balance being required to maintain the diffusion rate.

Furthermore it should be possible to predict the effect of foil thickness with this simple model. For $\delta' = .015$ cm

$$J' = (3.76 \times 10^{-5})\ (6.02 \times 10^{-5} - C_3')\ (60)/(.015)$$

$$= (3.4 \times 10^{-5})\ (C_3')\ (60) \qquad (A.24)$$

$$C_3' = 2.53 \times 10^{-5} \text{ moles O/cm}^3$$

$$J' = 5.25 \times 10^{-6} \text{ moles O/cm}^2\text{-min}$$

or about 65% of that in the thin foils.

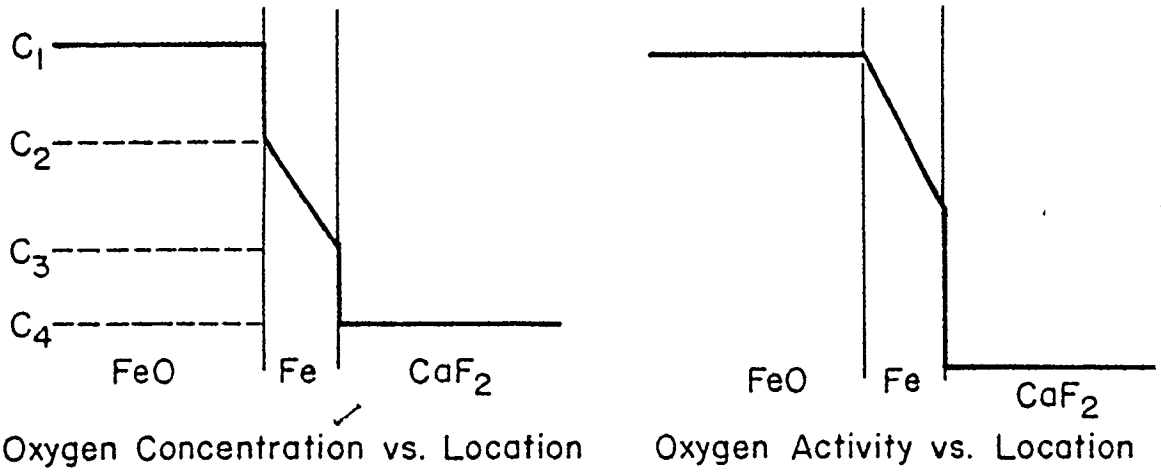

Figure A.3: Possible Oxygen Concentrations and Activities Through the Foil

APPENDIX 5

Estimation of the Rate of the Reverse Reaction

In principle there exists an oxygen concentration in the foil at the CaF_2/foil interface which is in equilibrium with the CaF_2 used in the experiments (C_3 as defined in Appendix 5). This concentration will be denoted by C_3^*. At this concentration, the following relationship holds:

$$J_{net} = \vec{J}^* - \overleftarrow{J}^* = 0 \quad \text{i.e.} \quad \vec{J}^* = \overleftarrow{J}^*. \tag{A.25}$$

If C_3^* can be estimated independently, then $\vec{J}^*$ and hence $\overleftarrow{J}^*$ can be estimated. Since this $\overleftarrow{J}^*$ is dependent on the CaF_2 only, it will be independent of C_3 (if no concentration gradients exist in the CaF_2). Thus, this value of $\overleftarrow{J}^*$ can be compared directly with the experimentally measured rates in order to evaluate the relative importance of the reverse reaction. It remains to estimate C_3^*.

For this order of magnitude estimation, henrian behaviour is assumed. The FeO - CaF_2 phase diagram (Figure A.4) demonstrates a large miscibility gap. On this basis we estimate $a_{FeO} = 1$ at 1 wt% FeO in CaF_2 in contact with pure Fe. For the reaction

$$2Fe + O_2 \rightarrow 2FeO, \quad \Delta G^\circ = -75 \text{ kcal}$$

$$\therefore \; - RT \ln \frac{(.01)^2}{(1)(P_{O_2})} = -75{,}000 \tag{A.26}$$

$$\therefore \; P_{O_2} = 2.2 \times 10^{-14} \text{ atm}.$$

Since $P_{O_2} = 2.2 \times 10^{-10}$ results in an oxygen concentration in Fe of 6×10^{-5} moles O/cm^3, we can estimate $C_3^* = 6.10^{-9}$ moles O/cm^3. Thus $\overleftarrow{J}^*$ may be evaluated as $\overleftarrow{J}^* = \overrightarrow{J}^* = (2.2 \times 10^{-3})\ (6 \times 10^{-9})$ $= 1.3 \times 10^{-11}$ moles O/cm^2 - sec.

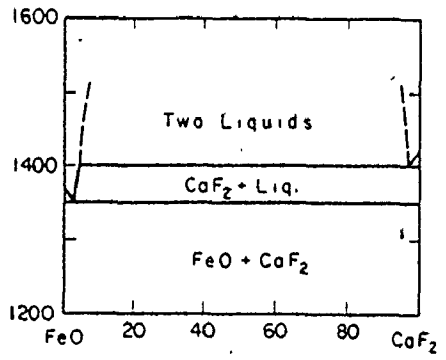

Figure A.4: Phase Diagram for FeO - CaF_2

REFERENCES

1. I.B, King and S. Ramachandran: The Physical Chemistry of Steelmaking, M.I.T. Symposium, 125, Wiley, (1958).

2. S. Ramachandran, I.B. King and N.J. Grant: Trans. Met. Society A.I.M.E., 1549, (1956).

3. K. Yamada: M. Eng. Thesis, McMaster University, (1977).

4. L.S. Darken: Trans. A.I.M.E., Inst. Met. Div., Tech. Publ., 2443 (1948).

5. Kirkendall and Smigelskas: Trans. A.I.M.E., 171, 130, (1947).

6. L.S. Darken: Trans. A.I.M.E., 175, 184, (1948).

7. P.G. Shewmon: Diffusion in Solids, McGraw-Hill, (1963).

8. de Groot and Mazur: Non-Equilibrium Thermodynamics, North Holland, (1962).

9. J.S. Kirkaldy: Energetic Phenomena IV. ed Mueller, Gordon and Breach, p. 242, (1968).

10. L. Onsager: Proc. Nat. Acad. Sci., 46, p. 241, (1945-46).

11. de Groot and Mazur: p. 64

12. Kirkaldy and Lane: Can. J. Phys. 42, 1643, (1964).

13. Kirkaldy and Lane: Can. J. Phys. 44, 2059, (1966).

14. J.R. Manning: Phys. Rev. 124, 470.

15. Zeibold and Cooper: Acta. Met. 13, 465, (1965).

16. J.G. Kirkwood, et al: J. of Chem. Phys., 33, 1505, (1960).

17. Bockris and Reddy: Modern Electrochemistry, Vol. 1, Plenum, (1970).

18. C.R. Masson, et al: J. Chem. 49, 683, (1971).

19. K. Schwerdtfeger and H. Keller: Private Communication, also Met. Trans. 10B, 551, (1979).

20. Kirkaldy: Can. J. Physics 57, 719 (1979).

21. Cooper: Physical Chem. of Glasses, 6, 55, (1965).

22. A. Varshneya: Ph.D. Thesis, Case Western Reserve Univ., (1970).

23. D. Okongwu: Ph.D. Thesis, McMaster University, (1973).

24. Okongwu, Lu, Hamielec and Kirkaldy: J. of Chem. Phys., 58, 777, (1973).

25. Okongwu, Lu and Kirkaldy: Metal-Slag-Gas Reactions and Processes. Electrochemical Society, (1975).

26. Nagata and Goto: J. Electrochem. Soc., 123, 1814, (1976).

27. K.S. Goto: Transport Properties in Complex Slags at High Temperature, Proceedings of Conference on Physical Chemistry and Steelmaking, Versailles, October, 1978.

28. Sugawara, Nagata and Goto: Met. Trans. B., 8B, 605, (1977).

29. B. Langanke and H. Schmalzried: Ber. Bunsenges. Phys. Chem., 83, 59, (1979), also B. Petuskey and H. Schmaltzried: Ber Bunsenges. Phys. Chem., 84, 218, (1980).

30. Y. Takata, Kawasaki Steel Corp.: Private communication.

31. W-K. Lu: Trans. ISIJ, 11, 32, (1971).

32. C. Wagner: The Physical Chemistry of Steelmaking MIT Symposium (1958), p. 237, Wiley.

33. Klaus J. Vetter: Electrochemical Kinetics, Academic Press, New York, 1967.

34. Guggenheim: Thermodynamics - An Advanced Treatment, North Holland Publishing, Amsterdam, 1967.

35. Berzins and Delahay: J. Am Chem. Soc. 77, (1955), 6448.

36. Gerischer and Krause: Z Physick. Chem. N. F. 10 (1957); 264:14 (1958), 184.

37. Matsuda, Oka and Delahay: J. Am Chem. Soc. 81, (1959).

38. E. Yeager: Overpotential Measurements - Techniques of Electrochemistry, ed. by Yeager and Salkind: Wiley Interscience (1972).

39. Susbrelles and Delahay: J. Electroanal Chem. 17, (1968), 289.

40. K. Schwerdtfeger, N. Nowack and D. Krause: Submitted to Ironmaking and Steelmaking.

41. R. Prange: Ph.D. Dissertation, Tech. Univ. Clausthal, (1980)

42. A.D. Graves et. al: Advances in Electrochemistry and Electrochemical Engineering, Vol. 4, Ed. P. Delahay, J. Wiley and Sons, N.Y., 1966, p. 174.

43. H.H. Bauer: Electrodics, Georeg Theime Stuttgart, 1972

44. John Newman: Electrochemical Systems, Prentice-Hall, Englewood Cliffs, N.J., 1973.

45. Swisher and Turkdogan: Trans. Met. A.I.M.E., 239, (1967), 426.

46. Tankins and Gokcen: Trans. A.S.M., 53, (1961), 843.

47. K.S. Goto, Tokyo Institute of Technology: Private Communcation.